Ollscoil na hÉireann

NATIONAL UNIVERSITY OF IRELAND

Investigation of Solution-Phase and On-Chip Binding of C-Reactive Proteins and Antibodies

A Thesis Presented to
The National University of Ireland
for the degree of
Doctor of Philosophy

by

Ethel Noonan

Head of Department
Prof. Martyn Pemble

Supervised by
Dr. Aidan Quinn

Tyndall National Institute
University College Cork
December 2014

Table of Contents

Declaration by Candidate:

This is to certify that the work I am submitting is my own and has not been submitted for another degree, either at University College Cork or elsewhere. All external references and sources are clearly acknowledged and identified within the contents. I have read and understood the regulations of University College Cork concerning plagiarism.

Signature of candidate: _____

Date: _____

Abstract

Gold nanoparticles can self-assemble into nanostructures in the presence of suitable linker molecules. The self-assembly of gold nanoparticles functionalized with C-reactive protein (CRP) antibodies in the presence of CRP antigen linker molecules was explored. A ratio of antigen linker molecules to nanoparticle (2:1) that resulted in rapid nanoparticle self-assembly was identified, evidenced as a distinct solution colour change from red to blue within 5 minutes. Higher linker molecule- nanoparticle ratios (12:1, 18:1, 72:1) resulted in slow formation of nanostructures and only a slight solution colour change (even after periods of several days), the rate being dependent on the number of available binding sites. The propensity of nanoparticles to rapidly assemble into nanostructures at certain linker molecule-nanoparticle ratios was corroborated employing citrate-stabilized nanoparticles and di-isothiocyanate terminated metal organic rhenium linker molecules whereby again rapid formation of nanostructures was dependent on a specific molecule-nanoparticle ratio as distinct from other molecule-nanoparticle ratios. UV-visible spectroscopy and scanning electron microscopy characterization confirmed visual observations. Surface-based assays also show much promise in application to point-of-care detection. It was of interest to determine if surface-based assays void of complex chemical processes and elaborate equipment could compete with laboratory-based assays in terms of specificity, stability and sensitivity but also offer faster and inexpensive diagnosis. The binding of CRP antibody to silanised silicon-silicon oxide substrates implemented using the organosilane APTES and the subsequent binding of CRP antigen to this immobilised CRP antibody was explored. The binding event of CRP antigen to surface immobilised CRP antibody was electrically characterised in ambient conditions. The formation of the antibody-antigen complex resulted in a corresponding decrease of the sensor capacitance at a CRP antigen concentration of 20 µg/mL (2 hours). However, it was demonstrated that nanoparticle amplification can facilitate rapid visual surface-based detection of CRP antigen of between 5 µg/mL and 20 µg/mL.

Acknowledgements

I wish to thank my supervisor Dr. Aidan Quinn for giving me the opportunity to read for a Ph.D. in the Nanotechnology Group at Tyndall National Institute. I am grateful for his advice, support and encouragement throughout the years as well as his pleasant, approachable and good-humoured nature. Thanks also to my co-supervisor Prof. Martyn Pemble and advisor Dr. Hugh Doyle for much valuable input during my Ph.D. and to my external examiner Prof. James Mc Laughlin.

I wish to thank Dr. Helen Braven of BBI Solutions (a partner in the EC FP7 Funmol project) for the many suggestions and advice regarding experimental work and to Dr. Nicolas Sassiat and Mr. Liam Floyd for performing simulations. Thanks to all colleagues at Tyndall and particularly within the Nanotechnology Group for much assistance at various stages of my Ph.D.

There was never a dull moment at Tyndall. I have many happy memories of fun times shared with the large postgraduate group at Tyndall, especially those of the Nanotechnology Group, providing so much cheer, chat and laughs creating an harmonious work environment. We have created great memories that I will cherish forever. Thanks also to the Tyndall Postgraduate Student Committee with whom I spent a term of two years, in particular to the talented Dr. Tuhin Subhra Maity for the many invites to various Indian cultural events. Thanks to my BFFs outside of Tyndall and housemates, especially Emilie, Andrea and babyDan. We had great times together.

I wish to thank those who formed the stepping-stones to my arrival at Ph.D. research, namely Dr. Siobhan Ni Ghriofa of The State Laboratory who advised me to pursue Ph.D. research, Dr. John Fox who carved my research path and Prof. Declan McCormack for inspiring my desire to research in the area of Nanotechnology. I am grateful to all.

I wish to thank my parents Pat and Helena for laying the foundation from which all of my educational achievements to date are based and my siblings Patrick, Michael and Ursula, nieces Doireann, Lilly and Aoibheann and nephew Rory for all of their love, support, wit and humour xxxx

To the Universe

There is always a way

Chapter 1

Introduction

1.1 Historical perspective

Gold, element 79 in the periodic table, has been prized for millennia. Gold is a noble metal among rhenium, ruthenium, rhodium, palladium, silver, osmium, iridium and platinum. The electron configuration of these elements imparts a certain chemical resistance to corrosion and oxidation. Since its extraction in the 5th millennium BC in Bulgaria[1] gold has been used in a diverse range of applications from gold bands in dentures, as used by the Etruscans, to electronic circuit components some centuries later. Colloidal gold appeared ~500 BC in Egypt and China[1] and was used throughout the middle ages for its perceived medicinal and curation powers. “Aurum potabile” or “potable gold” was used for treatment of dysentery, tumours and diagnosis of syphilis.[2] The intense colours of gold sols resulted also in their use in art and ceramics for more than 2000 years. An excellent illustration of this is the Lycurgus Cup found in the British museum, in London, crafted by Romans in the 4thC AD.[3] The cup changes colour depending on the lighting conditions. In reflected light it appears green - in transmission a bright red colour can be seen. The work of Barber deduced that the presence of a mix of gold and silver alloy particles of approximately 70 nm in size in the glass matrix of the vase was crucial to obtain the scarlet red colour.[4,5]

The contemporary view of colloidal gold nanoparticles can be attributed to Michael Faraday. In 1857 Faraday reported formation of deep red solutions upon reduction of chloroaurate ($AuCl_4$) aqueous solution with white phosphorous in a 2-phase CS_2- water mixture (phosphorous dissolved in carbon disulphide).[6] He reported that colloidal solutions he had synthesised exhibited colours ranging from ruby red to amethyst. He listed the factors impacting the colour of these solutions and deduced that “the mere variation in the size of particles gave rise to a variety of resultant colours.[7] Faraday observed the crucial size and shape dependence on the resulting solution colours and properties of nanostructures. Much research has been conducted since Faraday’s initial observations with regard to optimising synthesis routes to develop nanoparticles with tunable plasmonic properties. Major advances in understanding the role of the various reaction parameters have allowed tight control over size and shape monodispersity, which has been essential in understanding the correlation between nanoparticle morphology and optical response.

In 1908, Mie presented a solution to Maxwell's equations which facilitated the calculation of the extinction and scattering efficiencies of small metal particles.[8,9] Later Stratton introduced a more formal approach, which is commonly used today.[10] Mie's application of Maxwell's equations to explain the strong absorption of green light by a subwavelength gold sphere under plane-wave illumination established the foundation of an understanding of this phenomenon. In 1951 Turkevich[11,12] developed one of the most popular approaches for the synthesis of gold nanoparticles using citrate reduction of $HAuCl_4$ in H_2O. Great advancement has been made with regard to fabrication methods also, which provide us with good control over the composition and morphology of nanostructured metals. A wide variety of lithographic[13,14,15] and other physical methods have been devised and sophisticated characterisation techniques and modelling methods have also dramatically enhanced the field.

Faraday's experiments with colloidal gold were the beginning of today's nanotechnological revolution. Faraday went on to publish an excellent paper on small particle optics that constituted a Bakerian lecture in 1857.[7] A sol prepared by Faraday is still displayed in the Royal Institution of Great Britain.[2] Its violet colour is immediate visual proof of the reluctance of the gold colloidal particles to aggregate into a more massive gold sample despite the strong thermodynamic impulse to do so. Establishing an understanding of these phenomena has led to the evolution of gold from use in beautiful art as depicted in the Lycurgus Cup to the use of DNA to bind gold nanoparticles in 1996,[16] to the approval of Verigene[17] by the FDA in 2012[18], a gold nanoparticle diagnostic device to identify infectious bacteria. The sprinkling of gold once used to beautify art pieces now appears possible to vastly improve efficiency of solar cells to enabling more sensitive bio-detection.

1.2 Birth of nanotechnology

Since this technological milestone in 1857 an estimated 12.4 billion dollars[19] has been invested in research in the area, development of multiple research groups, publication of thousands of journal articles and has resulted in the birth of some of the huge research fields, namely nanotechnology, nanoelectronics, nanoplasmonics and bio-nanotechnology. The terms "nanomaterials" and "nanotechnology" have also been defined by the American Society for testing and materials and International

Organisation for Standardisation. Nanotechnology is described as technology based on materials with an upper size limit of ~100 nm in at least one of the dimensions[2] - nanoparticles being a number of atoms or molecules bonded together (these particles usually containing 10^6 atoms or fewer). Nanostructures are intermediate in size between individual atoms and aggregates large enough to be termed bulk material.

The properties of colloidal metals are strikingly different to those of their bulk counterparts due to the high surface to volume ratio,[20] quantum size effects[21] (in sub 1 nm NPs) and electrodynamic interactions.[22] Such unique metal nanoparticle optical, electrical, magnetic and mechanical properties make them a very attractive choice for, in particular, chemical and biological sensors[23] and also other novel applications. Bulk gold's familiar yellow colour is caused by a reduction in reflectance of light at the end of the spectrum.[24] When gold is subdivided into tiny particles, the ratio of the diameter to the wavelength becomes important and when particles of gold are small enough, the colour of gold is ruby red due to their strong absorbance of green light at ~520 nm corresponding to the frequency at which a plasmon resonance occurs with the gold.[2] Characteristically noble metals exhibit a strong absorbance band in the visible region of the spectrum[25,26] which is indeed a small particle effect and is as a result of this surface plasmon resonance (SPR). All conduction metals support plasmons but the plasmon resonances of coinage metals (Cu, Ag, Au) lie closer to the visible region of the spectrum allowing plasmon excitation by standard optical sources and methods.[27]

Plasmons are the collective oscillation of the electron gas in a metal.[14] Optical waves can couple to these electron oscillations in the form of propagating surface waves or localised excitations, depending on the geometry. Small noble metal particles with dimensions from a few up to several 100 nanometers support localised surface plasmon oscillations that create large electromagnetic fields at the nanoparticle surface. The electric field of an incoming light wave induces a polarisation of the (free) conduction electrons with respect to the much heavier ionic core of a spherical nanoparticle.[28] The positive charges in the particle are assumed to be immobile and the negative charges, that is, the conduction electrons,[29] move under the influence of external fields. Therefore, a displacement of the negative charges from the positive ones occurs when

the metallic nanoparticle is placed in an electric field, i.e. there results a net charge difference at the nanoparticle boundaries.

As a consequence, a dipolar oscillation of the electrons is created (with a particular time period), and this is known as the surface plasmon oscillation. The collective oscillation of the electrons is also sometimes denoted as the "dipole particle plasmon resonance" to differ from plasmon excitations that occur in bulk metal surfaces.[27] The surface plasmon resonance is the coherent excitation of all the "free" electrons within the conduction band, leading to an in-plane oscillation.[14] The term "surface" stems from the fact that although all electrons are oscillating with respect to positive-ion background, the main effect producing the restoring force is the surface polarization.[2] Plasmons also exist in the bulk and at the surface of large chunks of material. However, because of a mismatch between the plasmon dispersion relation and that of the photon, the plasmons cannot be excited by ordinary plane-polarised light. Oscillating frequency is critically determined by 4 factors: the density of the electrons, the effective electron mass, the shape and the size of the charge distribution.[30] Therefore, the dielectric constant of the surrounding medium, the electronic interactions between the stabilising ligands and the nanoparticle and the size, shape and monodispersity of the nanoparticles all have a strong impact on the position, size and shape of the surface plasmon band.[31]

With control over the composition and morphology of nanostructured metals, the next goal was to bridge the basic (wet chemical) fabrication of these nanoplasmonic building blocks and bring all of the advancements to the stage where these developments can bridge the gap between nanomaterials and successful technological applications. Among the possible applications of the above mentioned surface plasmon band property of colloidal gold, detection is the one that has been most successful thus far. The ability of surface plasmon band to be altered in an easy, controlled and reproducible way by a change in the environment or nanoparticle properties, in particular localised surface plasmon bands in metal nanoparticles displaying extreme sensitivity to environmental changes,[32] therefore being excellent transducers for sensing devices, naturally led researchers to use them as sensors to detect organic, inorganic and biological targets.[33,34,35] The extremely high extinction co-efficients[36] and the strong distance dependent optical properties of gold nanoparticles enable the nanoparticles to be ideal

colour reporting groups - extinction co-efficients are 3-5 orders of magnitude greater than that of organic compounds. This has been applied in biosensing because the local refractive index may change significantly when a target analyte binds to a biomolecule receptor that has been previously bound to the nanoparticles. The property of nanoparticles to feature a changing SPB in solution depending on the mean distance between them has therefore been extensively exploited in the field of biodetection and sensing having been used for biosensing since 1956.[37]

1.3 Bridging between nanomaterials and technological applications

The assembly and integration of nanoscale objects is of pivotal significance for the design and fabrication of nanodevices. Chemists have already made important progress in relation to precisely controlling size and shape of nanoscale objects as well as their surface chemistries[34]. There are hundreds if not thousands of procedures available that allow for crafting the sizes, shapes, material properties or surface chemistries of nanoscopic particles[19] using a multitude of syntheses. Various methods have been employed in the assembly of gold nanoparticles, using DNA,[38] polymer[39,40] and organic ligands.[41] Nanoscale objects can be easily assembled into aggregated nanostructures through self-assembly. Self-assembly refers to the process by which nanoparticles or other discrete components spontaneously organise due to direct specific interactions and/or indirectly through their environment.[42] Self-assembly is typically associated with thermodynamic equilibrium, the organised structures being characterised by a minimum in the systems Gibbs energy. Self-assembly is generally simple and low cost,[43,44] being governed by the balance of attractive forces (covalent or hydrogen bonded, electrostatic attraction between oppositely charged ligands, depletion forces or dipole-dipole interactions) and repulsive forces (steric forces and electrostatic repulsion between ligands of like charge).[42]

Solution-phase nanoparticle-based sensing through self-assembly is a simple yet powerful detection modularity. Because many molecules of interest, particularly biological molecules, are in the aqueous phase, it is desirable to have a sensitive and specific detection system that is homogeneous with the phase of the target molecule therefore decreasing the need for extended sample preparation. Aggregation-based detection has become a mainstay in the clinical community since the development of the

latex agglutination test (LAT) in 1956.[37] The assembly of gold nanoparticles and the accompanying colour change have been the subject of intense research particularly in the past decade with numerous molecular or bio-molecular optical sensing platforms being developed based on the nanoparticle assembly principle.[45,46,47,48] The colour changes observed upon assembly of the plasmonic nanoparticles originate from the coupling between the localised surface plasmons of the nanoparticles that result in lower energy excitation and red-shifted absorbance bands.

Organisation of nanoparticles into self-assembled structures paves the way for reducing the size of optoelectronic devices and components such as plasmon waveguides, focusing lenses, light generation and optical switches, chemical and biological sensors, adaptive materials, photonics, electronics and photovoltaics.[49] At present, many nanoparticle based opto-electronic components are made with top-down nanofabrication techniques, rather than bottom up self-assembled approaches. One key limitation of these fabrication methods is that it is difficult to obtain small separations (<10 nm) and curvatures.[13] E-beam lithography, although having nanometre resolution, is limited to thin films, has low throughput and is prohibitively expensive,[50] whereas plasmonic characteristics of gold nanoparticles can be tuned spectrally down to the sub 50 nm resolution beyond the possibilities of lithographically structured films.[15]

However, a major challenge for nanoparticle assembly is the lack of metrology to characterise the kinetics and structures *in situ* during the assembly process. In the last 20 years a large number of experimental and theoretical studies have been carried out aimed at understanding the physical properties of the aggregation phenomena and key factors in driving nanoparticle assembly formation. It is of importance to characterise the process of self-assembly in a much more rigorous manner than at present, by moving the “proof of concept” experiments to the quantitative assessment of the self-assembled structures. There are a number of questions regarding the molecular mechanism. Lack of such fundamental information mainly explains the current limitations facing linker-mediated self-assembly of inorganic nanoparticles.

1.4 Solution-phase detection of biomolecules

Nanoparticles are stabilised as a result of capping ligands on the surface. If prepared with $HAuCl_4$ as gold source and stabilised using trisodium-citrate, it leads to the coverage of citrate anions on the surface. The dissolved ions in the solvent readily cover the surface of the nanoparticles forming a film called the double layer enabling them to remain as a sol and not precipitate out of solution, due to the presence of this charged double layer surrounding each colloidal nanoparticle that produces a Coulomb barrier to aggregation. Helmholtz, Gouy and Chapman and then Stern studied the structure of the double layer. Depending on the surface potential of the nanoparticles and the cation affinity for the surface material, the ions may bond or adsorb on the nanoparticle surface creating an inner and outer Helmholtz plane. The Stern layer is delimited by a virtual plane (Stern plane) touching the ions aggregated on the surface. Ions in the Stern layer interact with counter ions of the solvent (by the means of the electrostatic force) by attracting them to accommodate the local surface charge thus creating a second layer. However in this case, the distribution of counter ions through space is diffuse and increases gradually to reach the bulk concentration. Conversely, ions presenting the same charge as the ones in the Stern layer also loosely occupy the second layer so that their local concentration decays to reach the bulk value.

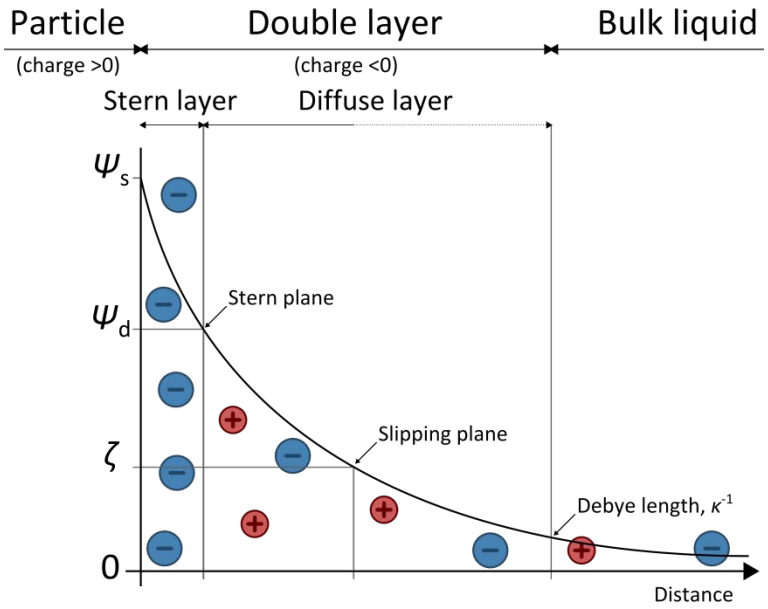

Figure 1.1: Schematic detailing the structure of the double-layer at an electrode surface, surface potential, ψ_s; potential at the Stern layer, ψ_d; potential at the slipping plane, ζ. [51]

The resulting repulsive double layer interaction between the particles makes the sol very stable against aggregation. However, it is desirable to cause aggregation of these nanoparticles for the formation of assemblies with desirable novel properties. There are various different types of attractive and repulsive forces and whether or not the particles aggregate depends on the equilibrium between these attractive (covalent or hydrogen bonding, electrostatic attraction between oppositely charged ligands, depleting forces or dipole-diploe interactions) and repulsive forces (static forces and electrostatic repulsion between ligands of like charge).

Aggregation processes for colloidal particles result from the coupling between two main interactions: particle fluid interactions which play a role in the motion of particles within a flow and govern the number of particle-particle encounters, as well as their time and spatial locations and secondly the collision step[52] described by Derjaguin-Laudau-Verwey-Overbeck (DLVO) theory. This theory is based on the principle that pairwise interaction forces, which arise from the interplay of attractive van der Waals forces and repulsive Coulomb forces, screened by Debye-Huckel ion clouds, dominate. Van der Waals forces originate from the electromagnetic fluctuations due to the incessant movements of positive and negative charges within all types of atoms, molecules and bulk materials. They are therefore present between any two material bodies, usually acting in an attractive fashion to bring the bodies together.[19] This theory demonstrates that two surfaces (typically nanoparticle surfaces) can come into strong adhesive contact when the potential or charge they carry is lowered by a more effective ion binding (in the Stern layer) or by improving the double-layer screening by the means of an increase of the electrolyte salt concentration. However, if the surface potential or charge is not substantially decreased, the two surfaces may still adhere in a less stable and reversible configuration. The Derjaguin-Laudau-Verwey-Overbeck theory has been widely employed in colloid science to study particle-particle interactions, colloidal stability, coagulation, sedimentation, filtration, and the behaviour of electrolyte solutions.[2]

Adsorption of ions and molecules on the surfaces of solid particles is a critical step in nanoparticle assembly. The thermodynamic driving force for adsorption at a surface is typically described using the concept of Gibbs energy. The overall Gibbs energy change for adsorption from solution onto a surface is a function of the chemical composition

and structure of the solid, as well as the nature of the solution. For a fixed set of solution parameters, however, the influence of particle size on the adsorption can be described thermodynamically by an adsorption coefficient, which can be determined experimentally by measuring the extent of surface adsorption as a function of solution concentration. The relationship among this adsorption coefficient, Gibbs energy, and crystal size can be defined using a classical thermodynamic approach. To describe the influence of particle size on adsorption at particle surfaces, a simple Langmuir-type adsorption isotherm can be employed. In the Langmuir isotherm, the probability of a molecule adsorbing at any surface location is independent of the total surface coverage and dependent only on whether the specific adsorption site is already occupied. Since at equilibrium the surface coverage by adsorbate is dependent on the concentration of adsorbate molecules in solution through the isotherm, the charge on the nanoparticle's surface will be a function of the concentration of adsorbate in solution.

Aggregation occurs through two mechanisms. Aggregates can be formed primarily through the addition of single nanoparticles to a growing cluster, that is, cluster-particle aggregation, and second, clusters of all sizes can assimilate into larger clusters, that is, cluster-cluster aggregation. An aggregating colloid can switch from one mechanism to the other depending on the number of depleted nanoparticles in the solution. However, all nanoparticle aggregation processes begin with the formation of a nanoparticle dimer from two isolated nanoparticles. Particles may adhere together if their activation energy is larger than the energy barrier encountered.

Monte Carlo simulations, Brownian dynamic simulations and the kinetic approach based on the population balance equations have been applied to describe these aggregation processes and have been the subject of numerous experimental, theoretical and computational studies.[53,54,55,56] However, the mechanisms by which single nanoparticles assemble to form extended and branched chains is still not well understood and then poorly controlled which is a major limitation for their effective application. A better understanding of the mechanism and dynamics of the growth reaction during self-assembly relies on the precise control of the assembly over time and the ability to image the assembly at different stages of the process.

UV-visible spectroscopy provides characterisation of the transverse and longitudinal plasmon absorption bands of metallic nanoparticle aggregates.[35] Highly dispersed gold nanoparticles (Au NPs) (effectively considered as single particles) in solution should exhibit only a single peak, while linked Au NP pairs or larger aggregates show two absorbance maxima.[48] The first peak located near the resonance peak for single particles is attributed to the transverse plasmon excitation in coupled spheres, while the second peak at a higher wavelength is attributed to the longitudinal plasmon resonance of the Au NP aggregates. When gold NPs assemble, the resonance at wavelengths close to 530 nm generally decreases in intensity and undergoes a slight red shift. In addition, the peak at higher wavelengths appears as a red-shifted shoulder. This is due to the decrease in the number of single NPs and the formation of dimers and oligomers. The frequency and intensity of the aggregated system depends on the degree of aggregation as well as orientation of the individual particles within the aggregate. Also an increase in the full width at half max (FWHM) of the new peaks is evident. This is mainly explained by the increase in the number density of the chains leading to a branched network. Importantly, the increase in the assembly degree is also signified by an increase in the solution transparency.[57]

1.5 Employing biofunctionalised nanomaterials in biosensing

Although localised surface plasmon resonance spectroscopy is a totally non-selective sensor platform, a high degree of analyte selectivity can be conferred using the specificity of surface attached ligands and passivation of the sensor surface to non-specific binding. The nanoparticles in solution are rarely ‘‘naked’’. Their surface is usually covered with stabilising molecules, which, due to their affinity for the gold surface prevent the agglomeration and the further growth of the nanoparticles. Self-assembled monolayers (SAMs) are easily grafted to a nanoparticle surface. The properties of the gold nanoparticles are then in large part determined by the monolayer which can bind specifically with particular biological materials including proteins, peptides, nucleic acids, DNA, RNA, genes, oligomers, aptamers, ribosomes, lipids, fatty acids or carbohydrates.[58] The biologicals may be functionally active, offering binding, catalytic or therapeutic activity (eg. antibody or enzymes) or alternatively may be passively utilised as an inert coating or scaffolding material.

Gold nanoparticles unique optical and electrical properties offer applicability to a wide range of applications. Gold is one of the few metals noble enough to survive as a nanoparticle under atmospheric conditions. It is chemically inert, robust, has low toxicity, possible shape modulation, facile preparation and modification and excellent binding specificity of gold nanoparticles that offer a suitable platform for functionalisation with a wide variety of organic or biological ligands for the selective binding and detection of small molecules and biological targets.[59,60,12] The integration of biomolecules with gold nanoparticles can generate materials that combine the properties of the nanoparticles with the molecular recognition components of biomolecules.

Functionalisation is possible using ligands terminated in functionalities imparting desired surface properties. It is desired to have control of volume or ratio of biomolecules per nanoparticle and also having their binding sites in access to the environment while at the same time avoiding over-conjugation as non-specific chemical or electromagnetic interaction can result in heterogeneous attachment and impair activity in the final conjugate. It is necessary to maintain the optical function and activity of both participants and control over inter-particle distance. Capping molecules are employed to achieve this as they act not only to maintain a good dispersion of particles but also to selectively respond toward external stimuli. Therefore the distribution of capping molecules is highly relevant.

1.6 Protein-functionalised nanomaterials

Proteins have a vast array of potential sizes and surface chemistries that can be used to control the structure and functionality of nanoparticle-based materials providing versatile building blocks for nanoparticle assembly. Molecular interaction can be tailored and used to create ordered assemblies designing particles with stimuli responsive inter-particle interactions and morphological or functional features that result in directional interactions. Antibodies are serum proteins. They belong to the family of glycoproteins known as immunoglobulins. They are produced by white blood cells, the B lymphocytes on differentiation into plasma cells, in response to a foreign (non-self) substance. The foreign substance is termed an immunogen so defined because it evokes an immune response. Secreted antibodies circulate in the blood and serve as the effectors of humoral immunity by searching out and neutralising or eliminating foreign

substances such as viruses or bacterial toxins. In most instances an individual antibody is highly specific and will recognise one substance only[61], this substance is termed the antigen. In assays and sensors based on antibodies, the analyte is either the corresponding antigen for the antibody used or a part of it.

Antibodies are heterogeneous with respect to physiochemical properties and function but have similar basic structures. They consist of two kinds of polypeptide chains: heavy chains (50-70 kDa) and light chains (~25 kDa). Identical light-chain-heavy chain pairs are linked by disulphide bridges and non-covalent interactions. This results in a Y-shaped structure. The light and heavy chains are made up of a number of segments or domains, each of approximately 110 amino acids. The light chains contain two domains, whereas the heavy chains have 3-5. It is the amino-terminated domains of both the light and heavy chains that are responsible for recognition and binding of antigen.[62]

Antibody preparations may be polyclonal, affinity-purified monospecies or monoclonal.[63] A polyclonal antiserum will contain many different antibody molecules with varying affinities and specificities. Monoclonal antibodies in contrast are produced *in vitro* by a single clone of antibody-producing cells and therefore all molecules from the clone have the same specificity and affinity. The choice of which antibody preparation to use depends on the antigen, the application of the assay and the time and money available. For monoclonal antibodies the purity of the antigen is not as important due to the cloning and selection procedures used during their production. Monoclonal antibodies offer the advantage that once a suitable and stable clone has been found, virtually unlimited quantities of a particular antibody can be produced. However, the production of a monoclonal antibody with the correct characteristics for any given assay is expensive and time consuming. Polyclonal antibody production however, is much cheaper and quicker. In general the use of monoclonal antibodies increases the reaction specificity but potentially at the expense of the reaction sensitivity.

The functional properties of the protein depend on the physiochemical characteristics of the system in which they are contained.[62] The elemental properties of the protein are the amino acid composition, structure, conformational stability, charge, shape, size, the extent of polarity and hydrophobicity and the nature of protein-protein interactions. The

most important characteristics of the medium influencing the functioning properties of proteins are the solvent nature, pH, ionic strength, temperature, redox state and the presence of interfaces.[64] An antibody will combine specifically with the corresponding antigen. Even a small change, for example, the substitution of one amino acid for another, moving a chemical group from one carbon to another, or using the mirror image of a chemical group may change the antibody-antigen fit from very good to weak or non-interacting. This qualifies them as very good biomaterials for use in sensing devices. The intermolecular forces which contribute to the stabilisation of the antibody-antigen complex are the same as those involved in the stabilisation of the configuration of proteins or other macromolecules. These include hydrogen bonds, ionic bonds, hydrophobic interactions and van der Waals forces. Since the strength of each of these interactions is weak compared to that of a covalent bond, a large number of such interactions are required to form a strong antibody-antigen bond. As each of these non-covalent interactions operates over a small distance, generally less than 1 angstrom, a strong antibody-antigen interaction therefore depends on a very close fit between the antibody and the antigen. Antigens contain numerous epitopes, which are the part of an antigen molecule to which an antibody attaches itself, but binding to a unique epitope is a highly specific interaction, providing the capacity for antibody-antigen recognition in solutions containing many different biomolecules. Once bound they are unlikely to desorb as attachment to the surface at one point on the protein increases the probability of binding a neighbouring site on the protein. However desorption requires the concurrent breaking of a large number of bonds, which is energetically unfavourable.

1.7 C-reactive protein

In 1930 Tillet and Francis observed a substance in the serum of individuals with pneumococcus infections that formed a precipitate when mixed with the polysaccharide coat of streptococcus pneumonia.[65] They noticed that this activity was absent from the sera of healthy individuals. MacLeod and Avery subsequently characterised this substance as a protein and introduced the term “acute phase” to describe the serum of patients with various acute infections.[66] C-reactive protein (CRP) is a non-specific protein secreted by the human body during the acute phase of the inflammation process and has historically been used to detect and predict the outcome of various infections, inflammatory and necrotic processes and to assess the efficacy of treatment for those processes.[67,68]

This protein has been highly conserved during evolution. It belongs to a family of pentameric proteins known as pentraxins. It has the same functional and structural homology as a protein that is detected in high concentrations in the hemolymph of the horseshoe crab (Limulus polyphemus), a "living fossil.[69] CRP comprises five identical, non-covalently bound subunits arranged in cyclic symmetry and each subunit consists of 206 amino acid residues.[70] The outer diameter is ~ 11.13 nm, the inner diameter ~ 3.52 nm and the height ~ 3.03 nm. CRP exists in at least two distinct forms in conformation, i.e. pentamer (or native) CRP (pCRP) and modified CRP (mCRP). The molecular weight of pCRP is 115 kDa. The mCRP is the subunit of pCRP and its molecular weight is 23 kDa.[70] The structure of CRP contains an area where the calcium-binding loop from one protomer coordinates into the calcium site of a second protomer to form the pentameric structure. This configuration allows for the binding of the ligand phosphocholine and provides information concerning conformational changes related to calcium binding.

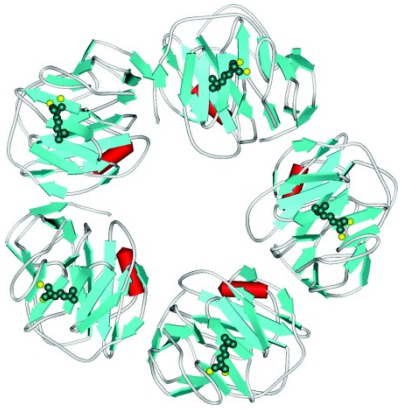

Figure 1.2: Computer-generated image of the structure of C-Reactive Protein. [71]

CRP is one of the most consistently increased and fastest reacting acute-phase proteins (biological half-life of 19 hours), suggesting that it is part of the innate immune response. Concentrations may increase 1000-fold or more within 24–48 hours of tissue injury. Serum concentrations rise above 5 μg/mL after about 6 hours and peak at around 48 hours. The plasma half-life of CRP is constant under all conditions of health and disease so that the sole determinant of circulating CRP concentrations is the synthesis rate which thus directly reflects the intensity of the pathological processes stimulating

CRP production. When the stimulus for increased production completely ceases, the circulating CRP concentration falls off rapidly at almost the rate of plasma CRP clearance.

C-reactive protein (CRP) is a widely recognised indicator of inflammation.[72] Recent prospective studies have demonstrated that increased CRP concentrations within the reference interval are an indication of myocardial infarction, stroke, sudden cardiac death and peripheral vascular disease in apparently healthy adults.[63,73] On the basis of available evidence, the American Heart Association and the Centre for Disease Control (CDC) have issued guidelines for the utility of CRP in the primary prevention of coronary syndromes.[68] The guidelines include specific recommendations that pertain to the laboratory aspect of CRP and defined cut-points for clinical interpretation: CRP concentrations <1 μg/mL (9 nM) are considered low, 1-3 μg/mL (9-27 nM) average and >3 μg/mL (>27 nM) high relative risk.[68] Mild inflammation and viral infections generally cause CRP concentrations to increase to ~10-50 μg/mL (0.09-0.45 μM), whereas active inflammation and bacterial infections generally cause concentrations to increase to between 50-200 μg/mL (0.45-1.8 μM). Concentrations >200 μg/mL (>1.8 μM) are seen in more severe infections and in trauma. [68]

CRP is now widely accepted as a biomarker for detection of possible onset of cardiovascular heart disease (CVD) as a result of increased levels of this protein [20, 21, 23] with patients with a CVD disorder and/or myocardial infarction at the time of admission to hospital being noted to have CRP levels >3 μg/mL [23] the requirement now is therefore for point-of-care (POC) testing of CRP for risk stratification of coronary disease. It is important that a patient suspected of CVD must be diagnosed as quickly, effectively and comprehensively as possible, so it is crucial that the assay can be carried out quickly and hence at the POC, which would also enable on-going monitoring of a potential condition.

CRP is therefore not only useful as a biomarker for evaluating inflammatory reactions, but also cardiovascular disease (CVD). Compared with other novel and traditional markers of coronary heart disease (CHD), CRP was shown to be the strongest predictor of future coronary events. High-sensitivity methods are therefore required for the measurement of CRP for the purpose of assessing risk of cardiovascular disease in apparently healthy individuals. C-reactive protein (CRP) assay applications fall into

two main categories: low-medium sensitivity tests (> 6 μg/ml, 55 nM) *e.g.*, latex agglutination tests, used for detection of an acute inflammatory response; and high sensitivity tests (< 1 μg/ml, 9 nM), *e.g.*, ELISA (Enzyme-linked immunosorbent assay) or lateral flow tests. In routine clinical analysis, CRP levels are determined by ELISA tests. These assays are well established and detection limits down to 0.8 nM (0.1 μg/mL) are available (Dade Behring Inc, now Siemens Medical, IL, USA).[74]

1.8 Detection of C-reactive protein

Expected merits relating to the performance of sensors include specificity, stability, sensitivity, range of detection, low cost and speed. With laboratory-based methods, many such factors are attained as standard and are therefore very reliable, consistent methods of detection. However, the emphasis is now shifting towards transferring sensing methods to point-of-care (POC) settings. Therefore speed, cost and portability should now be the prevailing issues while at the same time maintaining merits expected of biosensors such as specificity, stability and sensitivity.

The latex agglutination test (LAT) is one of the earliest assay methods for sensing CRP.[37] The method is still used today but is only semi-quantitative and insentitive, resulting in poor correlation with the clinical status of the patient.[70] In the LAT and similar tests, biomolecularly specific antibodies are conjugated to latex microspheres which, when mixed with a solution (blood, urine) containing target antigen, cause the latex spheres to form visible aggregates (15 min to 1 hour).[75]

Enzyme-linked immunosorbent assay (ELISA) is the gold standard in protein-based diagnostics. ELISA provides a quantitative, specific and sensitive approach, with excellent detection capabilities of 0.8 nM (0.1 μg/mL) and can be applied with the use of monoclonal antibodies specific to pCRP or mCRP for immunosensing. In conventional ELISA the signal generation mechanism consists of the chemical transformation of the enzyme substrate into a coloured or chemiluminescent product which is usually detected with a plate reader. This signal generation mechanism allows for the quantification of the target molecule because the colorimetric or chemiluminescent signal is proportional to the number of enzymes attached to the immunocomplex by means of the immunoreaction.[43] However, ELISA is a heterogeneous assay requiring a number of manipulations (coating of plates with antibody, incubation with a sample, extensive washings, adding reagents for enzyme

amplification reaction and reading the signal) taking several hours to perform and requires trained personnel, expensive reagents and high sample and reagent consumption, as well as the disadvantage of a relatively high false positive rate due to non-specific bindings.[70] This method is therefore not suitable for point-of-care health assessment.

Lateral flow immunoassays are also commonly employed and use imaging processing algorithms specifically designed for a particular test and medium, whereby line intensities can be correlated with analyte concentrations. Sensing techniques that compete with ELISA and lateral flow assay but that offer faster and inexpensive diagnosis through POC systems are highly desirable. Therefore a plethora of novel detection techniques and applications for the detection of analytes of interest have been proposed. While many of these techniques eloquently demonstrate effective application of such techniques in laboratory settings, many factors pertinent to transfer of laboratory-based assays to point-of-care analysis are mostly not addressed.

An "inverse sensitivity" approach has been applied to ELISA for detection of analytes at low concentrations, whereby the signal generated is larger at lower target molecule concentrations than at higher concentrations.[76] This removes the ambiguity associated with differentiating slight variations of the same colour, enabling visual detection. However, the use of hydrogen peroxide solutions required in the reduction of gold ions, are unstable. [76] Non-specificity was evident linked to the number of incubation and washing steps. Lengthy assay times of hours are involved.[77] Inverse sensitivity has also been applied to plasmonic nanosensors whereby the enzyme glucose oxidase is employed, but also involves lengthy assay times. [78]

Nanoparticle self-assembly offers an attractive alternative to traditional and lateral flow assay technologies and also many recently developed techniques. DNA has been successfully employed to organize nanoparticles into assemblies, representing much advancement in the field.[79, 80] However, the interactions are sensitive to temperature changes which results in the requirement for active temperature control.[81] Self-assembly involving small DNA origami has been demonstrated but again temperature limitations are evidenced.[82] Artificial proteins have also been designed [83, 84] and applied in the self-assembly of metallic colloids.[85] By adjusting the ratio of protein to particles, the self-assembly could be tuned between formation of large films and smaller

nanoparticle nanostructures. Assay times of hours are involved. Analyte binding has previously been employed to prevent nanoparticle self-assembly. [86] In the presence of analyte molecules, which bind to the synthetic receptor, nanoparticle assembly is prevented. However, the approach is limited to one analyte molecule concentration and does not address a scenario whereby alternative concentrations may not result in the required coverage of receptors with analyte molecules to prevent aggregation.[86] Surface enhanced raman spectroscopy (SERS) has also been employed in protein detection [87] including single-spot multiplex protein detection. [88] Silver nanoparticle aggregates have also been employed in SERS detection of CRP [89, 90]

1.9 Surface-based detection of biomolecules

A biosensor is derived from the coupling of a ligand-receptor binding reaction to a signal transducer. [91] Much biosensor research has been devoted to the evaluation of the relative merits of various signal transduction methods including optical,[92] radioactive,[93] electrochemical,[94] piezoelectric,[95] magnetic,[96] micromechanical [97] and mass spectrometric.[98] Research in the field of biosensors was initiated by Clark, who designed a biosensor to detect the presence of oxygen.[91] This was inspired by the critical need to monitor oxygen levels of patients undergoing surgery. Another huge area in biosensor technology is glucose detection. A modification of Clark's biosensing system led to the first blood glucose sensing device, an area of diagnostics now dominated by sensors, starting with the first commercial approaches for glucose detection produced by Yellow Spring Instruments (YSI INC 1975).[91] These earliest biosensors were catalytic systems that integrated particular enzymes with transducers that converted the biological response into an electrical signal. The next generation of biosensors, affinity biosensors, took advantage of different biological elements, such as antibodies, receptors (natural or synthetic) and nucleic acids. In all of these interactions, the binding between the target analyte and the immobilised biomolecule or the transduction element is governed by an affinity interaction such as the antibody-antigen, DNA – DNA or the protein-nucleic acid binding. The specificity of the biosensor is given by the immobilised molecule.[91] The development of blood glucose control and monitoring technology has achieved significant progress over the last decade. This offers patients a means of real-time measurement of blood glucose level, thus improving their quality of life. Several commercial test kits have been employed in routine

diagnostic tools, including those utilising chemical strips and those used to test blood and urine levels by sampling specimens directly into the strip followed by visual reading of the colour charts. In 2006, the first real-time continuous glucose monitoring system, DexCom7 was approved by the FDA and in 2007 its lifetime was extended from 3 days to 7 days. The latest Continuous Glucose Monitoring System facilitates 5 days of continuous glucose monitoring and was approved by the FDA in 2008. [99, 100] The Clearblue Pregnancy Test is an example of a current sensing technology with a digital reader. It is over 99% accurate, reading "Pregnant" or "Not Pregnant" and also indicates how many weeks since conception occurred, 1 – 2, 2 – 3 or more than 3 weeks (3+) being as accurate as an ultrasound scan at dating pregnancy. [101]

Generally surfaces are chemically modified to better control the organisation and the orientation of immobilised species and therefore their biological function. Silicon surfaces attach alkylsilanes through the formation of Si – O - Si bonds between the silanol groups present on the oxidised silicon surfaces and the hydrolysed organosilane molecules. The presence of NH_2 end groups on the surface has a major importance in biological application as it allows proteins or other molecules with carboxyl groups (functional groups that are commonly found in biomolecules) to be attached in a simple way. Trifunctional alkoxysilanes R-Si$(OR)_3$ are the most common precursors to introduce organic groups because of the variety of such silanes commercially available – (3-Aminopropyl)triethoxysilane (APTES) being one of the most popular. APTES is widely used in affinity based biosensors because the silane group can tightly bind to silicon or glass substrates, while its amine group can form covalent bonds.[102]

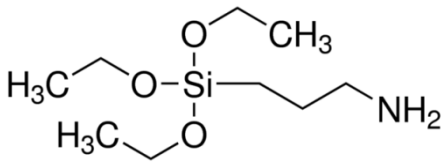

Figure 1.3: Structure of (3-Aminopropyl)triethoxysilane (APTES).

Various interfacial processes may be possible (covalent binding to the surface, lateral polymerisation of adsorbed silanes, 3D polymerisation).[103,104,105,106] Silane grafting is expected to occur in two steps in the presence of water molecules, firstly the ethoxy groups are hydrolysed either in the liquid phase or at the interface, depending on the experimental procedure. Secondly the Si-O-Si bonds are formed with surface silanol groups. However these processes are difficult to evidence and strongly depend on the hydration state. The silane layer may be unstable in the aqueous media used for biological applications - partial hydrolysis of the siloxane bonds may cause desorption.[107] Hydrogen bonding interactions with surface silanols alone result in weakly attached silane molecules on silica surfaces. APTES is an aminosilane and has three ethoxy groups per molecule and is capable of polymerising in the presence of water which can give rise to a number of possible surface structures. It is necessary to have water at the interface to form APTES multilayers in organic solvents and the number of protonated amine and hydrolysed ethoxy groups in the silane layers depends on the amount of surface water present. In general, anhydrous solvents with a trace amount of water and low silane concentration are desirable for the preparation of smooth APTES-derived silane layers. Solvent rinsing procedures and drying methods are also critical to the quality of monosilane layers.

Drying procedures have therefore been used to ensure that covalent bond formation proceeds through condensation of hydrogen bonded silanol groups and have been carried out under a nitrogen stream under vacuum or in an oven. During heat curing, silanes condense very rapidly to siloxanes. Curing increases the number of siloxane bonds in the APTES films up to a max of three and can be carried out at ambient or related temperatures. Mild curing results in binding of the first half of the monolayers to the silicon and the remaining absorbed or partially polymerised APTES is therefore removed quickly. Curing is optimised in the presence of surface water and at curing temperatures greater than 150ºC. Consensus has been that chemical bonding between silane molecules and silica surfaces is necessary to ensure hydrolytic stability of attached silane layers as hydrolysis of the Si-O-Si linkages can occur under certain conditions.[108] These procedures are necessary as hydrolytic stability of the attached aminosilane layers is vital for applications in aqueous media.

1.10 Electrical characterisation of antibody-antigen binding

Materials on the nanoscale not only display strikingly different optical, chemical and magnetic properties but unique electrical properties also, compared to those of their macroscopic counterparts. Methods for immobilising probe protein on solid supports range from covalent binding and affinity ligand capture, to simple physical absorption. If a protein is immobilised on the surface of an electrode pair, it introduces a capacitance component in the impedance response of the sensor. This originates from the low dielectric permittivity of the immobilised macromolecule. Further, when the pair of modified electrodes is exposed to another protein that couples to the immobilised protein, a complex is formed. The dielectric layer covering the electrode will thicken resulting in a corresponding decrease of the sensor capacitance. The capacitance is determined by the thickness and dielectric properties of the insulating layer and the solid/solution interface both of which constitute the dielectric. Electrochemical impedance and capacitance biosensors have been employed to study antibody-antigen binding and protein binding at surfaces and demonstrate much potential as a point-of-care sensing means. Capacitative immunosensors are made of successive layers deposited on a solid support. Each immobilised layer must have suitable electrical properties and the recognition element must retain its activity. Small capacitance changes might be expected for antibody-antigen recognition without amplification. The sensitivity is given by the ratio of change of the total capacitance C_t to the change in capacitance C_a due to the antigen binding. The sensitivity tends to 1 when C_i is large compared to C_a. This means that a change due to the binding of antigen will produce a maximum change in the sensor output when the initial capacitance, formed by the insulating layer and the antibody layers, is very large. [109] The capacitance of the antibodies depends on properties that cannot be used as design parameters. The only parameter left to be optimised, from a design point of view, is the thickness of the insulating layer. In order to have a maximum capacitance this layer should have a minimum thickness and be non-porous and non-soluble.

1.11 Nanoparticle amplification

Due to the low intrinsic signal of biomolecules the binding of antigen to antibody results in small and extremely localised conformational and charge related changes in the antibody structure which have proven difficult to measure with sufficient sensitivity and selectivity. A tracer is therefore often used to generate a signal for example, optical, electrochemical, or radioisotopic decay, which enables quantitation of the amount of bound antigen. There are many types of label used to monitor the antibody-antigen binding reaction including particles, metal and dye sols, radionuclides, enzymes, substrates and co-factors and electrochemically active compounds. The number of target molecules can then be converted to a specific measure. Traditionally radioisotopes and fluorophores have been used but challenges relating to poor stability, low sensitivity and difficult sample processing exist. The need for simple and reliable detection methods has led to the development of various inorganic nanoparticle-based probes, incorporating the remarkable magnetic, optical or plasmonic properties as previously described. This has resulted in much diversity in the scope of bioassays.[110, 111] Dielectrophoresis can be utilised as a means to position nanoparticle labels between electrodes for electrical characterisation. Dielectrophoresis is the translational motion of neutral matter caused by polarisation effects in a non-uniform electric field. [112] Uniform electric fields will exert force upon a charged particle and a neutral particle will be polarised but will not move relative to the electrodes. However, non-uniform electric fields also exert force on neutral particles. A neutral particle in a non-uniform field will still be polarised with both charges being equal, however, the field acting on these charges is not equal and therefore a net translational motion will result, with the particle either moving to or away from the region of highest field. The dielectrophoretic force experienced by a particle is dependant on the particle radius, the dielectric constant of the suspending medium, the root-mean-square of the electric field amplitude, the angular frequency and the real part of the Clausius-Mossotti factor which considers the complex permittivities of the particle and the medium. Negative dielectrophoresis, i.e. a particle is repelled from the region of highest field, occurs when the real part of the Clausius-Mossotti factor is negative. Conversely, if the real part of the Clausius-Mossotti factor is positive then positive dielectrophoresis occurs, i.e. the particle is attracted to the region of highest field. In the case of gold nanoparticles suspended in water the real part of the Clausius-Mossotti factor is always positive for frequencies

below 10^{18} Hz. [113] The permittivity of gold nanoparticles is larger than that of bulk gold partly due to their small size and partly due to the interfacial charge layer that is used to stabilise them. Increasing the conductivity of the solution and/or increasing the effective permittivity of the particle can lower the crossover frequency from positive to negative dielectrophoresis.

Considerable effort is being made to overcome the limitations of conventional bioassays by developing biosensors that can provide continuous *in situ* and rapid measurement of biomolecular activity in clinical diagnostics. Point-of-care (POC) devices capable of comprehensive diagnosis would decrease dramatically the time period involved from blood collection to analysis. This is of prime importance when assessing health conditions that can rapidly occur and worsen, for example, rapid diagnosis of heart problems is crucial to administer the appropriate treatment and to increase the chances of survival of the patient. Monitoring the evolution of the disease requires the analysis of cardiac markers to be performed periodically, therefore need for fast and accurate POC devices for detecting cardiac markers and more generally for detecting markers relevant to diseases that can evolve rapidly in varying circumstances.

POC testing for CRP at a GP surgery or hospital is therefore advantageous, in addition to testing at a range of near-patient settings, for example, at a patient's home. POC sensing at a GP surgery or hospital can improve clinical decision-making, patient management and referrals (urgent, non-urgent), monitoring and management of conditions with potential impact on mortality and morbidity. It facilitates provision of an immediate result and rapid decision-making and an improvement of care for remote practices. A high degree of accuracy is required in addition to the need for quality control, calibration and maintenance, and the means to transfer and integrate the result within the clinical records system. Whereas POC testing for certain diseases and conditions is feasible at a patient's home or near-patient setting, for example CRP, utilising visual semi-quantitative detection means which can facilitate provision of an immediate result and also monitoring of ongoing potential conditions which can then direct appropriate medical care. The use of a patient's mobile phone can alternatively communicate test data *via* a smartphone app electronically to a testing facility such as a

hospital laboratory for analysis following which the result can be provided to the patient electronically, eliminating the requirement for frequent attendance at a GP surgery or hospital setting to monitor such conditions.

Sensing technology should be sensitive, cost effective, lightweight, selective, rapid, inexpensive, easy to fabricate, user friendly and biocompatible. [114] The first biosensing application of gold nanoparticles was the pregnancy test developed in 1976 [115] in which the functionalization of the nanoparticles with specific antibodies provided their anchoring at the test window while their extremely high extinction coefficient provided sufficient signal in the colorimetric detection of the human gonadotropic hormone. The pregnancy test has not seen any innovation in over 30 years with the exception of adding a digital component. US start-up Lia has developed an FDA approved flushable and biodegradable pregnancy test. [116] As with other over-the-counter pregnancy tests it looks for the presence of human chorionic gonadotropin in urine. It is a colorimetric test relying on visual detection – one red line for a negative result and two red lines for a positive result and is over 99% accurate. It is engineered from paper and not plastic having special perforations to help the test break down easily when flushed or composted. It provides for a more private, convenient alternative for pregnancy testing reducing patient anxiety while also creating a more environmentally friendly alternative to the plastic methods currently on the market. Plastic accounts for approximately 52% of the cost of such tests. The global market for at home pregnancy and ovulation testing is at over $900 million. [116] Such a visual detection method is a most attractive detection method to enable rapid detection of analytes of interest at the point-of-care.

1.12 Scope of the thesis

The scope of this thesis is the exploration and characterisation of solution phase and surface-based binding of C-reactive protein (CRP) antigen to CRP antibody for the purpose of determination of the potential of visual threshold point-of-care detection of CRP. It was required to determine if merits standard of laboratory-based CRP detection such as specificity, stability, sensitivity could be maintained in addition to incorporating rapidity, cost-efficiency and portability - merits expected of point-of-care sensors.

Nanoparticle self-assembly is envisaged as an attractive technique for POC sensing of CRP. Metal nanoparticles have high indices of refraction and produce strong light scattering facilitating visual detection. A visual detection method, even if the result is only semi-quantitative (e.g. threshold detection) is a most attractive detection method to enable rapid screening of and timely intervention for treatment of diseases pertinent to our time, void of complex chemical processes and elaborate equipment. Employing just gold nanoparticles functionalized with CRP antibodies and CRP antigen linker molecules, solution-phase recognition-induced nanoparticle self-assembly was employed to discern if control of the rate of the self-assembly process could be achieved to enable rapid detection of CRP while maintaining specificity, stability and sensitivity facilitating application to POC sensing.

Surface-based assays also show much promise in application to POC sensing. It was of interest to determine if surface-based assays void of complex chemical processes and elaborate equipment could compete with laboratory-based assays in terms of specificity, stability and sensitivity but also offer faster and inexpensive diagnosis. The binding of CRP antibody to silanised silicon-silicon oxide substrates implemented using the organosilane APTES and the subsequent binding of CRP antigen to this immobilised CRP antibody was explored. Electrical characterisation of the binding event of CRP antigen to surface immobilised CRP antibody in ambient conditions assessed the reaction occurring at the biosensor surface. The use of nanoparticles as tracers in surface-based assays was evaluated as a means to quantify the amount of bound antigen. The binding of CRP antigen to surface immobilised CRP antibody was marked by gold nanoparticles functionalised with CRP antibodies (antiCRP NPs) marking the presence of CRP antigen and analysed numerically employing imageJ to determine the sensitivity, speed of response and limits of detection of the method.

1.13 References

1. Compton, D,; Cornish, L, The third order nonlinear optical properties of gold nanoparticles in glasses, part 1. *Gold Bull* **2003**, 36, 10 - 16.

2. Ghosh, S K,; Pal, T, Interparticle coupling effect on the surface plasmon resonance of gold nanoparticles: from theory to applications. *Chemical Reviews* **2007**, 107, 4797-4862.

3. The British Museum. (**2018**, April 21), *Collection Online*. Retrieved from http://www.britishmuseum.org/research/collection_online/collection_object_details.aspx?objectId=61219&partId=1&searchText=lycurgus+cup&page=1

4. Barber, D.J,; Freestone, I.C, An investigation of the origin of the colour of the lycurgus cup by analytical transmission electron-microscopy. *Archaeometry* **1990,** 32, 33-45.

5. Hornyak, G.L,; Patrissi, C.J,; Oberhauser, E.B *et al*, Effective medium theory characterization of Au/Ag nanoalloy porous alumina composites. *Nanostructured Materials* **1997**, 9, 571-574.

6. Quinten, M, Optical effects associated with aggregates of clusters. *Journal of Cluster Science* **1999**, 10, 319-358.

7. Faraday, M, The bakerian lecture: “experimental relations of gold (and other metals) to light". *Philos Trans R Soc London Ser A* **1957**, 147, 145 - 181.

8. Mie, G, Beitrage zur optik truber medien, speziell kolloidaler. *Ann Phys* **1908**, 25, 1 - 65.

9. El-Sayed, M.A, Some interesting properties of metals confined in time and nanometer space of different shapes. *Acc Chem Res* **2001,** 34, 257-264.

10. Stratton, J.A. (**1941**). *Electromagnetic Theory*. New York, NY: McGray-Hill.

11. Grabar, K.C,; Freeman, R.G,; Hommer, M.B,; Natan, M.J, Preparation and characterization of Au colloid monolayers. *Analytical Chemistry* **1995**, 67, 735-743.

12. Bigall, N.C,; Eychmueller, A, Synthesis of noble metal nanoparticles and their non-ordered superstructures. *Philos Trans A Math Phys Eng Sci* **2010,** 368, 1385-1404.

13. Barrow, S.J,; Funston, A.M,; Gomez, D.E,; Davis, T.J,; Mulvaney, P, Surface plasmon resonances in strongly coupled gold nanosphere chains from monomer to hexamer. *Nano Lett* **2011**,11, 4180-4187.

14. Fan, J.A,; Wu, C,; Bao, K *et al,* Self-assembled plasmonic nanoparticle clusters. *Science* **2010,** 328, 1135-1138.

15. Li, M,; Johnson, S,; Guo, H,; Dujardin, E,; Mann, S, A generalized mechanism for ligand-induced dipolar assembly of plasmonic gold nanoparticle chain networks. *Adv Funct Mater* **2011**; 21, 851-859.

16. Mirkin, C.A,; Letsinger, R.L,; Mucic, R.C,; Storhoff, J.J, A DNA-based method for rationally assembling nanoparticles into macroscopic materials. *Nature* **1996**, 382, 607-609.

17. Luminex. (**2018**, April 21), *Clinical Instruments*. Retrieved from https://www.luminexcorp.com/clinical/instruments/the-verigene-system/

18. Zhang, Y,; Wong, T,; Yang, C,; Ooi, K, Dynamic aspects of electroosmotic flow. *Microfluidics and Nanofluidics* **2006**, 2, 205-214.

19. Bishop, K.J.M,; Wilmer, C.E,; Soh, S,; Grzybowski, B.A, Nanoscale forces and their uses in self-assembly. *Small* **2009**, 5, 1600-1630.

20. Schmid, G,; Simon, U, Gold nanoparticles: assembly and electrical properties in 1-3 dimensions. *Chemical Communications* **2005**, 697-710.

21. Toyozawa, Y, Theory of localized spins and negative magnetoresistance in the metallic impurity conduction. *J. Phys. Soc. Jpn* **1962,** 17, 986 - 1004.

22. Klauk, H,; Schmid, G,; Radlik, W, *et al.* Contact resistance in organic thin film transistors. *Solid-State Electronics* **2003,** 47, 297-301.

23. Abbas, A,; Kattumenu, R,; Tian, L,; Singamaneni, S. Molecular linker-mediated self-assembly of gold nanoparticles: understanding and controlling the dynamics. *Langmuir* **2013,** 29, 56-64.

24. Lam, C.C,; Leung, P.T,; Young K, Explicit asymptotic formulas for the positions, widths and strengths of resonances in Mie scattering. J. Oct. Soc. Am **1992**, 9, 1585-1592.

25. Alvarez, M.M,; Khoury, J.T,; Schaaff, T.G,; Shafigullin, M.N,; Vezmar, I,; Whetten, R.L, Optical absorption spectra of nanocrystal gold molecules. *Journal of Physical Chemistry B.* **1997**, 101, 3706-3712.

26. Link, S,; El-Sayed, M.A, Spectral properties and relaxation dynamics of surface plasmon electronic oscillations in gold and silver nanodots and nanorods. *Journal of Physical Chemistry B* **1999**, 103, 8410-8426.

27. Moores, A,; Goettmann, F, The plasmon band in noble metal nanoparticles: an introduction to theory and applications. *New Journal of Chemistry* **2006**, 30, 1121-1132.

28. Beeram, S.R,; Zamborini, F.P, Selective attachment of antibodies to the edges of gold nanostructures for enhanced localized surface plasmon resonance biosensing. *J Am Chem Soc* **2009**, 131, 11689 - 11691.

29. Millaruelo, M,; Eng, L.M,; Mertig, M, *et al*, Photolabile carboxylic acid protected terpolymers for surface patterning. Part 2: photocleavage and film patterning. *Langmuir* **2006**, 22, 9446-9452.

30. Yockell-Lelievre, H,; Desbiens, J,; Ritcey, A.M, Two-dimensional self-organization of polystyrene-capped gold nanoparticles. *Langmuir* **2007**, 23, 2843-2850.

31. Kelly, K.L,; Coronado, E,; Zhao, L.L,; Schatz, G.C. The optical properties of metal nanoparticles: The influence of size, shape, and dielectric environment. *Journal of Physical Chemistry B* **2003,** 107, 668-677.

32. Brian, B,; Sepulveda, B,; Alaverdyan, Y,; Lechuga, L.M,; Kall, M, Sensitivity enhancement of nanoplasmonic sensors in low refractive index substrates. *Opt Express*, **2009**, 17, 2015-2023.

33. Saha K,; Agasti, S.S,; Kim, C,; Li, X,; Rotello, V.M, Gold Nanoparticles in chemical and biological sensing. *Chemical Reviews* **2012,** 112, 2739-2779.

34. Boulos, S.P,; Davis, T.A,; Yang, J.A, *et al*, Nanoparticle-protein interactions: a thermodynamic and kinetic study of the adsorption of bovine serum albumin to gold nanoparticle surfaces. *Langmuir* **2013**, 29, 14984-14996.

35. Yang, M,; Chen, G,; Zhao, Y, *et al*, Mechanistic investigation into the spontaneous linear assembly of gold nanospheres. *Physical Chemistry Chemical Physics* **2010**, 12, 11850-11860.

36. Blakey, I,; Merican, Z,; Thurecht, K.J, A method for controlling the aggregation of gold nanoparticles: tuning of optical and spectroscopic properties. *Langmuir* **2013,** 29, 8266-8274.

37. Plotz, C.M,; Singer, J.M, The latex fixation test. I. Application to the serologic diagnosis of rheumatoid arthritis. *The American journal of medicine* **1956**, 21, 888-892.

38. Maye, M.M,; Kumara, M.T,; Nykypanchuk, D,; Sherman, W.B,; Gang, O, Switching binary states of nanoparticle superlattices and dimer clusters by DNA strands. *Nature Nanotechnology* **2010**, 5, 116-120.

39. Shenhar, R,; Norsten, T.B,; Rotello, V.M, Polymer-mediated nanoparticle assembly: structural control and applications. *Advanced Materials*. **2005**,17, 657-669.

40. Frankamp, B.L,; Uzun, O,; Ilhan, F,; Boal, A.K,; Rotello, V.M, Recognition-mediated assembly of nanoparticles into micellar structures with diblock copolymers. *J Am Chem Soc* **2002**, 124, 892-893.

41. Sardar, R,; Heap, T.B,; Shumaker-Parry, J.S, Versatile solid phase synthesis of gold nanoparticle dimers using an asymmetric functionalization approach. *J Am Chem Soc* **2007**, 129, 5356 - 5357.

42. Nie, Z,; Petukhova, A,; Kumacheva, E, Properties and emerging applications of self-assembled structures made from inorganic nanoparticles. *Nature Nanotechnology* **2010,** 5, 15-25.

43. de la Rica, R,; Stevens, M.M, Plasmonic ELISA for the detection of analytes at ultralow concentrations with the naked eye. *Nature Protocols* **2013**, 8, 1759-1764.

44. Glotzer, S.C,; Horsch, M.A,; Iacovella, C.R,; Zhang, Z.L,; Chan, E.R,; Zhang, X, Self-assembly of anisotropic tethered nanoparticle shape amphiphiles. *Current Opinion in Colloid & Interface Science* **2005,** 10, 287-295.

45. Banerjee, P,; Conklin, D,; Nanayakkara, S,; Park, T-H,; Therien, M.J,; Bonnell D.A, Plasmon-induced electrical conduction in molecular devices. *ACS Nano*. **2010**, 4, 1019-1025.

46. Barnard, A.S,; Chen, Y, Kinetic modelling of the shape-dependent evolution of faceted gold nanoparticles. *J Mater Chem* **2011**, 21, 12239-12245.

47. Abbas, A,; Tian, L,; Kattumenu, R,; Halim, A,; Singamaneni, S, Freezing the self-assembly process of gold nanocrystals. *Chemical Communications* **2012**, 48, 1677-1679.

48. Malola, S,; Lehtovaara, L,; Enkovaara, J,; Hakkinen, H, Birth of the localized surface plasmon resonance in mono layer-protected gold nanoclusters. *ACS Nano* **2013**, 7, 10263-10270.

49. Xie, Y,; Guo, S,; Guo, C, *et al*, Controllable two-stage droplet evaporation method and its nanoparticle self-assembly mechanism. *Langmuir* **2013**, 29, 6232-6241.

50. Gierhart, B.C,; Howitt, D.G,; Chen, S.J,; Smith, R.L,; Collins, S.D, Frequency dependence of gold nanoparticle superassembly by dielectrophoresis. *Langmuir* **2007**, 23, 12450-12456.

51. Sassiat, N. P. 2011, Formation and electrical interfacing of nanocrystal-molecule nanostructures. PhD Thesis. University College Cork.

52. Henry, C,; Minier, J-P,; Pozorski, J,; Lefevre, G, A new stochastic approach for the simulation of agglomeration between colloidal particles. *Langmuir* **2013**, 29, 13694-13707.

53. Meakin, P, Work with fractals: fractals. *Science* **1989,** 245, 1515-1516.

54. Li, G,; Sander, L.M,; Meakin, P, Self-similarity of diffusion-limited aggregates and electrodeposition clusters. *Phys Rev Lett* **1989,** 63, 1322-1322.

55. Meakin, P,; Muthukumar, M, The effects of attractive and repulsive interaction on two-dimensional reaction-limited aggregation. *J Chem Phys* **1989**, 91, 3212-3221.

56. Meakin, P,; Tolman, S, Diffusion-limited aggregation. *Proc. royal Soc. A.* **1989**, 423, 133-148.

57. Jain, P.K,; El-Sayed, M.A, Surface plasmon coupling and its universal size scaling in metal nanostructures of complex geometry: Elongated particle pairs and nanosphere trimers. *J. Phys. Chem. C* **2008,** 112, 4954-4960.

58. Van Lehn, R.C,; Alexander-Katz, A, Ligand-mediated short-range attraction drives aggregation of charged mono layer-protected gold nanoparticles. *Langmuir* **2013,** 29, 8788-8798.

59. Parolo, C,; de la Escosura-Muniz, A,; Polo, E,; Grazu, V,; de la Fuente, J.M,; Merkoci, A, Design, preparation, and evaluation of a fixed-orientation antibody/gold-nanoparticle conjugate as an immunosensing label. *ACS Appl.Mater. Interfaces* **2013,** 5, 10753-10759.

60. Makarova, M,; Mandal, S.K,; Okawa, Y,; Aono, M, Ordered monomolecular layers as a template for the regular arrangement of gold nanoparticles. *Langmuir* **2013**, 29, 7334-7343.

61. Chen, Y,; Munechika, K,; Ginger, D.S, Bioenabled nanophotonics. *MRS Bull* **2008**, 33, 536-542.

62. Majumdar, R,; Manikwar, P,; Hickey, JM, *et al,* Effects of salts from the hofmeister series on the conformational stability, aggregation propensity, and local flexibility of an IgG1 monoclonal antibody. *Biochemistry* **2013**, 52, 3376-3389.

63. Mohammed, M-I,; Desmulliez, M.P.Y, Lab-on-a-chip based immunosensor principles and technologies for the detection of cardiac biomarkers: a review. *Lab on a Chip* **2011**, 11, 569-595.

64. Elghanian, R,; Storhoff, J.J,; Mucic, R.C,; Letsinger, R.L,; Mirkin, C.A, Selective colorimetric detection of polynucleotides based on the distance-dependent optical properties of gold nanoparticles. *Science* **1997**, 277, 1078-1081.

65. Tillet, W.S,; Francis, T, Seroligical reaction in pneumonia with a non-protein somatic fraction of pneumococcus. *J Exp Med* **1930**, 52, 561-571.

66. MacLeod, C, ; Avery, O.T, The occurrence during acute infections of a protein not normally present in the blood. II. Isolation and properties of the reactive protein. *J Exp Med* **1941**, 73, 191-200.

67. Ledue, T.B,; Rifai, N, Preanalytic and analytic sources of variations in C-reactive protein measurement: Implications for cardiovascular disease risk assessment. *Clinical Chemistry* **2003**, 49, 1258-1271.

68. Lee, W-B,; Chen, Y-H,; Lin, H-I,; Shiesh, S-C,; Lee, G-B, An integrated microfluidic system for fast, automatic detection of C-reactive protein. *Sensors and Actuators B-Chemical* **2011**, 157, 710-721.

69. Kushner, I, C-Reactive Protein in rheumatology. *Arthritis and Rheumatism* **1991**, 34, 1065-1068.

70. Hu, W.P,; Hsu, H.Y,; Chiou, A, *et al*, Immunodetection of pentamer and modified C-reactive protein using surface plasmon resonance biosensing. *Biosens Bioelectron* **2006,** 21, 1631-1637.

71. Black, S,; Kushner, I,; Samols, D, C-reactive protein. J Biol Chem, **2004**, 279, 48487 – 48490.

72. Bini, A,; Centi, S,; Tombelli, S,; Minunni, M,; Mascini, M, Development of an optical RNA-based aptasensor for C-reactive protein. *Anal Bioanal Chem* **2008**, 390, 1077-1086.

73. Yousuf, O,; Mohanty, B.D,; Martin, S.S, *et al*, High-sensitivity C-reactive protein and cardiovascular disease a resolute belief or an elusive link? *Journal of the American College of Cardiology* **2013,** 62, 397-408.

74. FUNMOL project proposal document.

75. Haes, A.J,; Stuart, D.A,; Nie, S.M,; Van Duyne, R.P, Using solution-phase nanoparticles, surface-confined nanoparticle arrays and single nanoparticles as biological sensing platforms. *Journal of Fluorescence* **2004**, 14, 355-367.

76. De la Rica, R.; Stevens, M.M, Plasmonic ELISA for the ultrasensitive detection of disease biomarkers with the naked eye. *Nature nanotechnology* **2012,** 7, 821-824.

77. De la Rica, R.; Stevens, M.M, Plasmonic ELISA for the detection of analytes at ultralow concentrations with the naked eye. *Nature Protocols* **2013**, 8, 1759-1764.

78. Rodriguez-Lorenzo, L.; de la Rica, R.; Alvarez-Puebla, R.A.; Liz-Marzan, L.M.; Stevens, M.M, Plasmonic nanosensors with inverse sensitivity by means of enzyme-guided crystal growth. *Nature Materials* **2012**, 11, 604-60.

79. Mirkin, C.A.; Letsinger, R.L.; Mucic, R.C.; Storhoff, J.J, A DNA-based method for rationally assembling nanoparticles into macroscopic materials. *Nature* **1996**, 382, 607 – 609.

80. Alivisatos, P. A.; Johnsson, K. P.; Peng, X.; Wilson, T. E.; Loweth, C. J.; Bruchez Jr, M. P.; Schultz, P. G, Organisation of “nanocrystal molecules” using DNA. *Nature* **1996**, 382, 609 – 611.

81. Parolini, L.; Kotar, J.; Di Michele, L.; Mognetti, B. M. Controlling self-assembly kinetics of DNA-functionalised liposomes using toehold exchange mechanism. *ACS Nano* **2016**, *10*, 2392–2398.

82. Snodin, B.E.; Romano, F.; Rovigatti, L.; Ouldridge, T.E.; Louis, A.A.; Doye, J.P, Direct simulation of the self-assembly of a small DNA origami. *ACS Nano* **2016**, 10, 1724-37.

83. King, N.P.; Bale, J.B.; Sheffler, W.; McNamara, D.E.; Gonen, S.; Gonen, T.; Yeates, T.O.; Baker, D, Accurate design of co-assembling multi-component protein nanomaterials. *Nature* **2014**, 510, 103-108.

84. Mejias, S.H.; Sot, B.; Guantes, R.; Cortajarena, A.L, Controlled nanometric fibres of self-assembled designed protein scaffolds. *Nanoscale* **2014**, 6, 10982-10988.

85. Gurunatha, K.L.; Fournier, A.C.; Urvoas, A.; Valerio-Lepiniec, M.; Marchi, V.; Minard, P.; Dujardin, E, Nanoparticles self-assembly driven by high affinity repeat protein pairing. *ACS Nano* **2016**, *10* , 3176–3185.

86. Aili, D.; Selegard, R.; Baltzer, L.; Enander, K.; Liedberg, B, Colorimetric protein sensing by controlled assembly of gold nanoparticles functionalised with synthetic receptors. *Small* **2009**, 5, 2445 – 2452.

87. Smolsky, J; Kaur, S,; Hayashi, C,; Batra, S.K,; Krasnoslobodtsev, A. V, Surface-enhanced raman scattering-based immunoassay technologies for detection of disease biomarkers. *Biosensors* **2017,** 7, 1 - 21.

88. Foscan, M,; Cracian, A.M,; Potara, M,; Leordean, C,; Vulpoi, A,; Maniu, D,; Astilean, S, Flexible and tunable 3D gold nanocups platform as plasmonic biosensor for specific dual LSPR-SERS immuno-detection. Sci. Rep **2017,** 7, 1 – 11.

89. Guarrotxena, N,; Bazan, G.C, Anti-tags: SERS-encoded nanoparticle assemblies that enable single-spot multiplex protein detection. *Adv. Mater* **2014**, 26, 1941 – 1946.

90. Kim, H,; Kim, E,; Choi, E, Baek, C. S,; Song, B,; Cho, C-H,; Jeong, S. W, Label-free C-reactive protein SERS detection with silver nanoparticle aggregates. *RCS Adv*, **2015**, 5, 34720 – 34729.

91. Mascini, M,; Tombelli, S, Biosensors for biomarkers in medical diagnostics. *Biomarkers* **2008**, 13, 637-657.

92. Hall, D, Use of optical biosensors for the study of mechanistically concerted surface adsorption processes. *Anal Biochem* **2001**, 288, 109-125.

93. Wang, J,; Cai, X.H,; Rivas, G,; Shiraishi, H,; Farias, P.A.M,; Dontha, N, DNA electrochemical biosensor for the detection of short DNA sequences related to the human immunodeficiency virus. *Analytical Chemistry* **1996,** 68, 2629-2634.

94. Thevenot, D.R,; Toth, K,; Durst, R.A,; Wilson, G.S, Electrochemical biosensors: recommended definitions and classification. *Biosens Bioelectron* **2001**, 16, 121-131.

95. Horacek, J,; Skladal, P, Improved direct piezoelectric biosensors operating in liquid solution for the competitive label-free immunoassay of 2,4-dichlorophenoxyacetic acid. *Analytica Chimica Acta* **1997**, 347, 43-50.

96. Miller, M.M,; Sheehan, P.E,; Edelstein, R.L, *et al* A DNA array sensor utilizing magnetic microbeads and magnetoelectronic detection. *Journal of Magnetism and Magnetic Materials* **2001**, 225, 138-144.

97. Raiteri, R,; Grattarola, M,; Butt, H.J,; Skladal, P, Micromechanical cantilever-based biosensors. *Sensors and Actuators B-Chemical* **2001,** 79, 115-126.

98. Natsume, T,; Nakayama, H,; Isobe, T, BIA-MS-MS: biomolecular,interaction analysis for functional proteomics. *Trends in Biotechnology* **2001,** 19, S28-S33.

99. Mamkin, I,; Ten, S,; Bhandari, S,; Ramchandari, N, Real-time continuous glucose monitoring in the clinical setting: the good, the bad and the practical. *J. Diabetes Sci. Technol* **2008**, 2, 882 – 889.

100. Wang, H-C,; Lee, A-R, Recent developments in blood glucose sensors. *J Food Drug Anal*, **2015**, 23, 191 – 200.

101. SPD Swiss Precision Diagnostics GmbH. (**2018**, April 21), *Pregnancy Tests.* Retrieved from http://www.clearblue.com/pregnancy-tests

102. Hsiao, V.K.S,; Waldeisen, J.R,; Zheng, Y,; Lloyd, P.F,; Bunning, T.J,; Huang, T.J, Aminopropyltriethoxysilane (APTES)-functionalized nanoporous polymeric gratings: fabrication and application in biosensing. *J Mater Chem* **2007**, 17, 4896-4901.

103. Stang, P.J, Abiological Self-assembly via coordination: formation of 2D metallacycles and 3D metallacages with well-defined shapes and sizes and their chemistry. *J Am Chem Soc* **2012,** 134, 11829-11830.

104. Howarter, J.A,; Youngblood, J.P, Optimization of silica silanization by 3-aminopropyltriethoxysilane. *Langmuir* **2006,** 22, 11142-11147.

105. Kim, J,; Seidler, P,; Wan, L.S,; Fill, C, Formation, structure, and reactivity of amino-terminated organic films on silicon substrates. *Journal of Colloid and Interface Science* **2009**, 329, 114-119.

106. Smith, E.A,; Chen, W, How to prevent the loss of surface functionality derived from aminosilanes. *Langmuir : the ACS journal of surfaces and colloids* **2008**, 24, 12405-12409.

107. Aissaoui, N,; Bergaoui, L,; Landoulsi, J,; Lambert, J-F,; Boujday, S, Silane layers on silicon surfaces: mechanism of interaction, stability, and influence on protein adsorption. *Langmuir* **2012**, 28, 656-665.

108. Asenath-Smith, E,; Chen, W, How to prevent the loss of surface functionality derived from aminosilanes. *Langmuir* **2008**, 24, 12405-12409.

109. Rayner, G.H,; Ford, L.H, Capacitance measurement. *Journal IEE* **1961**, 7, 171 - 172.

110. Peng, H-I,; Miller, B.L, Recent advancements in optical DNA biosensors: exploiting the plasmonic effects of metal nanoparticles. *Analyst* **2011**, 136, 436-447.

111. Dykman, L,; Khlebtsov, N, Gold nanoparticles in biomedical applications: recent advances and perspectives. *Chem Soc Rev* **2012**, 41, 2256-2282.

112. Pohl, H. A. (**1978**). *Dielectrophoresis: the behavior of neutral matter in nonuniform electric fields*. Cambridge, UK: Cambridge University Press.

113. Gierhart, B. C.; Howitt, D. G.; Chen, S. J.; Smith, R. L.; Collins, S. D, Frequency dependence of gold nanoparticle superassembly by dielectrophoresis. *Langmuir* **2007,** 23, 12450-12456.

114. Mascini, M,; Tombelli, S, Biosensors for biomarkers in medical diagnostics. *Biomarkers* **2008, 1**3, 637-657.

115. Bain, C.D,; Whitesides, G.M, Formation of monolayers by the coadsorption of thiols on gold - variation in the length of the alkyl chain. *J Am Chem Soc* **1989**, 111, 7164-7175.

116. Lia Diagnostics Inc. (**2018**, April 21), *How Lia Works*. Retrieved from https://meetlia.com/why-lia/

Chapter 2

Solution-Phase Formation and Characterization of Nanoparticle-Biomolecule Assemblies *via* C-Reactive Protein Antibody-Antigen recognition

2.1 Introduction

Nanoparticle self-assembly is envisaged as an attractive technique to facilitate point-of-care (POC) detection of C-reactive protein (CRP). Metal nanoparticles have high indices of refraction and produce strong light scattering facilitating visual detection. A visual detection method, even if the result is only semi-quantitative (e.g. threshold detection) is a most attractive detection method to enable rapid screening of and timely intervention of CRP, void of complex chemical processes and elaborate equipment.

To facilitate such POC detection, a rapid, inexpensive assay is required while concurrently maintaining such expected merits of biosensors such as specificity, stability and sensitivity. Many recently developed techniques for biomolecular detection focus on achieving lower and lower limits of detection, for example, 100 pg/mL, 17 pg/mL and 1 fg/mL.[1, 2, 3] However, these techniques are mostly not amenable to POC settings due to requirement for elaborate experimental techniques and/or equipment [4, 5] or specific experimental requirements such as temperature control. [2, 6]

Employing just gold nanoparticles functionalized with CRP antibodies and CRP antigen as linker molecules, solution-phase recognition-induced nanoparticle self-assembly was employed to discern if control of the rate of the self-assembly process could be achieved to enable rapid detection of CRP while maintaining specificity, stability and sensitivity of the assay facilitating application to POC sensing of CRP.

It was also of interest to discern if control of the rate of the recognition-induced nanoparticle self-assembly process could be corroborated employing nanoparticles of differing size and functionality. In that regard 60 nm citrate-stabilised gold nanoparticles were employed using $Re_2(DMAA)_4(NCS)_2$ as linker molecules.

2.2 Experimental

2.2.1 Formation and UV-visible characterization of NP-CRP assemblies

UV-visible spectroscopic analysis was performed using an Agilent 8453 spectrophotometer. All glassware and cuvettes were cleaned using aqua regia (3:1 HCl:HNO_3) to remove any metal residue and piranha solution (3:1 H_2SO_4:H_2O_2) to remove organic residue. **Warning** these solutions are very corrosive reacting violently with organic material and so must be handled with extreme care. Glassware and cuvettes were then rinsed thoroughly using ultrapure deionized water. UV-visible spectra were recorded of the phosphate buffered saline (PBS) solution and of the CRP antibody functionalized 40 nm diameter gold nanoparticle solutions (BBI Solutions) diluted to optical density 2 with Phosphate Buffered Saline solution. Aliquots of purified C-reactive protein (CRP) antigen solution (BBI Solutions) were added to the antibody functionalized gold nanoparticle solutions (BBI Solutions), equating to ratios of antigen linker molecules to nanoparticles of 2:1, 12:1, 18:1 and 72:1. Solutions were gently stirred with a magnetic stir bar. UV-visible spectra of these solutions were recorded in the wavelength range 400 nm < λ < 800 nm at time intervals of 2-10 minutes. Resultant nanoparticle solution colour changes were visually observed over time.

2.2.2 Determination of robustness and specificity of formation process

Solution stability was investigated, employing UV-visible analysis as described above, whereby no CRP antigen solution was added to the CRP antibody functionalized nanoparticle solution and absorbance measured over a 5 hour time frame. Similarly robustness, where harsh stirring conditions were employed at a temperature of 50°C and specificity, where a goat anti-mouse antibody functionalized 40 nm gold nanoparticle solution was used in place of the monoclonal anti-human CRP antibody functionalized nanoparticle solution. It is required for the primary antibody (goat) to be raised against (anti) the species of the specimen, i.e anti-human. Goat anti-human CRP antibody recognizes human CRP. An aliquot of antigen solution was added equating to a ratio of antigen linker molecules to nanoparticle of 2:1.

2.2.3 Formation of NP- $Re_2(DMAA)_4(NCS)_2$ assemblies

Control of the rate of nanoparticle self-assembly process was corroborated employing citrate-stabilised gold nanoparticles and a di-isothiocyanate terminated metal organic rhenium linker $Re_2(DMAA)_4(NCS)_2$. Citrate-stabilised gold nanoparticle solutions with nanoparticle core diameter of d = 60 nm were purchased from BBI. Ultrapure deionized water was used in all experiments. To improve the stability of the citrate-stabilised nanoparticle solutions, 3 mM aqueous tri-sodium citrate was added prior to use (1:1). The bi-functional linker molecule $Re_2(DMAA)_4(NCS)_2$ was dissolved in acetone. UV-Visible absorption spectra were recorded of these nanoparticle solutions using an Agilent 8453 spectrophotometer. 2 µL aliquots of 10 µM $Re_2(DMAA)_4(NCS)_2$ linker solution were added to each of the nanoparticle solutions at 2 - 10 minute intervals, followed by mixing and recording of UV-visible spectra, in addition to visual observation of nanoparticle solution colour changes

2.2.4 Scanning electron microscopy characterization of assemblies

Aliquots of nanoparticle solution were removed at various intervals during each nanoparticle assembly formation experiment. Scanning electron microscopy (SEM) characterisation was performed (JSM-7500F JEOL UK Ltd) on these aliquots of solution following dilution by a factor of 100 and drop deposited on to individual silicon substrates (rendered hydrophilic by immersion in H_2SO_4 for 30 minutes followed by immersion in HCl : methanol (1 : 1) solutions for 30 minutes). For each substrate, at least 100 nanostructures were counted at random locations using the Step Function on the SEMs motorized stage. The numbers of each sized nanostructure formed for each time interval were recorded. These numbers provide the experimental concentrations of each sized nanostructure formed which are then used in a set of generation-recombination models and rate equations developed by Dr Nicolas Sassiat during his Ph.D. within the Nanotechnology Group at Tyndall. [7] This phenomenological model based on a system of rate equations (superseding an initial full random-walk approach) is implemented using MATLAB routines developed by Dr Sassiat. The model can accommodate and essentially fit the distributions of nanostructure populations found experimentally through SEM analysis and facilitates estimation of the enthalpies of reaction for molecular decoration of nanoparticle surfaces and nanoparticle association on the basis of the values of the optimised fit parameters.

2.3 Results and Discussion

2.3.1 Formation and UV-visible characterization of NP-CRP assemblies

C-reactive protein (CRP) antibody functionalized 40 nm diameter gold nanoparticle solution, diluted to optical density 2 with phosphate buffered saline, exhibits a single absorption peak in the UV-visible spectrum at λ_{max} = 531 nm, see figure 2.1 (a) and a ruby red colour. It consists of highly dispersed single nanoparticles. Stability of the nanoparticle solutions and batch-to-batch variability is affected by the protein covering on the gold particle which acts to passivate the surface (i.e. prevent the salt collapse associated with citrate-capped particles). The amount of protein and the conformation on the surface will affect this, see figure 2.1 (b) whereby on dilution with PBS solution resulted in the collapse of the gold nanoparticle solution. The nature of the protein interaction with the gold surface and the storage buffer will also affect whether the protein remains on the particle surface during storage. The stability is however established on dilution of the nanoparticle solution with buffer and monitored over lengthy time intervals using UV-visible absorption spectroscopy, see figure 2.1 (a).

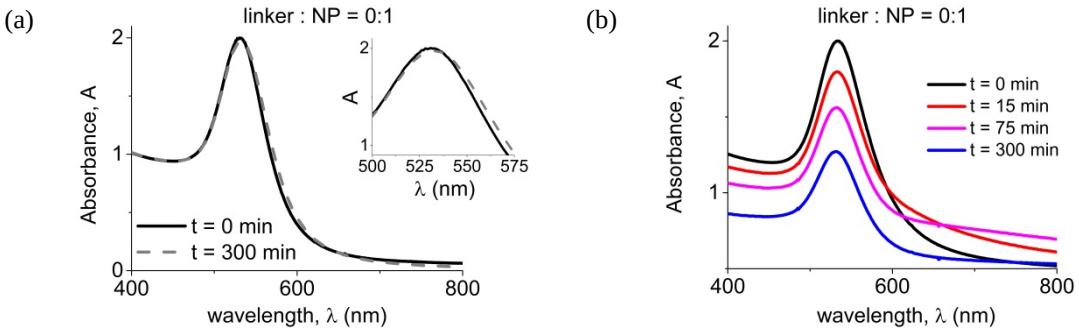

Figure 2.1: UV-visible absorbance spectra recorded versus wavelength (λ) over 300 minutes, of C-reactive protein (CRP) antibody-functionalised 40 nm diameter gold nanoparticle (a) stable solution to which no CRP antigen linker molecules have been added, (b) unstable solution to which no CRP antigen linker molecules have been added.

Directed assembly of CRP antibody functionalized gold nanoparticles occurred through addition of CRP antigen linker molecules. Concentrations of antigen linker molecules corresponding to nanoparticle-molecule ratios of 2, 12, 18 and 72 molecules per nanoparticle were used, see table 2.1.

Volume & Concentration antigen	Molarity (nM)	# antigen molecules per NP
10 µL @ 0.01 mg/mL	0.6 nM	2
60 µL @ 0.01 mg/mL	3.6 nM	12
9 µL @ 0.1 mg/mL	5.4 nM	18
18 µL @ 0.2 mg/mL	22 nM	72

Table 2.1: Table of 4 different concentrations of CRP antigen added to an optical density 2 antiCRP NP solution, with the corresponding solution molarity and average number of molecules available in solution per nanoparticle.

The spectral signature of red-shifted and broadened absorption bands and two absorption maxima is ascribed to the assembly of nanoparticles forming nanostructures, see figure 2.2. UV-visible absorbance spectra recorded versus wavelength over 60 minutes, representing nanoparticle-molecule formation where (a) 10 µL of 0.01 mg/mL CRP antigen solution is added to antiCRP nanoparticle solution @ optical density (OD) 2 (0.6 nM, 2 molecules per NP), (b) 60 µL of 0.01 mg/mL CRP antigen solution is added to antiCRP NP solution @ OD 2 (3.6 nM, 12 molecules per NP), (c) 9 µL of 0.1 mg/mL CRP antigen solution is added to antiCRP NP solution @ OD 2 (5.4 nM, 18 molecules per NP), (d) 18 µL of 0.2 mg/mL CRP antigen solution is added to antiCRP NP solution @ OD 2 (22 nM, 72 molecules per NP).

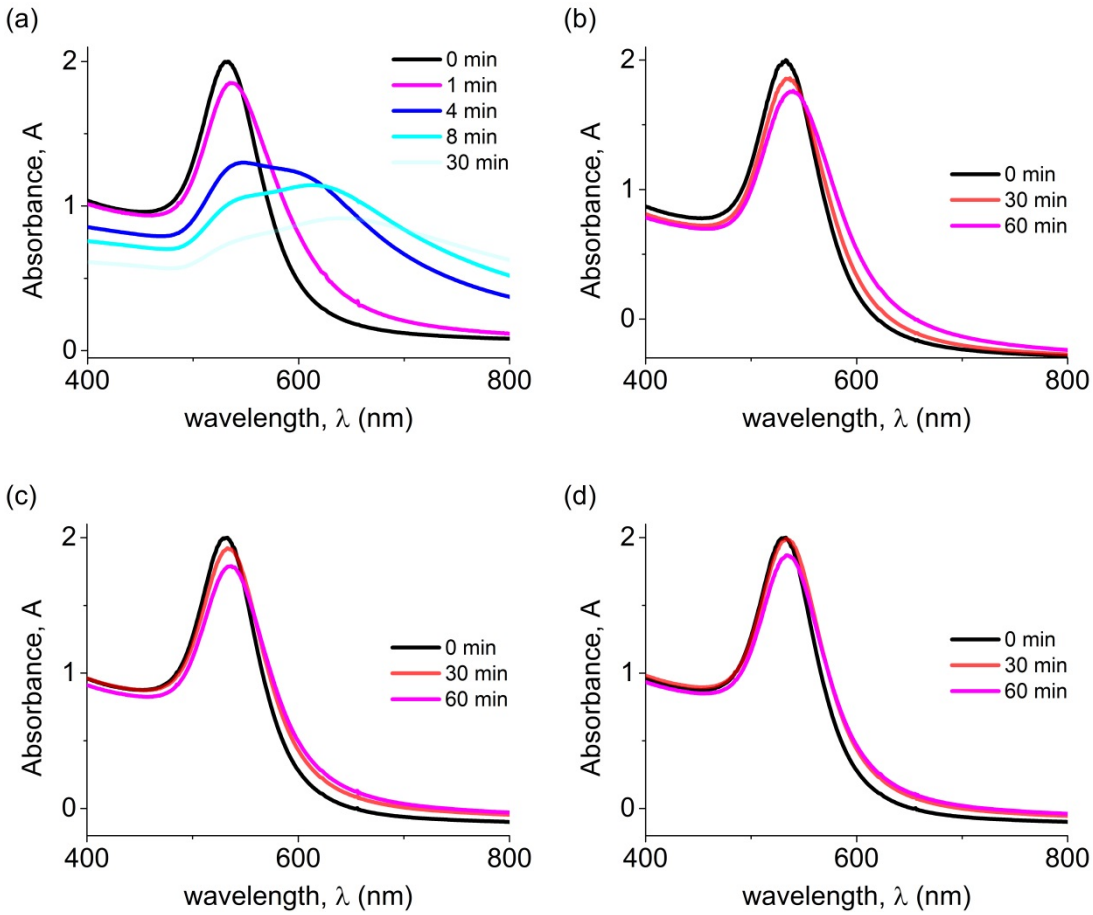

Figure 2.2: UV-visible absorbance spectra recorded versus wavelength (λ) over 60 minutes where (a) 10 µL of 0.01 mg/mL CRP antigen solution is added to antiCRP NP solution (0.6 nM; 2 molecules per NP), (b) 60 µL of 0.01 mg/mL CRP antigen solution is added to antiCRP NP solution (3.6 nM; 12 molecules per NP), (c) 9 µL of 0.1 mg/mL CRP antigen solution is added to antiCRP NP solution (5.4 nM; 18 molecules per NP) and (d) 18 µL of 0.2 mg/mL CRP antigen solution is added to antiCRP NP solution @ ~OD2 (22 nM; 72 molecules per NP).

The first peak located near the resonance peak for single nanoparticles is attributed to the transversal resonance peak/ plasmon excitation in coupled spheres. Overall the peak intensity at λ_{max} (531 nm) decreases in magnitude as a result of the decrease in the number of single nanoparticles and is red-shifted by up to 4 nm and broadened over a time frame of 60 minutes. As nanostructures form, the emergence of a second peak is evident at ~ 600 nm. As nanostructure formation progresses, this second peak intensifies and shifts to longer wavelengths which reflects the increase in chain length and the linear nature of the assembly. Increase in the full width at half max (FWHM) of the new peaks is mainly explained by the increase in the number density leading to a branched network. This second longer wavelength peak arising from the formation of dimers and

higher order nanostructures has previously been predicted theoretically and observed experimentally using optical transmission measurements on fabricated and synthesised dimer nanostructures. The intensity of the aggregated system depends on the degree of aggregation as well as orientation of the individual nanoparticles within the aggregates.[8,9,10]

The increase in the assembly degree was signified by a solution colour change from red to blue within 5 minutes when the concentration of linker molecules supplied in solution provided on average 2 linker molecules per nanoparticle, see figure 2.3 (b). The blue solution colour is ascribed to the formation of large nanostructures, see figure 2.2 (a) and figure 2.3 (a), facilitating visual detection of a CRP concentration of 0.06 µg/mL within 5 minutes. Nanoparticle- linker molecule ratios outside of a narrow range, for example, 12, 18, 72 resulted in only a vaguely discernable change in the tone of the red colored nanoparticle solution after 5 days, see figure 2.3 (d). Some decrease and red shift in absorbance was observed over long time intervals representing slow formation of small numbers of small nanostructures, see figure 2.2 (b) and figure 2.3 (c). As the number of CRP antigen linker molecules supplied in solution increases, the rate of formation of nanostructures decreases, see figure 2.2 (c) and (d) and figure 2.3 (c).

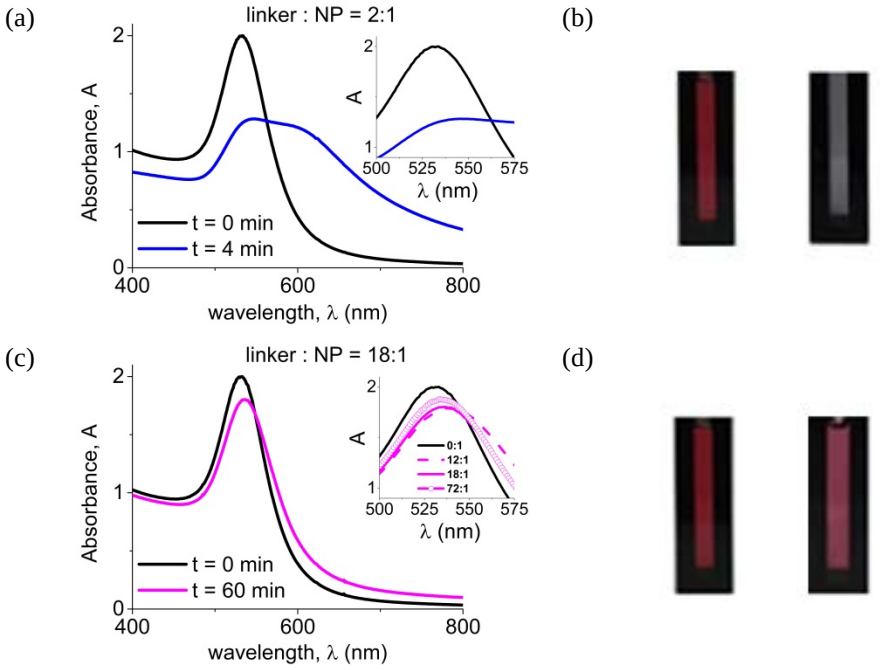

Figure 2.3: UV-visible absorption spectra of C-reactive protein (CRP) antibody functionalized 40 nm diameter gold nanoparticle solution to which (a) CRP antigen linker molecule-nanoparticle ratio = 2:1 and (c) CRP antigen linker molecule-nanoparticle ratio = 18:1. Corresponding photographs of C-reactive protein antibody functionalized 40 nm diameter gold nanoparticle solution taken (b) prior to addition of CRP antigen and 5 minutes following addition of CRP antigen solution (2:1), (d) prior to addition of CRP antigen and 5 days following addition of CRP antigen solution (18:1).

Of critical significance in any assay platform is determination of the range of detection for the particular analyte. In this technique employing 40 nm gold nanoparticles, the range of detection is limited by the number of CRP antibody molecules bound to the nanoparticle surface and also by the number of nanoparticles present, allowing a maximum number of molecules to bind to all available nanoparticles, irrespective of the quantity of molecules in solution. However, in the case of binding of molecules to all available CRP antibody molecules, nanostructure formation is prevented as an antigen shouldn't bind to an antigen. For nanostructure formation to occur there must be a nanoparticle/nanostructure which has an available antibody on its surface to which no antigen is bound, another nanoparticle/nanostructure which has an antigen bound to a surface attached antibody and a collision event of the surface bound antibody with the antibody bound antigen. When many of the nanoparticle antibody binding sites have been occupied with antigen linker molecules nanostructure formation is limited to slow formation of small numbers of small nanostructures, as is the case when the molecule-

nanoparticle ratio is 12 or greater, see figure 2.4 (c). It was found however when the molecule-nanoparticle ratio was 2:1 rapid formation of large numbers of large nanostructures occurred, facilitated by many available antibody binding sites on the nanoparticle surfaces and sufficient antibody bound antigen on the nanoparticle surface to facilitate rapid formation of large nanostructures, see figure 2.4 (b). Therefore, the upper limit of detection is actually lower than the maximum permittable number of antigen molecules that can bind per nanoparticle. This facilitates naked eye detection of CRP antigen that falls within certain concentration ranges: if the CRP antigen concentration falls within the upper limit of detection (LOD) (as determined by NP : molecule ratio) a rapid solution colour change from ruby red to blue will occur within 5 minutes. However, if the concentration is close to or much higher, this colour change is not seen. The possibility for detection across a range of CRP concentrations is facilitated by varying the number of nanoparticles present in the assay or the sample volume.

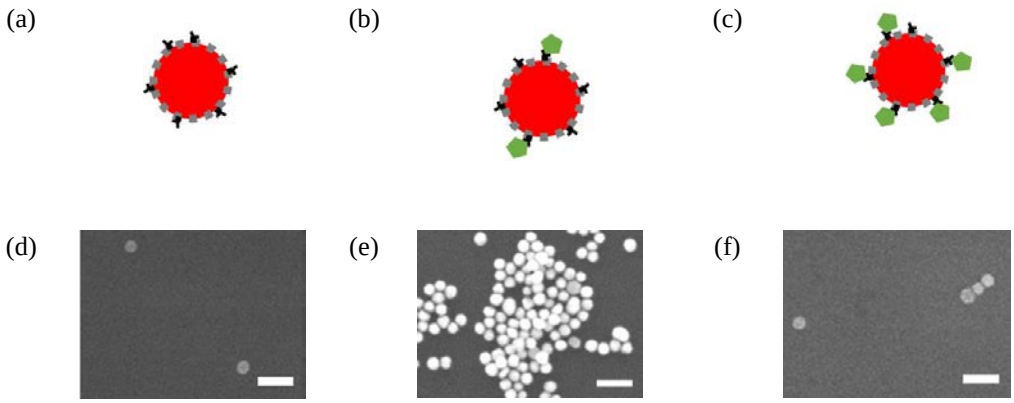

Figure 2.4: Schematics depicting the relative coverage of the antiCRP NPs with CRP antigen (a) antigen molecule-NP ratio = 0:1, (b) antigen molecule-NP ratio = 2:1 (c) antigen molecule-NP ratio = 18:1 and corresponding SEM images in (d), (e) and (f). SEM image scalebars = 120 nm.

2.3.2 Determination of robustness and specificity of formation process

The robustness of the nanostructure formation process was then investigated. An elevated temperature (37°C) was employed to check the stability of the antiCRP nanoparticle solution, i.e. if an elevated temperature was having a significant impact on the speed of formation of nanostructures. Figure 2.5 displays UV-visible absorption spectra recorded for the formation of nanostructures using CRP antibody functionalised gold nanoparticle solution to which 9 µL 0.1 µg/mL CRP antigen was added – the nanostructure formation process being carried out at temperatures of (a) 25°C (b) 30°C (c) 37°C and (d) 40°C.

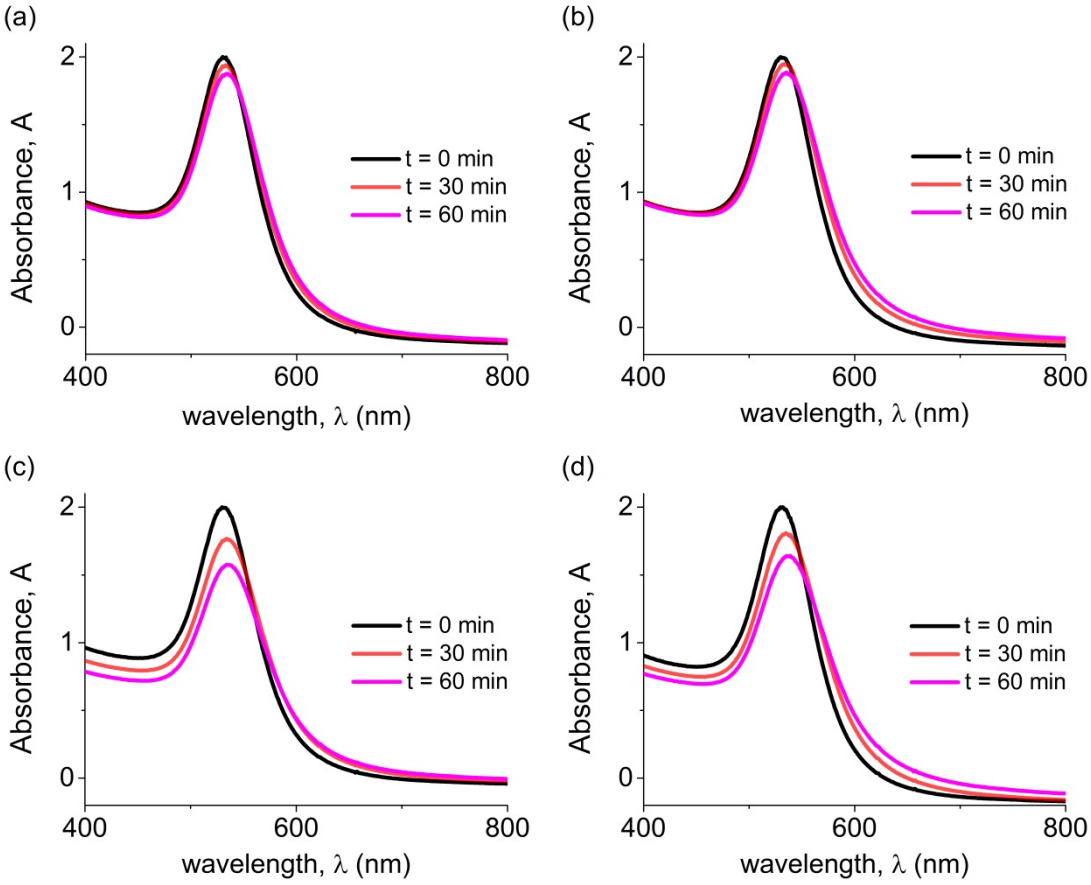

Figure 2.5: UV-visible absorbance spectra of antiCRP nanoparticle solution @ ~OD2 to which 9 µL of 0.1 mg/mL CRP antigen solution is added, recorded versus wavelength (λ) over 60 minutes, representing nanostructure formation at (a) 25°C (b) 30°C (c) 37°C and (d) 40°C.

Temperatures of 37ºC – 40ºC resulted in an increased rate of nanostructure formation, however, not to the extent that even after 60 minutes the colour change is not appreciable enough to detect with the human eye, i.e. at elevated temperatures of 37°C the solution still remained red days following addition of antigen linker molecules. Increased temperatures did not result in any adverse effects on the solution at an elevated temperature. Repeatability was also ascertained, see figure 2.6.

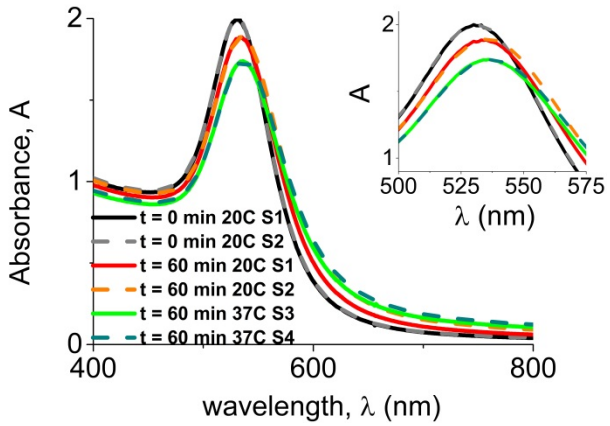

Figure 2.6: UV-visible absorption spectra, recorded versus wavelength over time, of two different C-reactive protein (CRP) antibody functionalized 40 nm diameter gold nanoparticle solutions, where the ratio of antigen linker molecules to nanoparticle is 18:1, performed at 20°C and two different C-reactive protein (CRP) antibody functionalized 40 nm diameter gold nanoparticle solutions where the ratio of antigen linker molecules to nanoparticle is also 18:1, performed at 37°C.

A control experiment was also carried out in parallel, to which no CRP antigen was added to determine the stability of the antiCRP NP solution at an elevated temperature of 37ºC, with harsh stirring, see figure 2.7.

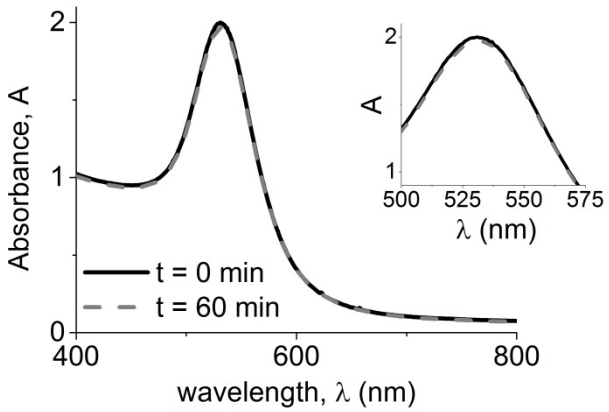

Figure 2.7: UV-visible absorption spectra recorded versus wavelength over time of C-reactive protein antibody functionalized 40 nm diameter gold nanoparticle solutions to which no CRP antigen linker molecules were added and where harsh stirring conditions at 37°C were employed.

Also gold nanoparticles functionalized with goat anti-mouse antibodies were used in place of CRP antibodies, see figure 2.8. In this case the number of antigen linker molecules per nanoparticle was also 2:1. Results demonstrated no red-shift of absorbance maxima to longer wavelengths or decrease in intensity. These results therefore ascertain robustness of the CRP antibody functionalized nanoparticle solutions to environmental conditions and specificity, with regard to nanoparticle self-assembly, i.e. dependence on presence of CRP antigen linker molecules to formation of nanostructures.

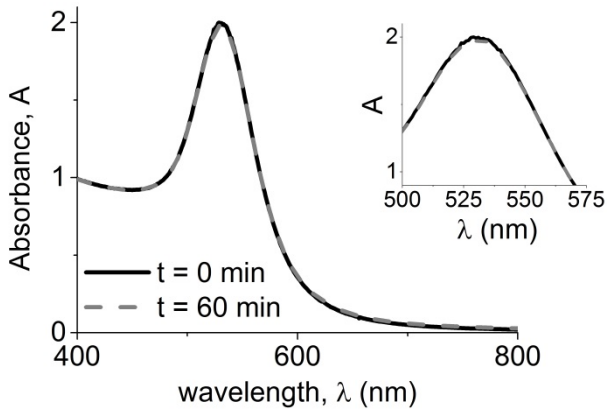

Figure 2.8: UV-visible absorption spectra recorded versus wavelength over time of a goat anti-mouse antibody functionalized 40 nm diameter gold nanoparticle solution (used in place of C-reactive antibody functionalized gold nanoparticle solution) where the ratio of antigen linker molecules to nanoparticle is 2:1.

2.3.3 Formation of NP- $Re_2(DMAA)_4(NCS)_2$ assemblies

Such control of the nanoparticle self-assembly process can be applied across different nanoparticle sizes and functionality as was additionally demonstrated employing 60 nm citrate-stabilized gold nanoparticle solution and $Re_2(DMAA)_4(NCS)_2$ linker molecules, which are ~1.2 nm in diameter as compared to the CRP antigen linker molecules which are ~ 11 nm in diameter. In this case many more $Re_2(DMAA)_4(NCS)_2$ linker molecules were required to replace the strong carboxylate-terminated citrate protectors. Supplying 1000 $Re_2(DMAA)_4(NCS)_2$ linker molecules per nanoparticle resulted in rapid nanoparticle assembly accompanied by a distinct solution color change, see figure 2.9 (a) while 14000 $Re_2(DMAA)_4(NCS)_2$ linker molecules per nanoparticle resulted in slow/restricted nanostructure formation, see figure 2.9 (b).

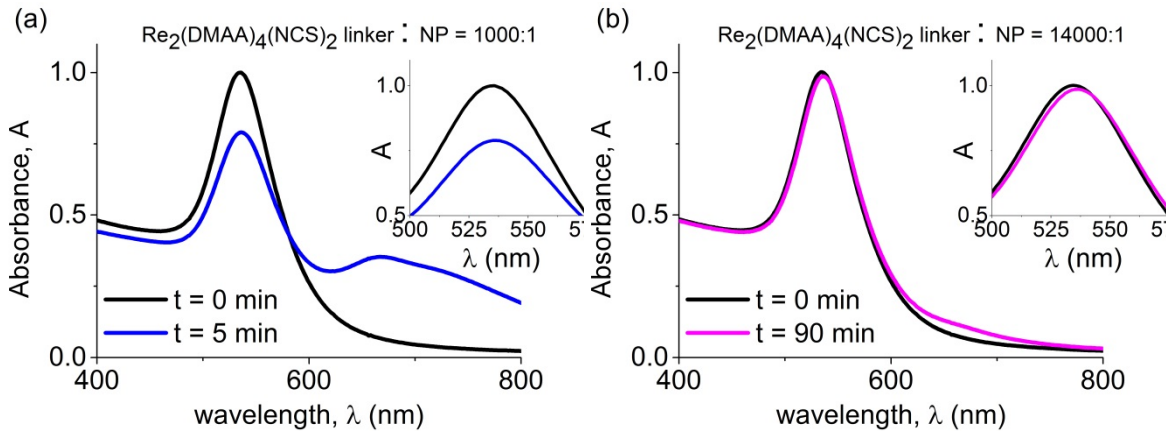

Figure 2.9: UV-visible absorption spectra, recorded versus wavelength over time, of citrate stabilized 60 nm diameter gold nanoparticle solutions to which (a) the ratio of $Re_2(DMAA)_4(NCS)_2$ linker molecules to nanoparticle is 1000:1 and (b) the ratio of $Re_2(DMAA)_4(NCS)_2$ linker molecules to nanoparticle is 14000:1.

2.3.4 Scanning electron microscopy characterization of assemblies

Scanning electron microscopy (SEM) is an excellent tool for the morphological study of nanoparticles and their assemblies but any solution must be dried onto a substrate before inserting into the SEM vacuum chamber. This drying process could possibly change the state of the solution species by inducing aggregation, dissociation or reorganisation which can add to ambiguities when interpreting SEM images.

To reinforce the UV-visible findings and ensure that the original solutions, on dilution with PBS solution, are composed of mostly monomers, aliquots of these solutions being analysed by UV-visible spectroscopy were removed at intervals for SEM analysis. To obtain reliable statistics of the nanoparticle/nanostructure population within a solution and also elimination of formation of nanostructures as a result of drying effects, the aliquots of solution removed from the diluted antiCRP NP solution under analysis were diluted by a factor of 100 to ensure a dilute sample and hence good spacing between nanoparticles/nanostructures deposited on the substrate. Individual silicon chips (substrate resistivity ~5 mΩcm) were used as substrates for SEM analysis. These substrates were rendered hydrophilic by immersion in H_2SO_4 and HCl : methanol (1:1) solutions for 30 minutes each. This ensured that the drop of solution spread out evenly over the substrate increasing the distance between nanostructures at the substrate surface. Single 50 µL drops of solution were deposited on each silicon chip. The excess solution was then wicked away by placing filter paper at the edge of the chip. The

remaining solution was allowed to air dry on the substrate and when dry, the substrate was rinsed in ultrapure deionised water and gently dried under a stream of nitrogen.

Following drop deposition and SEM imaging, manually counting the numbers of nanoparticles/nanostructures to obtain number populations of the various classes of nanostructures present was carried out. This illustrates that a dilution factor of 100 of the conjugate with PBS buffer resulted in close to 98% monomers, with only 3 dimers being present out of 162 nanostructures counted, thereby confirming that dilution of the antiCRP NP solutions with PBS solution and the drop deposition technique employed to prepare samples for SEM analysis did not result in the formation of "false" nanostructures and so is not only a suitable technique to confirm the stability of the gold conjugate upon dilution with PBS solution but also the drop deposition procedures used for preparation of SEM samples are suitable for application in quantifying the distribution of different classes of nanostructures formed *via* antibody-antigen recognition induced self-assembly on addition of CRP antigen to the gold conjugate solution. In order to quantify the distribution of nanoparticles and nanostructures on each individual substrate, representing the numbers formed at the various time intervals, SEM (JSM-7500F, JEOL UK Ltd.) was employed to record and statistically analyse the populations of monomers, dimers and higher order nanostructures.

For each substrate, at least 100 nanostructures were counted at 20+ random locations as determined using the "Step function" on the SEM's motorised sample stage, resulting in no more than 5 nanoparticles/nanostructures counted in each SEM image of area ~ 6 µm x 4.75 µm. Each image was inspected manually to count and thereby obtain the distribution of the different classes of nanostructures present for each image. Using the table of records for each sample, the mean value for each class is calculated. Figure 2.10 shows a typical SEM image containing dimers and a trimer. The histograms in figure 2.11, display the % of nanostructures containing each number of nanoparticles (NP) up to 10 NP per NS for the various time intervals for three repeat nanostructure formation experiments.

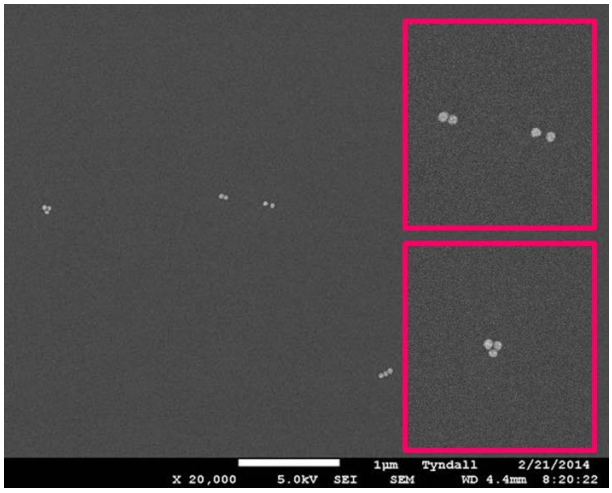

Figure 2.10: Typical scanning electron microscopy image used to determine the distribution of nanoparticles and nanostructures formed at various time intervals during the nanostructure formation process.

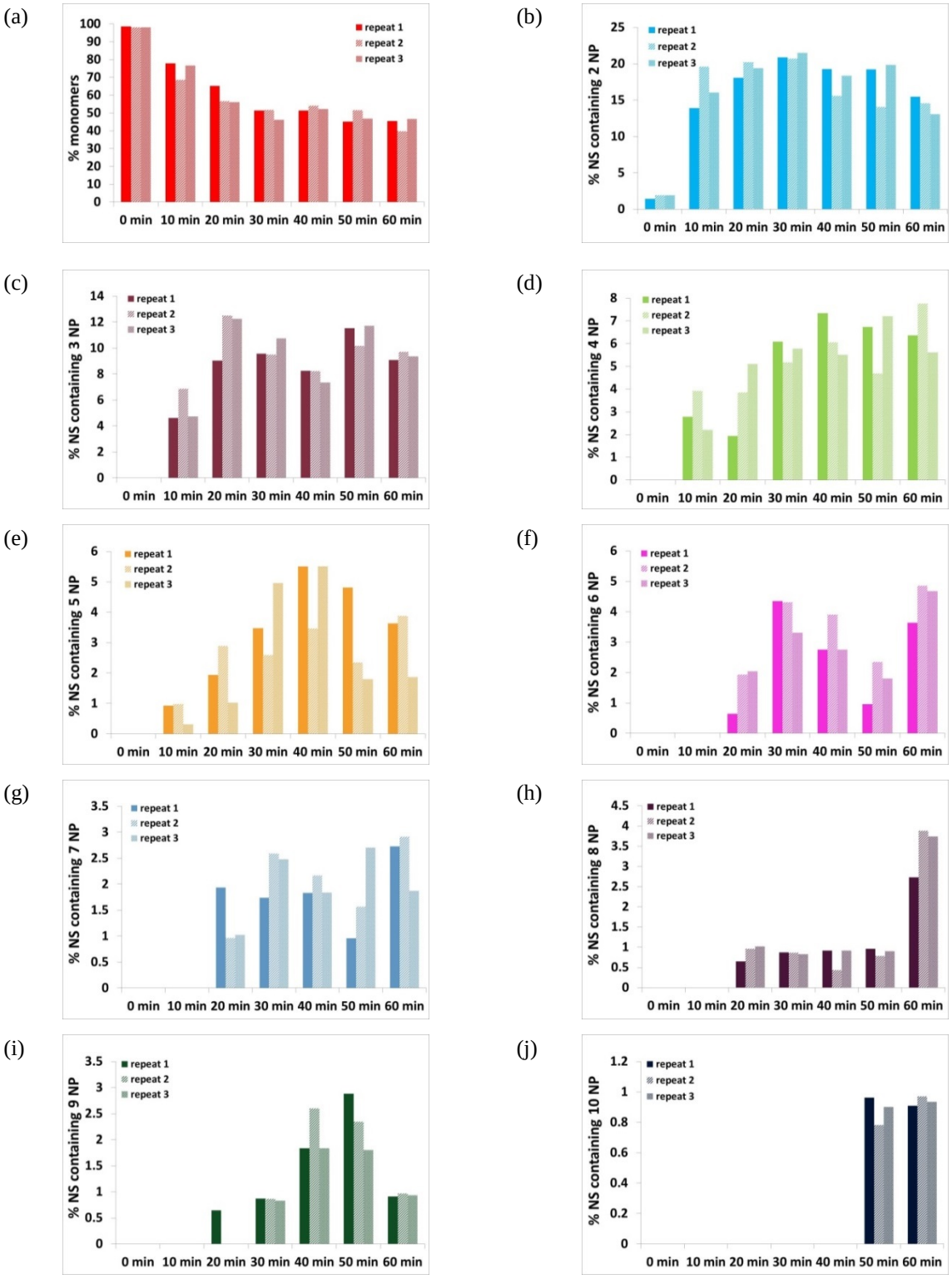

Figure 2.11: Histograms showing the distribution of nanostructures (NS) containing (a) one (b) two (c) three (d) four (e) five (f) six (g) seven (h) eight (i) nine (j) ten NP at various time intervals, present in the antiCRP NP solution following addition of 9 µL of 0.1 mg/mL CRP antigen solution (9 µL @ 0.1 mg/mL, 5.4 nM, 18 M:NP).

The histograms show the nanostructure distribution for each class of nanostructure based on numbers of the different classes of nanostructures manually counted from aliquots of solution drop deposited on substrates. Over 500 SEM images were taken across 21 substrates, with a minimum of 100 nanostructures counted at random locations for each substrate. It can be seen that a gradual decrease in the numbers of monomers occurs from 98% at the beginning of the nanostructure formation process to just 44% after 60 minutes. This correlates with the decrease in intensity of the transversal peak for the solution of gold nanoparticles as recorded with the UV-visible spectrophotometer.

After 10 minutes 15% of a total of 20% dimers have formed; 5% of a total of 12% trimers; 4% of a total of 8% nanostructures containing 4 nanoparticles and 1% of a total of 5% nanostructures containing 5 nanoparticles and after 20 minutes 19% of a total of 20% dimers have formed and 11% of a total of 12% trimers being formed. Formation of nanostructures containing 6, 7 and 8 nanoparticles emerges 20 minutes after commencement of the experiment, nanostructures containing 9 nanoparticles at 30 minutes and nanostructures containing 10 nanoparticles at 50 minutes with much less of them being formed and their formation being relied on more complex processes such as dissociation and formation of smaller clusters into larger ones. These results indicate that lower order nanostructures are eventually consumed in formation of higher order nanostructures which again correlates with the observations of the UV-visible analysis where a second peak at longer wavelength emerged as longer and branched chain nanostructure were formed.

These results are synopsised in figure 2.12 where prior to addition of CRP antigen 98% of nanostructures observed were single nanoparticles, see figure 2.12 (a). SEM analysis revealed that when the linker molecule: NP ratio = 2:1, 5% observed nanostructures were single nanoparticles with 78% nanostructures comprising 10 or more nanoparticles, see figure 2.12 (b) and when the linker molecule :NP = 18:1 18% observed nanostructures were single nanoparticles and only 4% nanostructures comprising 10 or more nanoparticles, see figure 2.12 (c).

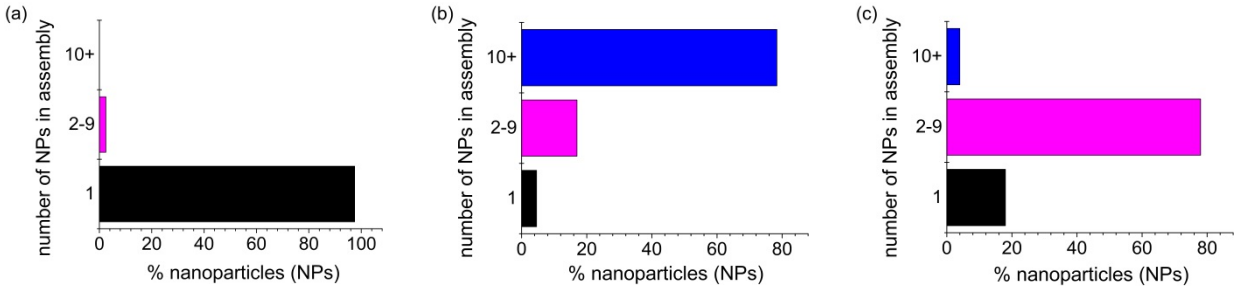

Figure 2.12: Scanning electron microscopy (SEM) analysis revealed that (a) 98% of nanostructures observed were single nanoparticles when linker molecule: NP = 0:1; (b) 5% observed nanostructures were single nanoparticles with 78% nanostructures comprising 10 or more nanoparticles when linker molecule: NP = 2:1, (c) 18% observed nanostructures were single nanoparticles and only 4% nanostructures comprising 10 or more nanoparticles when linker molecule :NP = 18:1.

One step further towards realising the benefits of formation of such assemblies involves modelling/simulation of the processes involved in the growth of these nanoparticle-biomolecule assemblies. This can, in part at least, be achieved by modelling the interactions in bulk solution between the nanoparticles and the molecules. Dr. Nicolas Sassiat developed a set of generation-recombination models and rate equations to do this. This section describes in brief and employs these set of rate equations to extract information pertaining to the growth of these assemblies over time in a given set of experimental conditions.

Modelling of the nanostructure formation process is not an easy task owing to the large number of parameters influencing this mechanism. The phenomenological model developed by Dr. Sassiat, based on a system of rate equations (superseding the initial full random-walk approach), see figure 2.13, captures many of these processes influencing the formation of nanostructures. The system of rate equations presented is of first order but non-linear. The high flexibility of the model, implemented using MATLAB routines developed by Dr Sassiat, allows for accounting of molecular decoration of nanoparticle surfaces quantitiatively, whereas effects like perturbation of the double layer around nanoparticle surfaces or solvation issues are qualitatively considered.

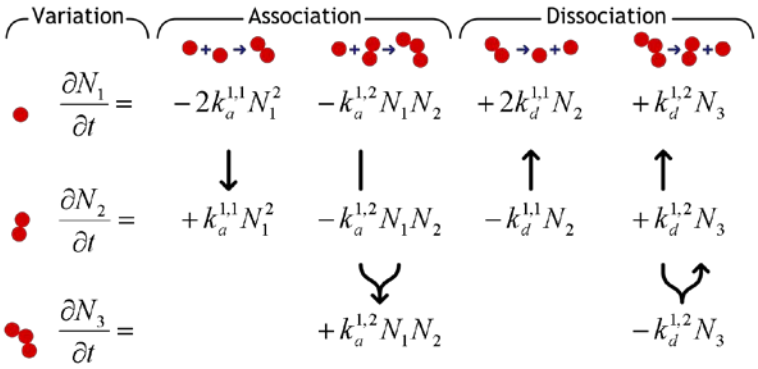

Figure 2.13: Equation for a three species system. [7]

On commencement of the nanostructure formation process, within the cuvette there are monodisperse nanoparticles, as demonstrated from control experiments and SEM counting statistics. In order to model the formation of nanostructures we need to know the numbers of nanoparticles and molecules present and thereby the concentrations of each at any given time. As the quantity and optical density of antiCRP NP solution and quantity and concentration of CRP antigen solution added to the cuvette is known, a good estimate of numbers of both nanoparticles and molecules present is therefore known. Thereby the concentration of each can be calculated (number normalised by the volume). As described earlier in the chapter, aliquots of solution are removed for SEM analysis during the experiment and also an aliquot of CRP antigen solution is added at the beginning. Even though these quantities are µL volumes (tiny) they are still taken into consideration when calculating concentration of the nanoparticles and molecules at various time points during the experiment. Therefore the number of nanoparticles and molecules at any time point in the experiment can be described. Mixing of the solution results in what should be an homogenous dispersal of both entities, so it is assumed that the distribution of nanoparticles and molecules is evenly dispersed, on average at all times.

These nanoparticles and molecules are moving around randomly. Locally self-diffusion exists due to the thermal energy carried by nanoparticles and molecules as described by the concept of random walk. In place of an analytical solution, Dr Sassiat utilised random walk simulations to estimate the rate of encounter of nanoparticles and molecules. The concept of random walk is widely used to model Brownian motion. Other factors governing the movement and transport of these nanoparticles and

molecules include diffusion and associated diffusion coefficients. Dr Sassiat addressed the classic Stokes Einstein relation to get an initial value for the translational diffusivity of 20 nm gold nanoparticles immersed in an aqueous solution. It is proportional to the thermal energy, inversely proportional to both the dynamic viscosity of the medium, and the hydrodynamic diameter of the diffusing nanoparticles taken as the nanoparticle diameter of 20 nm. The diffusivity of the molecules was accounted for by estimation according to values reported in literature for other molecules, which is accurate provided that the molecular mass is the leading term.

At the start the assemblies are simple single 40 nm nanoparticles. However, as dimers, trimers and higher order nanostructures form, the size and shape and therefore their diffusivity differs considerably. Ideally we need to know what the diffusivity is for any of the nanostructures involved. Dr. Sassiat employed a simple trend law employing geometric arguments based on nanostructure shapes observed.

So at the beginning there are just nanoparticles in the cuvette. CRP antigen molecules are then added and mixing results in an homogeneous mix of nanoparticles and molecules. In order for nanostructures to form, molecules need to collide with and bind to the nanoparticle surfaces. After collision, there are other factors which govern the propensity of a molecule to attach to the surface, such as the number of available binding sites on the surface, the number of available molecules in the pool and the adsorption rate constant. There are limited available binding sites on the surface of the nanoparticles, as determined by the number of CRP antibodies attached on the surface of the nanoparticles.

Modelling of the formation of nanostructures incorporates the processes of two mechanisms: molecules adsorbing and desorbing from nanoparticle surfaces and the association and dissociation of molecule bearing assemblies. The reverse reaction does not rely on a collision event. So nanoparticle growth implies four elementary rate coefficients: molecular linker coverage of a nanoparticle surface, h_a and molecular desorption from a nanoparticle, h_d, association of two clusters *via* linker molecules, driven by the coefficient k_a and dissociation of a cluster, driven by the coefficient k_d , see figure 2.14. Variations in populations of nanostructures are influenced by the balance between gains by the aggregation of lower order nanostructures or the dissociation of higher order nanostructures.

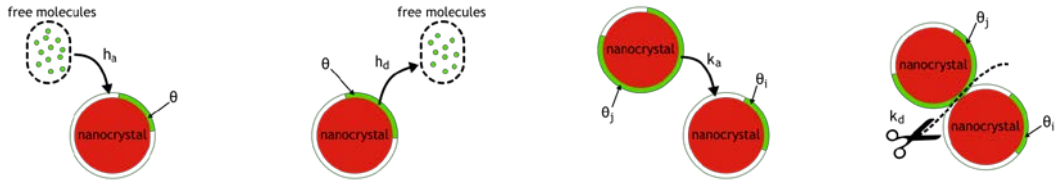

$$nc + ml \overset{h_a}{\rightarrow} (nc, ml) \qquad nc + ml \overset{h_d}{\leftarrow} (nc, ml) \qquad cl_i + cl_j \overset{k_a}{\rightarrow} cl_{i+j} \qquad cl_i + cl_j \overset{k_d}{\leftarrow} cl_{i+j}$$

Figure 2.14: Schematic (not to scale) of the four elementary steps involved in nanostructure growth. In the chemical equations, *nc*, *ml* and *cl* stand for nanoparticle, molecule and cluster, respectively. [7]

Once molecules begin to attach to the nanoparticle surfaces nanostructure formation can then commence. The formation of nanostructures does not require full coverage with molecules. In fact full coverage on all nanoparticles should prevent formation of nanostructures as all antibody binding sites would be occupied by antigen, which shouldn't bind to another antigen. When nanoparticles or nanoparticles and nanostructures collide, two situations accommodating the efficiency of binding/aggregation can be described: there is at least one CRP antigen molecule bound to the surface attached CRP antibody, or molecular stacking impedes the binding based on steric factor. Therefore a description of the influence of molecules in the system is incorporated in the rate constants. Rate constants can be split into three main components: the attempt frequency, *Z*, the likelihood of the reaction due to potential steric factor, *S* and the exponential factor due to the energy barrier to be overcome, *W*. Once in contact with the surface, anchoring is the next step, governed by anchor groups and recognition-induced effects. Once anchored the second step involves molecular rearrangement driven by intermolecular interactions. It is of interest to determine what the limiting process in the reaction is. Either the molecules are limiting and so the attempt frequency is not too often or the energy barrier to be overcome is limiting.

In order to model what is happening during the nanostructure formation process as described earlier in the chapter, we need to extract the numbers of different nanostructure types formed at various time points during this process. There are two ways of achieving this: firstly UV-visible spectroscopic analysis employing the Beer Lambert law which states that the absorbance is equal to the extinction coefficients multiplied by concentration and path length. However, to build the modelled spectrum of pure nanostructures, their extinction coefficients are required to be determined. The

extinction coefficients of pure monomers are obtained by recording the UV-visible spectrum of a solution of monodisperse nanoparticles before any modification. Generalised Multiple Mie (GMM) method to investigate the optical response (extinction cross-section) of clusters of spherical particles was employed by Dr. Gaetan Leveque, former researcher at Photonics Theory Group, Tyndall, to simulate the optical spectrum of dimers. However, at present it is not possible to get the experimental spectrum of individual higher order nanostructures, since there is no reliable technique to achieve mono-dispersed samples of such species and simulations based on Mie theory have the disadvantage that the computation of spectra becomes ever more complicated with higher order nanostructures.

For this reason, in this case, only population data is extracted from SEM counting statistics. A lengthy counting routine is performed manually on the SEM images taken. The numbers of nanostructures for each class is recorded for each image, as previously described. Using the table of records of each sample, the mean value of each class of nanostructures observed is calculated. The accuracy of the calculated concentration is subject to the maximum number of nanostructures taken into account. Choosing an unrealistically small value would introduce a bias in the statistics but a sufficiently large value ensures relevance to the family of concentrations. Compared to the Beer Lambert law fit, the analysis of SEM sample images offers the possibility of estimation of a broader range of entities that may be formed. Nanoparticle assemblies comprising up to ~10 nanoparticles can be counted for high accuracy.

The principle of curve fitting is based on comparing the locus of a suggested curve to the curve of the raw data. The difference between suggested points and measured points needs to be minimised, resulting in an R^2 value close to 1. The parameters which result in giving the best "fit" to the experimental data are outputted along with a graphical representation of the fit versus the experimental data. Experimental concentrations of nanostructures estimated for each time interval are represented by the red circles and the best fit curve by green circles. The energy barrier to be overcome is considered, originating from the concept developed in Arhennius' law, $k = Ae^{-Ea/(k_B T)}$, where k = rate constant, A = pre-exponential factor, E_a = activation energy, k_B = Boltzmann constant and T = absolute temperature in Kelvin, see figure 2.15. The corresponding activation energies can then be calculated so as to provide a value for the enthalpy of molecular binding and nanostructure formation, $\Delta H = E_a - E_d$.

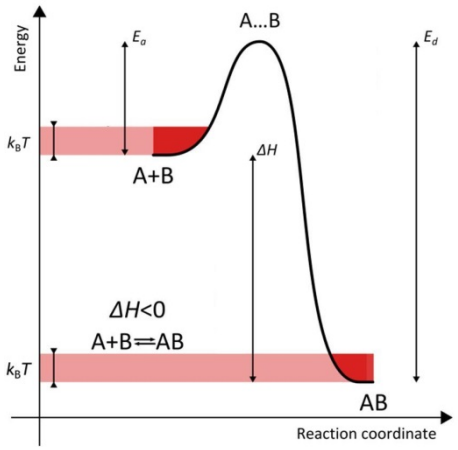

Figure 2.15: Energy diagram of the molecular decoration of nanoparticle surfaces and cluster formation along the reaction coordinate. [7]

It is shown that the model can accommodate and essentially fit the distributions of nanostructure populations found experimentally through scanning electron microscopy analysis, see figure 2.16. The corresponding activation energies can then be calculated so as to provide a value for the enthalpy of molecular binding and nanostructure formation, $\Delta H = E_a - E_d$, see table 2.2. These estimates indicate that the enthalpies of both processes are negative and so the reactions are exothermic. This indicates that a system comprising a linker molecule and a bare nanoparticle has its energy lowered when the molecule is bound on the nanoparticle surface and so bound nanoparticles are unlikely to dissociate. This leads to the conclusion that the products are more thermodynamically stable than the reactants. The formation of nanostructures is driven by antigen adsorption on an antibody functionalized nanoparticle surface and the association of antigen-bearing nanostructures. Previous work by Dr. Sassiat estimated the rate of encounter of 20 nm nanoparticles and $Re_2(DMAA)_4(NCS)_2$ linker molecules to be of the order of seconds. Considering the 40 nm nanoparticles employed in this work we can deduce that antigen binding on the nanoparticles is complete within a short time interval (seconds) and the nanoparticle coverage with antigen molecules remains the dominant factor in controlling the nanostructure formation process. The max number of antigen molecules that can bind on the nanoparticle surface was determined to be 8 which correlates with the number of antigen molecules determined experimentally which resulted in slow/restricted nanostructure formation.

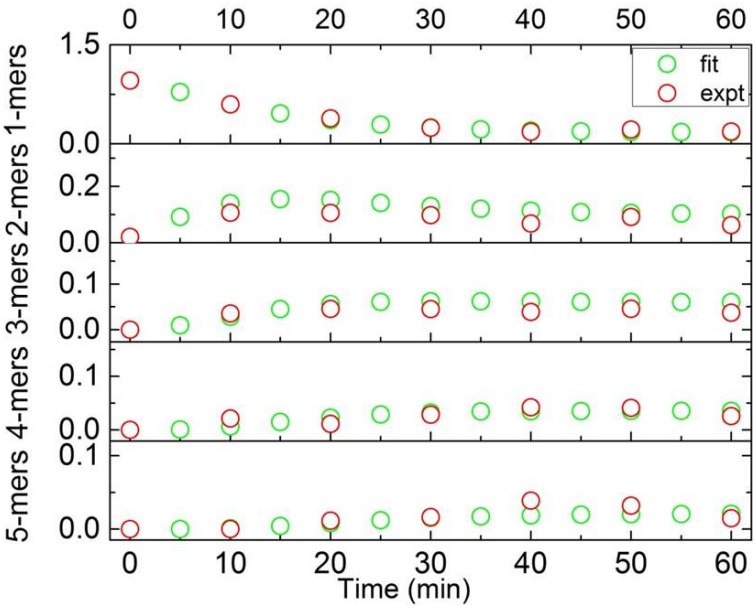

Figure 2.16: Experimental data fitting employing the rate-equation model for distributions of nanoparticle assemblies counted at various time intervals taken from a solution of CRP antibody-functionalised nanoparticle solution to which 9 µL 0.1 mg/mL CRP antigen solution was added.

Parameter	Output	Parameter	Output
R^2	0.913	$E_{a\ NP\ ml}$	120 meV
h_a ($\mu m^3 s^{-1}$)	5.4E-5	$E_{d\ NP\ ml}$	450 meV
h_d (s^{-1})	1.5E-5	$\Delta H_{NP\ ml}$	-330 meV
k_a ($\mu m^3 s^{-1}$)	4.9E-3	$E_{a\ cl\ cl}$	60 meV
k_d (s^{-1})	2.5E-3	$E_{d\ cl\ cl}$	400 meV
ml_{max}	8	$\Delta H_{cl\ cl}$	-340 meV

Table 2.2: Summary of the rate-equation output parameters at 60 minutes after commencement of the nanostructure formation process, corresponding to Figure 2.16.

2.4 Conclusions

Nanoparticle self-assembly was demonstrated as an attractive technique to facilitate point-of-care detection of C-reactive protein (CRP). A CRP antigen concentration of 0.06 µg/mL was detected evidenced as a distinct solution colour change from red to blue within 5 minutes. The strong light scattering of the gold nanoparticles facilitated this visual detection void of complex chemical processes and elaborate equipment, facilitating rapid inexpensive POC detection while concurrently maintaining the specificity, stability and sensitivity of the assay.

Employing just gold nanoparticles functionalized with CRP antibodies and CRP antigen as linker molecules, control of the rate of nanoparticle recognition-induced self-assembly was achieved between that of rapid formation of large nanostructures with associated solution colour change from red to blue within 5 minutes, and slow formation of small nanostructures over hours with no discernable solution color change. The key factor causative of that controlled self-assembly being the linker molecule-nanoparticle ratio and can be controlled to enable detection across a wide CRP concentration range.

Such control of the rate of nanoparticle self-assembly was corroborated employing nanoparticles of different functionality demonstrating applicability to detection of other molecules of interest. The self-assembly of 60 nm citrate-stabilized gold nanoparticle solution and $Re_2(DMAA)_4(NCS)_2$ linker molecules also resulted in a distinct solution colour change from red to blue within 5 minutes while elevated $Re_2(DMAA)_4(NCS)_2$ linker molecule concentrations resulted in slow/restricted nanostructure formation.

Such a sensitive, specific, stable, rapid detection mechanism provides for POC sensing at, for example, a GP surgery or hospital setting, using a hand-held spectrometer, facilitating provision of immediate and accurate test results. It also provides for detection at a range of near-patient settings, most particularly in resource-constrained settings, providing a simple, inexpensive visual detection means.

2.5 References

1. Chen, X.; Wang, Y.; Zhou, J.; Yan,W.; Li, X.; Zhu, J.J, Electrochemical impedance immunosensor based on three-dimensionally ordered macroporous gold film. *Anal. Chem* **2008**, *80*, 2133–2140.

2. Yuan, G.; Yu, C.; Xia, C.; Gao, L.; Xu, W.; Li, W.; He, J, A simultaneous electrochemical multianalyte immunoassay of high sensitivity C-reactive protein and soluble CD40 ligand based on reduced graphene oxide-tetraethylene pentamine that directly adsorb metal ions as labels. *Biosens Bioelectron* **2015,** 72, 237-46.

3. Prasad, S.; Selvam, A.P,; Reddy, R.K,; Love, A, Silicon nanosensor for diagnosis of cardiovascular proteomic markers. *J Lab Autom* **2013**, 18, 143-51.

4. Hu, W.P.; Hsu, H.Y.; Chiou, A.; Tseng, K.Y.; Lin, H.Y.; Chang, G.L.; Chen, S.J, Immunodetection of pentamer and modified C-reactive protein using surface plasmon resonance biosensing. *Biosens Bioelectron* **2006,** 21, 631-7.

5. Islam, M.S.; Kang, S.H, Chemiluminescence detection of label-free C-reactive protein based on catalytic activity of gold nanoparticles. *Talanta*. **2011,** 84, 752-8.

6. Liu, Z.; Li, W.; Han, G.C.; Yuan, S.; Chen, Z, Towards label-free impedance biosensors: CRP probe based on thiol schiff-nickel complex modified gold nanoparticles. *J. Electrochem. Soc* **2014,** 161, B75-B80.

7. Sassiat, N. P. 2011, Formation and electrical interfacing of nanocrystal-molecule nanostructures. PhD Thesis. University College Cork.

8. Yang, M,; Chen, G,; Zhao, Y, *et al*, Mechanistic investigation into the spontaneous linear assembly of gold nanospheres. *Physical Chemistry Chemical Physics* **2010**, 12, 11850-11860.

9. Malola, S,; Lehtovaara, L,; Enkovaara, J,; Hakkinen, H, Birth of the localized surface plasmon resonance in mono layer-protected gold nanoclusters. *ACS Nano* **2013**, 7, 10263-10270.

10. Jain, P.K,; El-Sayed, M.A, Surface plasmon coupling and its universal size scaling in metal nanostructures of complex geometry: elongated particle pairs and nanosphere trimers. *Journal of Physical Chemistry C* **2008**, 112, 4954-4960.

Chapter 3

Electrical Characterisation of C-Reactive Protein Antibody-Antigen Binding

3.1 Introduction

Employing just gold nanoparticles functionalised with C-reactive protein (CRP) antibodies and CRP antigen as linker molecules, control of the rate of *solution-phase* nanoparticle recognition-induced self-assembly was achieved resulting in visual detection of CRP within 5 minutes, demonstrating applicability to point-of-care (POC) sensing. Surface-based assays also show much promise in application to POC sensing. It was of interest to determine if *surface-based* assays void of complex chemical processes and elaborate equipment could compete with laboratory-based assays in terms of specificity, stability and sensitivity but also offer faster and inexpensive diagnosis.

The binding of CRP antibody to silanised silicon-silicon oxide substrates with gold micron-scale electrodes implemented using the organosilane (3-Aminopropyl)triethoxysilane (APTES) and the subsequent binding of CRP antigen to this immobilised CRP antibody was explored. When a protein is immobilised on the surface of an electrode pair it introduces a capacitance component in the impedance response of the sensor. When the pair of electrodes is exposed to another protein that couples to the immobilised protein, a complex is formed, resulting in a corresponding decrease of the sensor capacitance.

The binding of antigen to antibody however results in small and extremely localised conformational and charge related changes in the antibody structure which have proven difficult to measure with great sensitivity. Despite the limitations associated with surface-based assays, electrical characterisation of the binding event of CRP antigen to surface immobilised CRP antibody in ambient conditions facilitates characterisation of the reaction occurring at the biosensor surface in the presence of such limitations to determine if nanoparticle amplification would be required to facilitate rapid surface-based POC detection of CRP.

3.2 Experimental

3.2.1 Chemical modification of substrate surface through silanisation

Classical 100 mm wafers of silicon, p-type (~ 1 – 30 mΩ.cm) were used. Wafers were oxidised in a furnace providing a smooth natural 300 nm of silicon oxide. Electrodes were fabricated using optical beam lithography, metal evaporation and lift-off employing a mask composed of 500 nm thick gold electrodes and gap sizes with critical dimensions down to 1 µm. Also, larger contact pads for ease of probing. Substrate preparation involved immersion in R1165 followed by a solvent clean and plasma ashing 50 W 1.5 Torr 10 minutes (March GCM-200, March Instruments Inc.). The role of key parameters such as silane type, solvent used, reaction time and concentration has been researched extensively previously as described in literature. [1,2,3,4] In this research, liquid phase silanisation was performed under ambient conditions using APTES - (3-Aminopropyl)triethoxysilane 99% (Sigma Aldrich). APTES chemically modifies the surface without forming a layer of appreciable thickness. For practical purposes, it is readily available for purchase and relatively inexpensive. Silanisation conditions of 3% APTES in methanol: ultrapure deionised water 19:1 and a reaction time of 30 minutes were used. After immersion of the substrates in silane solution for 30 minutes, they were rinsed in methanol and then ultrapure deionised water and dried in a stream of nitrogen. The substrates were then cured in an oven at 120°C for 15 minutes. Following this they were immersed in 20 nm citrate-capped nanoparticle solution, optical density 1 for 3 hours to determine the efficiency of the pre-treatment and silanisation processes.

3.2.2 Surface immobilisation of CRP antibody and antibody-antigen binding

C-reactive protein antibody (CRP) was covalently bound to the silanised substrates. A temperature of 4°C was used and a concentration of 100 µg/mL prepared by dilution of the as supplied CRP antibody with phosphate buffered saline (PBS) solution. A 50 µL aliquot of this CRP antibody solution was placed on each substrate and kept in humid conditions at 4°C overnight (16 hours). Substrates were then rinsed with 10 mM PBS buffer + BSA before binding of CRP antigen. Again this process was repeated a number of times to ensure reproducibility (determining binding process using goat anti-mouse (GAM) conjugate to mark the presence of the CRP antibody). Control experiments were

performed to ensure that antiCRP NPs did not directly bind to the CRP antibody functionalised surface in the absence of CRP antigen. Binding of CRP antigen to CRP antibody was performed at antigen concentrations of 10 µg/mL and 20 µg/mL.

3.2.3 Electrical characterisation of CRP antibody-antigen binding

Substrates were mounted in a manual probe station (Wentworth Laboratories PML 8000) using low-leakage, manual, linear motion probe arms (Wentworth Laboratories PVX500) and shielded by a Faraday cage. Substrates were initially optically examined to ensure structural integrity of the devices. Measurements were performed using an Agilent E4980A LCR meter, incorporating VEE software interfaced to a PC. The influences of unwanted stray capacitance, e.g. cables are eliminated by calibration by performing an open and short measurement. Initially large voltage bias and frequency conditions were explored. It was found that instabilities, e.g. hysteresis were minimal at voltage biases ~ 20 mV. 100.025 kHz was employed as the frequency to characterise the binding event. Devices were characterised in ambient conditions. The source drain bias was swept in the sequence -20mV 0V +20mV 0V -20mV for all measurements to quantify the influence of hysteresis, obtaining therefore two different traces for a given bias polarity. Initial survey measurements of devices were performed using 20 data points per sweep with voltage step sizes of 2 mV. Later 80 data points were used with voltage step sizes of 0.5 mV.

3.2.4 ANSYS simulations

Simulations pertaining to the silicon-silicon oxide substrates and gold micron-scale device structures were performed by Mr Liam Floyd, Compound Semiconductors Group, at Tyndall National Institute using ANSYS Q3D Extractor. The device structure is laid out for Ground-Signal S-parameter measurements so in the simulations these were simulated and then the resistance, capacitance, line inductance and leakage conductance determined. A 3D model of the device structure was employed in the simulations. Capacitance values were simulated whereby a quasi-static electromagnetic field analysis using Finite Element Method (FEM) was employed. FEM involves splitting the entire volume of the structure under analysis into a 3D mesh involving

different shapes, for example, tetrahedrals, polygons and rectangular blocks. Initially a course mesh attempts a solution, whereby the regions where the quantities of electric and magnetic fields are changing most rapidly are examined, following which these regions are meshed more finely to reach the solution. This precedes matrix calculations to estimate the electric and magnetic fields. The electric and magnetic fields are considered separately but finally coalesced to reach a combined solution.

3.2.5 Dielectrophoresis

Prior to dielectrophoresis electrodes were solvent cleaned. Any residue on the electrodes impedes the dielectrophoretic trapping process. All chips were ashed in O_2 plasma (March Plasmod, 0.5 Torr, 20 W, 3 min). A waveform generator Agilent AG33220A was used to carry out dielectrophoresis. The samples were mounted in a manual Wentworth PML8000 probe station. A drop (10 μL) of nanoparticle solution, diluted 1:10 with ultrapure deionised water was placed on the substrate. AntiCRP nanoparticle solution diluted with ultrapure deionised water and also PBS solution was also employed. In most cases where the probes were lowered prior to adding a drop of the nanoparticle solution, damage to the electrodes was obvious even by optical inspection. Therefore, the probes were lowered to the substrate after the drop of nanoparticle solution had been added. Voltage and frequency parameters as well as trapping time were optimised.

3.3 Results and Discussion

3.3.1 Electrical characterisation of CRP antibody-antigen binding

Measured capacitance was employed as it resulted in greatest repeatability and reproducibility. Initially many measurements were performed on each device to determine stability and repeatability, with ΔC_{max} between repeat measurements = $1.1E^{-15}$ and between voltage steps = $3E^{-16}$. Following this, one measurement was performed per device, see figure 3.1.

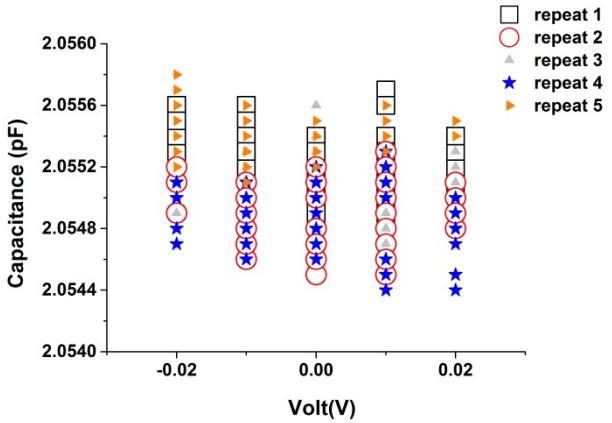

Figure 3.1: Five measurements in succession were carried out on devices. ΔC_{max} between repeat measurements = $1.1E^{-15}$ and between voltage steps = $3E^{-16}$.

Measured capacitance of devices on silicon-silicon oxide substrates prior to surface functionalisation revealed a clear differentiation between capacitances of row 1 and row 4 devices and row 2 and row 3 devices, likely due to electric field effects of neighbouring devices, i.e. row 1 and row 4 devices have devices adjacent to them on only one side while row 2 and row 3 devices have devices adjacent to them on both sides, see figure 3.2. This trend was accounted for in successive measurements.

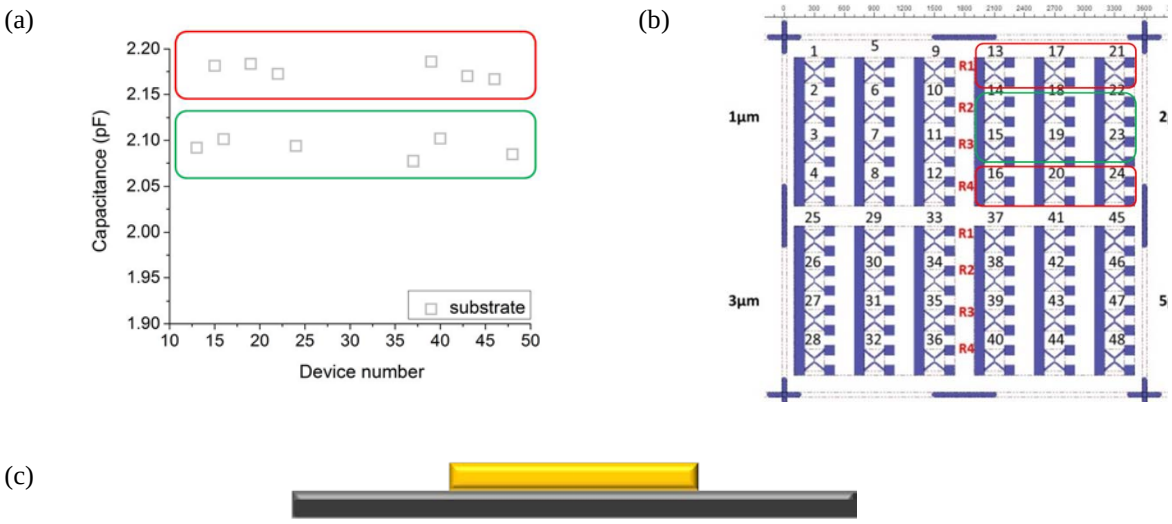

Figure 3.2: Measured capacitances (a) show a clear differentiation between those of row 1 and 4 devices and row 2 and 3 devices represented schematically in (b) prior to surface functionalisation, represented schematically in (c).

Measurements were performed dry on each 2 µm device (devices 12 – 24) and each 5 µm device (devices 37 – 48) for each process step commencing with the APTES functionalisation and antibody immobilisation steps, see figure 3.3.

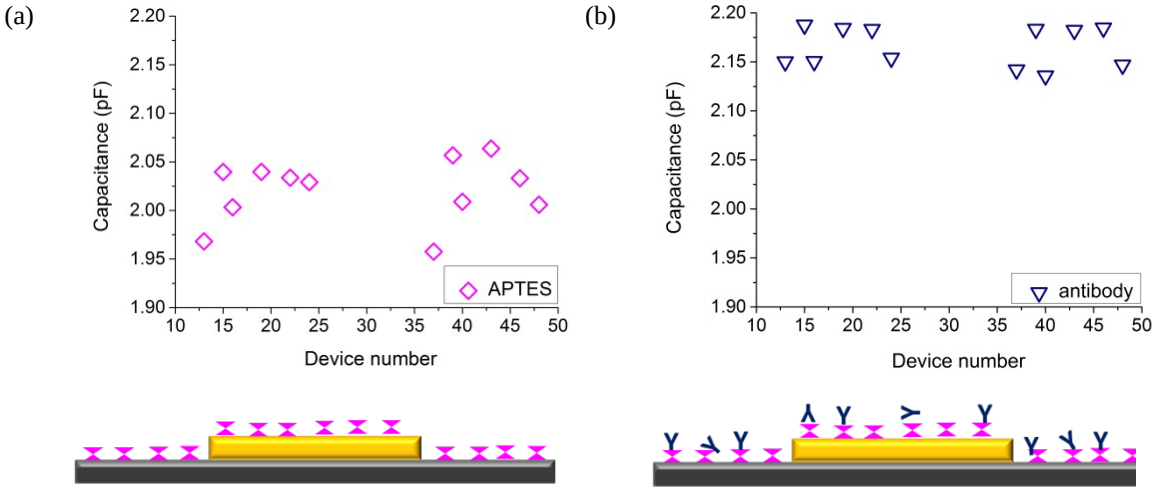

Figure 3.3: Measured capacitances of substrates (a) functionalised with APTES and (b) following C-reactive protein (CRP) antibody immobilisation.

A control measurement was performed whereby, substrates with CRP antibody immobilised were immersed in phosphate buffered saline (PBS) solution for 2 hours, to ensure integrity of the immobilised antibody layer post immersion in PBS solution, as employed in antigen binding steps. No appreciable change in capacitance was observed, see figure 3.4.

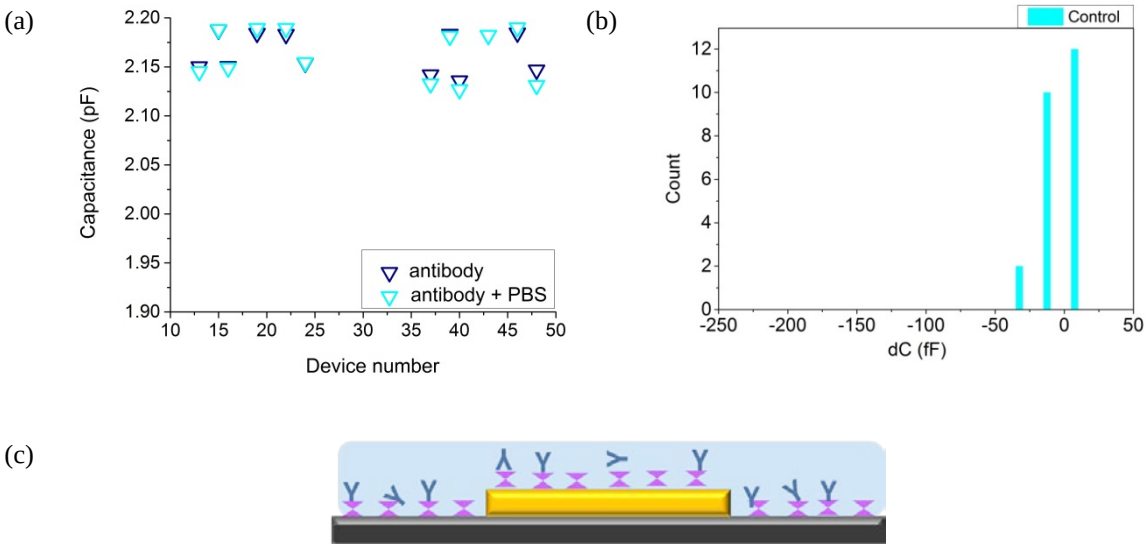

Figure 3.4: (a) Measured capacitances of substrates with C-Reactive protein (CRP) antibody immobilised and substrates with CRP antibody immobilised followed by immersion in phosphate buffered saline (PBS) solution for 2 hours, represented schematically in (c), demonstrates integrity of the immobilised antibody layer post immersion in PBS solution with (b) no appreciable change in capacitances.

The electrical characterisation which is of importance in detection of CRP is the characterisation of the binding of CRP antigen to CRP antibody. The measurement performed is a differential one. If there was no response to the control addition and there was a response to addition of CRP antigen then it was considered that a positive response specific to antigen binding antibody was seen. When antigen bound antibody, a resulting decrease in capacitance was observed. The limitations associated with the small signal intrinsic of biomolecular binding of antigen to antibody were evident. The magnitude of change in capacitance depended both on the concentration of the CRP antigen and also the length of time the devices were exposed to CRP antigen solution, see figure 3.5 whereby substrates were exposed to 10 µg/mL CRP antigen for 2 hours, figure 3.6 substrates exposed to 20 µg/mL CRP antigen for 10 minutes and figure 3.7

substrates exposed to 20 µg/mL CRP antigen for 2 hours, demonstrating detection of CRP antigen in a clinically relevant range.

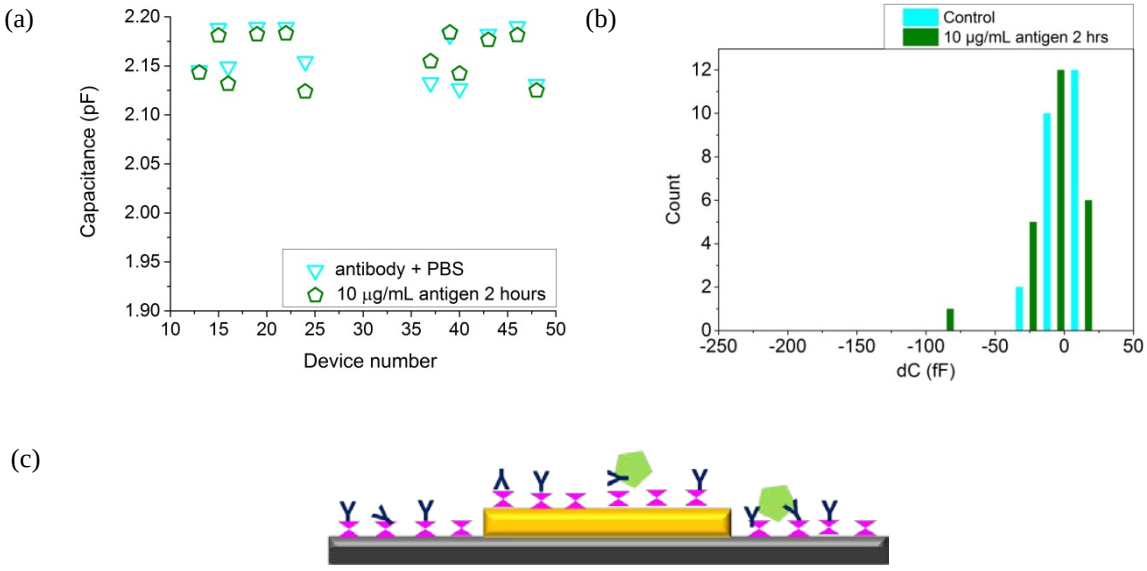

Figure 3.5: (a) Measured capacitances of substrates post C-reactive protein (CRP) antibody immobilisation and binding of CRP antigen (10 µg/mL 2 hours), (b) ΔC and (c) schematic representation.

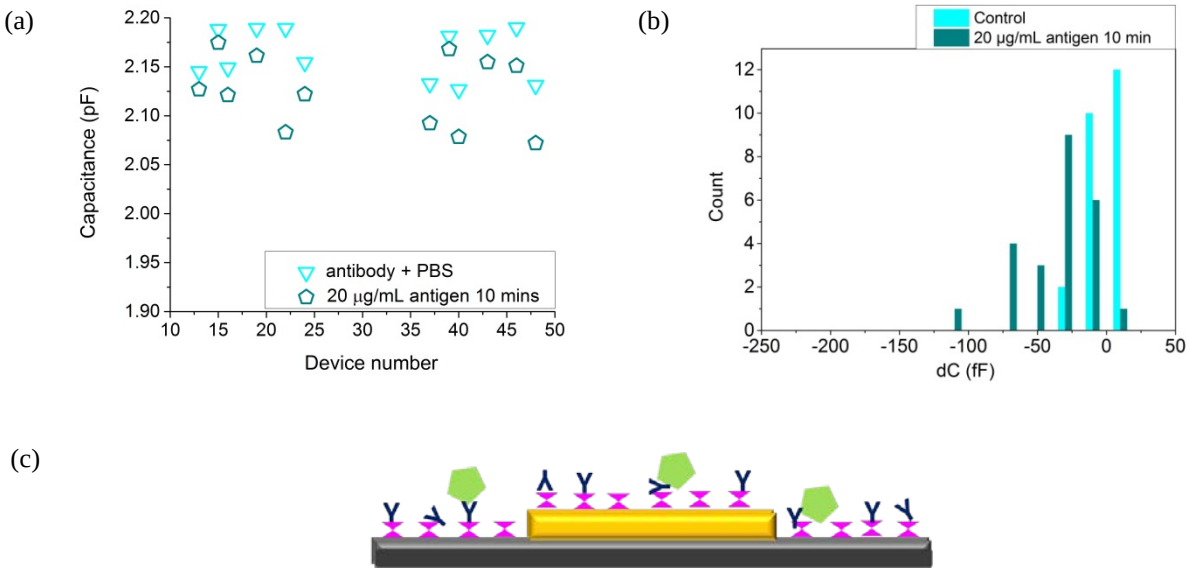

Figure 3.6: (a) Measured capacitances of substrates post C-reactive protein (CRP) antibody immobilisation and binding of CRP antigen (20 µg/mL 10 mins), (b) ΔC and (c) schematic representation.

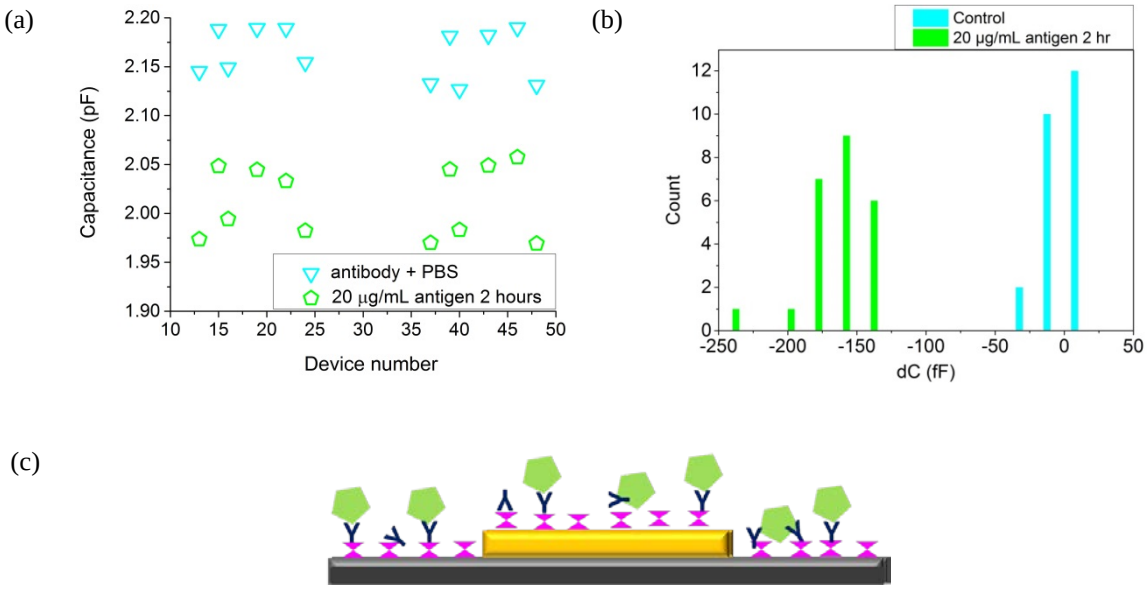

Figure 3.7: (a) Measured capacitances of substrates post C-reactive protein (CRP) antibody immobilisation and binding of CRP antigen (20 µg/mL 2 hours), (b) ΔC and (c) schematic representation.

3.3.2 ANSYS simulations

Simulations employing a 3D model of the device structure, see figure 3.8 (a), enabled prediction of the performance and improvement of substrates aimed towards surface-based point-of-care detection. Capacitance was simulated whereby a quasi-static electromagnetic field analysis using finite element method was employed. Initial simulations were performed taking the silicon to be lossless. The simulated values of line resistance, conductivity of the gold and line inductance agreed with calculated and previously reported values [5] with simulated leakage conductance = 0 as expected for lossless silicon. Simulations were then performed of the entire device structure setting the silicon resistivity at 3 S/m, see figure 3.8 (b) which is in agreement with measured capacitance values, see figure 3.2.

These simulations demonstrate that leakage through the substrate dominates the electrical response when measurements are taken at 100.025 kHz. When the silicon resistivity was set at 100 times better than the present upper resistivity of 3 S/m, i.e. 0.03 S/m, combined with measurement in the > 10 GHz regime, such losses are overcome, see figure 3.8 (c). Alternative means to overcome such losses include use of

quartz or ceramic substrates. However, simulations also reveal that water, even in the form of a layer of moisture on the device surface, contributes greatly to the capacitance response, see figure 3.8 (d) and even on elimination of losses through the substrate this contribution has to be considered. This guides further development of the process potentially enabling application to electrical surface-based point-of-care detection of analytes of interest.

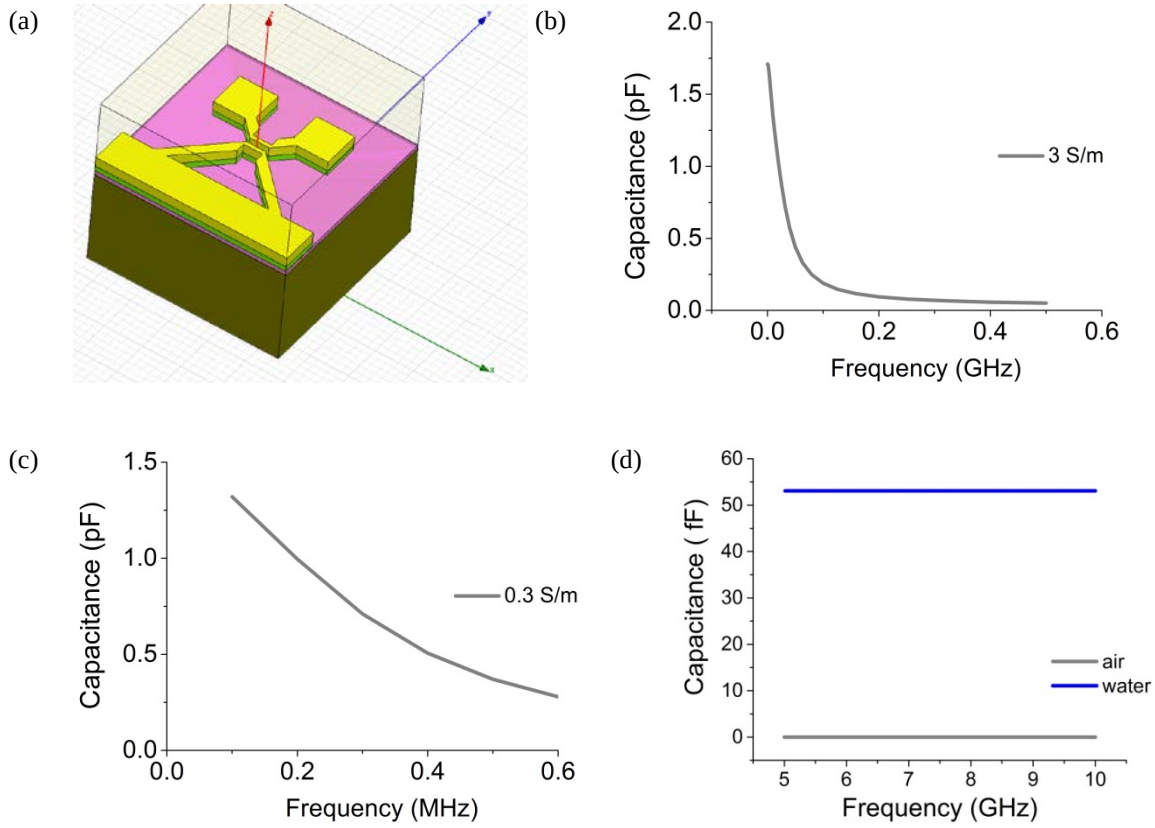

Figure 3.8: Simulations as performed in ANSYS employing a 3-D model of the device structure (a) (with exaggerated dimensions) and quasi-static electromagnetic field analysis using finite element method to estimate capacitance associated with lossless silicon-silicon oxide substrates and silicon with resistivity of (b) 3 S/m and (c) 100 times better than the present upper resistivity of 3 S/m (0.03 S/m). Also, (d) setting the silicon resistivity as lossless with the device structure covered in water.

3.3.3 Dielectrophoresis

While electrical characterisation facilitated characterisation of the reaction occurring at the biosensor surface in the presence of limitations such as small charge related changes, it was deemed advantageous to employ nanoparticle amplification to facilitate rapid point-of-care surface-based detection of CRP. Dielectrophoresis was explored as a means for the directed assembly of nanoparticles and nanostructures between gold micron-scale electrodes using AC electric fields with frequencies in the MHz range. [6,7,8] Voltage and frequency parameters as well as trapping time were optimised. The data shows a clear influence of the peak-peak voltage on the quantity of nanoparticles trapped. The SEM images show increasing numbers of nanoparticles trapped as $V_{p\text{-}p}$ was increased, see figure 3.9.

(a) (b)

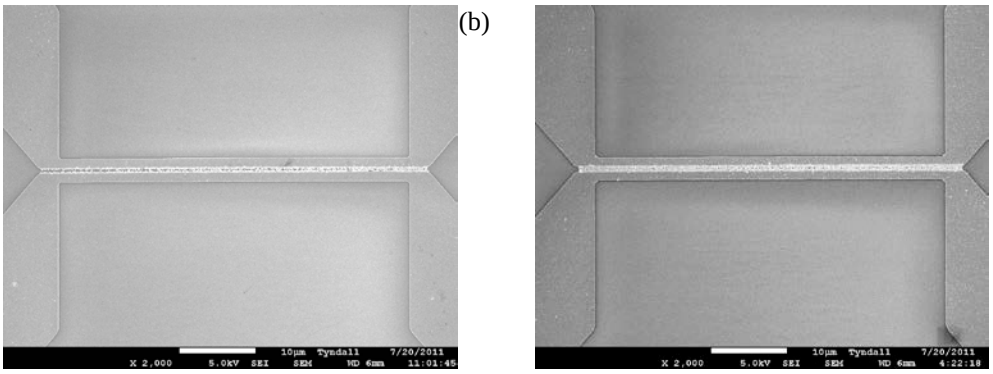

Figure 3.9: Scanning electron microscopy (SEM) images of microelectrodes (500 nm gaps) used to investigate the voltage required to overcome the electrostatic potential at the electrode-solution interface for d = 40 nm citrate-capped gold nanoparticles, (a) fdep = 1 MHz, tdep = 300 s, V = 8 V, (b) fdep = 1 MHz, tdep = 300 s, V = 10 V.

Hence f=1 MHz and peak-to-peak amplitude ($V_{p\text{-}p}$) in the range of 8 V ≤ $V_{p\text{-}p}$ ≤ 10 V being applied for 5 minutes resulted in trapping of particles in > 90% of devices, the process being repeated across 3 sets of 4 microgaps each on the same chip. On completion of dielectrophoresis substrates were briefly rinsed in ultrapure deionised water and blown dry in a gentle stream of nitrogen. Figure 3.10 illustrates positive dielectrophoresis of citrate-capped gold nanoparticles of core diameter 80 nm resulting in the directed assembly of the nanoparticles within the electrode gaps. Further, little or no trapping was observed in control gaps (no voltage applied). Scanning electron microscopy (SEM) imaging was used to determine the degree to which nanoparticles

were directly assembled between the electrodes. Imaging was the final step in each experiment. SEM data obtained at lower magnification for each device confirmed low incidence of nanoparticles outside the region in which dielectrophoresis was carried out, ruling out the possibility of random assembly.

(a) (b)

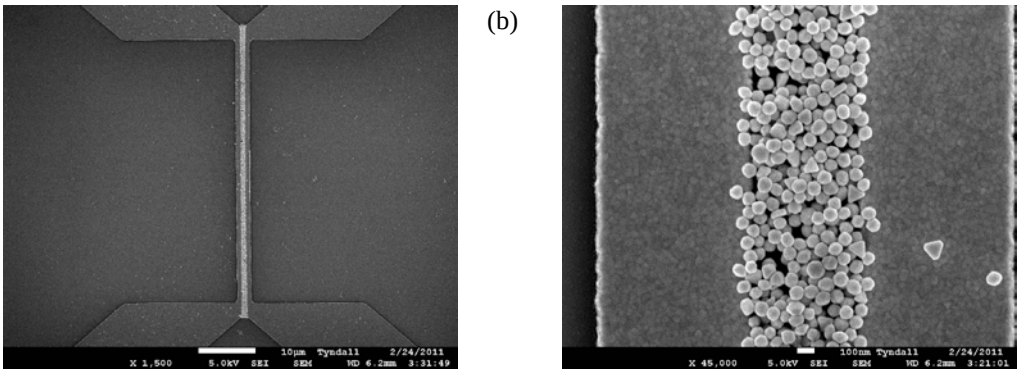

Figure 3.10: Scanning electron microscopy (SEM) images of microelectrodes (500 nm gaps) used for initial dielectrophoretic trapping of citrate capped gold nanoparticles with core diameters of d = 80 nm at fdep = 1 MHz, tdep = 300 s, V = 10 V.

However repeating this procedure using antiCRP NPs in ultrapure deionised water resulted in electrothermal effects having a significant influence on the dielectrophoretic process, see figure 3.11 (a). Furthermore, DEP trapping of antiCRP NPs and antiCRP nanostructures in 100 mM PBS buffer, required to mimic physiological conditions, resulted not only in negative dielectrophoresis as a result of the conductivity of the solution and overall negative real part of Clausius-Mossotti factor Re[$K(\omega)$] but also resulting damage to the electrodes, see figure 3.11 (b), even at low voltages and a range of frequencies, ruling out the potential of this proposed technique as a means to electrically characterise nanoparticle assemblies formed *via* CRP antibody-antigen recognition induced self-assembly.

(a) 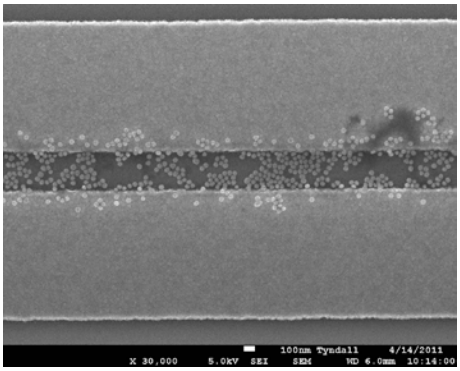 (b) 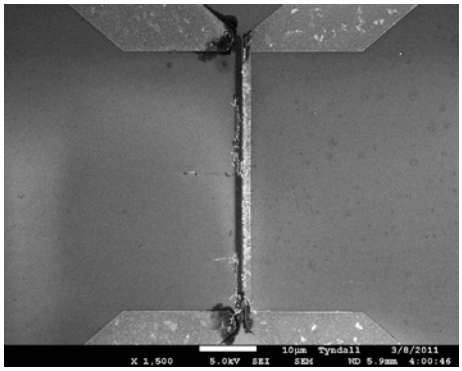

Figure 3.11: SEM images of microelectrodes (500 nm gap) displaying (a) partial trapping of CRP antibody functionalised gold nanoparticles dissolved in water (fdep = 1 MHz, tdep = 300s, V = 10 V), (b) damage as a result of trapping CRP antibody functionalised gold nanoparticles in 100 mM PBS buffer (fdep = 1 MHz, tdep = 300 s, V = 10 V).

3.4 Conclusions

The binding of CRP antibody to silanised silicon-silicon oxide substrates with gold micron-scale electrodes implemented using the organosilane (3-Aminopropyl)triethoxysilane (APTES) and the subsequent binding of CRP antigen to this immobilised CRP antibody was explored. The formation of the antibody-antigen complex resulted in a corresponding decrease of the sensor capacitance employing a CRP antigen concentration of 20 μg/mL for 2 hours.

It is concluded the molecular functionalization is successful for these devices and the net decrease in capacitance is a signature of successful binding of CRP antigen to CRP antibody immobilised on the substrate surface. Measurement protocols were reported and CRP was detected in a clinically relevant range mimicking point-of-care conditions. The binding of CRP antigen to CRP antibody however resulted in small charge related changes which were difficult to measure with great sensitivity.

The means to overcome limitations presented in using silicon-silicon oxide substrates in electrical detection of CRP was identified employing simulations performed in ANSYS. There lies potential in utilising this detection mechanism to establish a differential immunosensor where difference in response between a single antibody layer and an antibody layer to which antigen has bound can be detected. It presents a platform from which to work on to develop the electrical detection process further, using optimised electrode design and substrates and potentially real time measurements in buffer ideally in a flow through cell involving the addition of the sample containing CRP antigen yielding the result.

While the reaction occurring at the biosensor surface was electrically characterised in the presence of such limitations it was deemed advantageous to employ nanoparticle amplification to facilitate rapid point-of-care surface-based detection of CRP. In that regard dielectrophoresis was explored as a means for the directed assembly of nanoparticles and nanostructures between gold micron-scale electrodes. However it was demonstrated that the PBS solution employed to mimic physiological conditions did not accommodate positive dielectrophoresis. It was therefore deemed advantageous to consider nanoparticle amplification in surface-based assays without electrical detection.

3.5 References

1. Stang, P.J, Abiological self-assembly via coordination: formation of 2D metallacycles and 3D metallacages with well-defined shapes and sizes and their chemistry. *J Am Chem Soc* **2012,** 134, 11829-11830.

2. Howarter, J.A,; Youngblood, J.P, Optimization of silica silanization by 3-aminopropyltriethoxysilane. *Langmuir* **2006,** 22, 11142-11147.

3. Kim, J,; Seidler, P,; Wan, L.S,; Fill, C, Formation, structure, and reactivity of amino-terminated organic films on silicon substrates. *J. Colloid Interface Sci.* **2009,** 329, 114-119.

4. Aissaoui, N,; Bergaoui, L,; Landoulsi, J,; Lambert, J-F,; Boujday, S, Silane layers on silicon surfaces: mechanism of interaction, stability, and influence on protein adsorption. *Langmuir* **2012,** 28, 656-665.

5. Piatek, Z,; Baron, B,; Szczegielniak, T,; Kusiak, D,; Pasierbek, A, Self inductance of long conductor of rectangular cross section. *Przeglad Elektrotechniczny* **2012,** 88, 323-326.

6. Tran, E,; Duati, M,; Ferri, V, *et al*, Experimental approaches for controlling current flowing through metal-molecules-metal junctions. *Advanced Materials*. **2006**, 18,1323-1328.

7. Yaffe, O,; Scheres, L,; Puniredd, S.R, *et al*, Molecular electronics at metal/semiconductor junctions. Si inversion by sub-nanometer molecular films. *Nano Lett* **2009,** 9, 2390-2394.

8. Green, J.E,; Choi, J.W,; Boukai, A, *et al*, A 160-kilobit molecular electronic memory patterned at 10(11) bits per square centimetre. *Nature*. **2007,** 445, 414-417.

Chapter 4

Investigation of Surface-Based C-Reactive Protein Antibody-Antigen Binding

4.1 Introduction

The binding of CRP antibody to silanised silicon-silicon oxide substrates with gold micron-scale electrodes was implemented using the organosilane (3-Aminopropyl)triethoxysilane (APTES) and CRP antigen was subsequent bound to this immobilised CRP antibody. The formation of the antibody-antigen complex resulted in a corresponding decrease of the sensor capacitance representing successful molecular functionalization. The binding of antigen to antibody however resulted in small charge related changes which were difficult to measure with great sensitivity.

While electrical characterisation facilitated characterisation of the reaction occurring at the biosensor surface in the presence of such limitations it was deemed advantageous to employ nanoparticle amplification to facilitate rapid surface-based detection of CRP, void of elaborate equipment, applicable to POC detection of CRP. A tracer is often used to generate a signal, for example, optical, electrochemical, or radioisotopic decay, which enables quantitation of the amount of bound antigen. The number of target molecules can then be converted to a specific measure. Traditionally radioisotopes and fluorophores have been used but challenges relating to poor stability, low sensitivity and difficult sample processing exist. Nanoparticles offer a simple, sensitive alternative.

The binding of CRP antigen to surface immobilised CRP antibody was marked by gold nanoparticles functionalised with CRP antibodies (antiCRP NPs) and the numbers of bound nanoparticles analysed numerically employing imageJ software. Such nanoparticle tracers enable estimation of the amount of bound antigen and visual detection of CRP [1,2,3] demonstrating potential of nanoparticle tracers to facilitate rapid surface-based point-of-care detection of CRP.

4.2 Experimental

4.2.1 Binding of CRP antigen to surface immobilised CRP capture antibody

Substrate surface silanisation and immobilisation of CRP antibody was performed as described in chapter 3 of this thesis. Binding of CRP antigen to CRP antibody was performed at antigen concentrations of 5 μg/mL and 20 μg/mL. CRP antigen binding was marked by the presence of antiCRP NPs. Factors which may affect the binding of the nanoparticles to the CRP antigen were investigated, such as optical density and length of time of immersion to ensure that optimum binding was achieved. Control experiments were performed by replacing antiCRP NPs with BSA-capped NPs.

4.2.2 ImageJ analysis

In the imageJ programme the required scanning electron microscopy (SEM) image is selected. The size scale is set according to the scale as per SEM image. This relates the number of pixels in the image and the size of the features, which are in this case the nanoparticles (NP) and nanostructures (NS). The image is then cropped to include just the part of the SEM image excluding the SEM imaging details bar. The programme identifies and outlines the edges of NP/NS in the image. The image threshold can be adjusted to ensure that all NP/NS are selected and clearly defined by the edge outline line. The “smooth” function is then selected to remove background interference. The image is made binary and “dilate” function selected, which ensures that NP of a nanostructure (NS) assembly are combined together so as that the programme recognises them as a nanoparticle assembly as not as individual nanoparticles. The diameter of one NP is then measured using the “Analyse, measure” function. The entire image is selected, selecting all nanoparticles and nanostructures. The required measurements are set using the “Analyse, set measurements” function and all NP/NS in the image counted using the “Analyse, analyse particles” function. This outputs a list of results which includes the number of NS identified and the corresponding mean area. The areas corresponding to monomers, dimers etc. were recorded and from this, area ranges associated with each of the various NS sizes from monomers to assemblies containing 10 nanoparticles was established. This provided the number of each sized NS per SEM image.

4.3 Results and Discussion

4.3.1 Chemical modification of substrate surface through silanisation

It was crucial that the substrates, which chemical reactions are performed on to modify the surface to allow covalent coupling of the biological constituent, in this case *via* substrate silanisation, were sufficiently clean to eliminate any contaminants that would interfere with the functioning of the bio-layer and modified so as to generate the maximum number of available reactive hydroxyl groups for surface functionalisation. Control experiments were performed to ensure that neither citrate-capped gold NPs or antiCRP gold NPs bound non-specifically to the cleaned substrate surface. To investigate the degree of non-specific binding of antiCRP NPs to the silicon-silicon oxide substrate surface, substrates were immersed in antiCRP NP solution @ optical density (OD2) for 3 hours which equates to approximately 1.8E11 NPs supplied. This resulted in binding of on average 2 NPs per 6.5 x 4.5 µm area, 4E6 NPs binding per substrate, see figure 4.1 (a). Similarly, substrates were immersed in 20 nm citrate-capped gold NP solution @ OD1 for 3 hours, equating to approximately 7E11 NPs supplied. This resulted in on average 0 NPs binding per 6.5 x 4.5 µm area, 0 NPs binding per substrate, see figure 4.1 (b).

(a) (b)

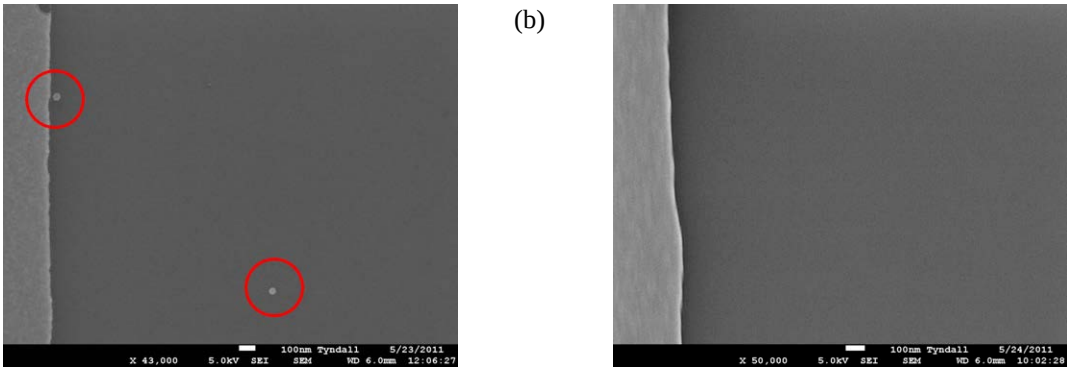

Figure 4.1: Scanning electron microscopy (SEM) images depicting the surface nanoparticle density on immersion of substrates post cleaning in (a) antiCRP NP solution at OD2 RT for 12 hours (≈ 2 particles binding per 6.5 µm x 4.5 µm area), (b) citrate-capped gold NP solution at OD1 RT for 12 hours (≈ 0 particles binding per 6.5 µm x 4.5 µm area).

Following substrate preparation the substrate surface was chemically modified through silanisation. The chemical and physical nature of the silane layer is of utmost importance as it directly influences the morphology and surface density of subsequently cross-linked molecules. The method used to determine the density and homogeneity of the silanisation layer formed involves immersion of the silanised substrates in a solution of 20 nm diameter citrate capped gold NPs. The negatively charged citrate capped gold NPs can bind to the positively charged amine group of the APTES molecules on the substrate surface.

APTES-functionalised substrates were immersed in citrate-capped NP-solution @ OD1 for 3 hours, equating to approximately 7E11 NPs supplied. This resulted in, on average 900 NPs binding per 6.5 x 4.5 μm area, 2E9 NPs binding per substrate, implying that there are at least 2E9 active APTES binding sites. The NP density obtained most likely represents the lower limit of available APTES binding sites, depicting a situation resulting from the electrostatic repulsion of citrate NPs rather than a limited population of APTES binding sites, see figure 4.2 (a). The number of bound NPs does not increase with longer immersion times despite possible unoccupied APTES binding sites on the surface, as the repulsive electrostatic forces exercised by neighbouring NPs prevent binding of further NPs on the substrate surface.

It is also of interest to determine the degree of non-specific binding of antiCRP NPs to the APTES-functionalised surface. In this case APTES-functionalised substrates were immersed in 40 nm antiCRP gold NP solution @ OD2 for 3 hours, equating to approximately 1.8E11 NPs supplied. This resulted in, on average 3 NPs binding per 6.5 x 4.5 μm area, 6E6 NPs binding per substrate, see figure 4.2 (b).

(a) (b)

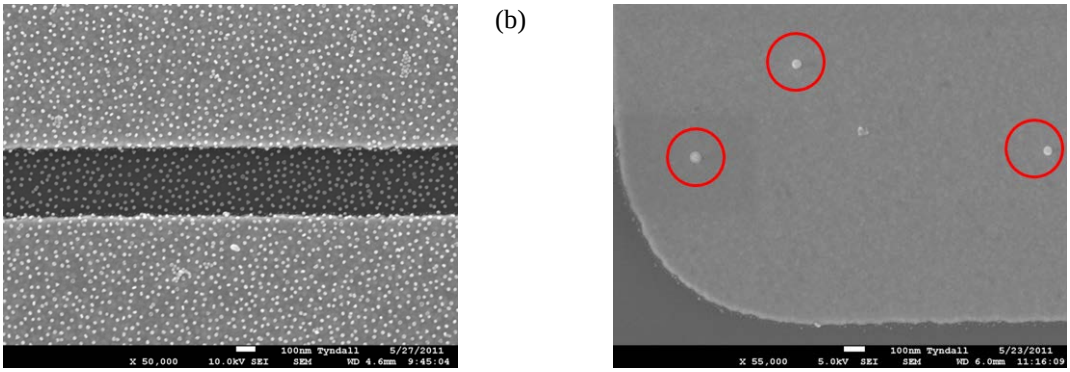

Figure 4.2: Scanning electron microscopy (SEM) images depicting the surface nanoparticle density on immersion of APTES functionalised substrates in (a) citrate-capped gold NP solution at OD1 RT for 3 hours (≈ 900 NPs binding per 6.5 µm x 4.5 µm area), (b) antiCRP gold NP solution at OD2 RT for 3 hours (≈ 3 NPs binding per 6.5 µm x 4.5 µm area).

4.3.2 Covalent attachment of CRP antibody

To determine the degree of binding of antiCRP NPs to the CRP antibody-functionalised substrate surface, antibody functionalised substrates were immersed in 40 nm gold antiCRP NP solution @ OD2 for 3 hours. This resulted in binding of, on average 8 NPs per 6.5 x 4.5 µm area, 1.7E7 NPs per substrate, equating to approximately binding of 1 in 100 resulting from non-specific binding, see figure 4.3.

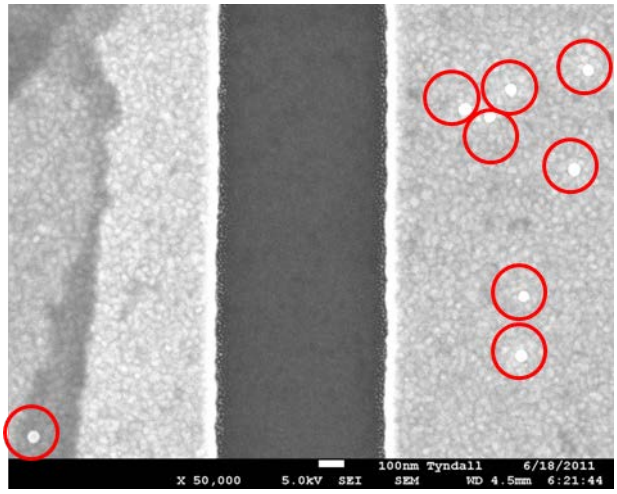

Figure 4.3: Scanning electron microscopy (SEM) image depicting the surface NP density on immersion of antibody functionalised substrates in 40 nm antiCRP gold NP solution at OD2 3 hours ≈ 8 NPs per 6.5 x 4.5 µm area (≈ 1.7E7 NPs binding per chip ≈ binding of 1 in 100 sites due to non-specific binding).

4.3.3 Binding of CRP antigen to surface immobilised CRP capture antibody

The detection of CRP antigen is determined by binding of the antigen to surface immobilised CRP antibody. The presence of CRP antigen is marked by antiCRP NPs. Substrates with antibody immobilised and antigen bound were immersed in 40 nm antiCRP gold NP solution @ OD2 for 1 hour. With approximately 2E9 APTES binding sites and approximately 5.4E12 antigens supplied, equates to approximately 2700 antigens per APTES site. With ≈ 1.8E11 NPs supplied and ≈ 9.8E8 NPs binding on the substrate surface, this results in binding of 1 in 2 APTES sites with antiCRP NPs. Figure 4.4 (a) displays the surface NP density of the antiCRP NPs on the substrate surface, marking the presence of the CRP antigen (20 μg/ml 2 hours). Each NP marks the presence of a CRP antigen molecule which has bound to a CRP antibody. Decreased binding activity results due to the orientation of the surface bound molecules, alteration of conformation of the receptor molecule on interaction with the surface, steric factor and altered kinetics.

As a control experiment, BSA passivated NPs were used in place of antiCRP NPs. Substrates with CRP antibody immobilised to which CRP antigen (20 μg/mL) was bound were immersed in 40 nm BSA passivated NP solution @ OD2 for 3 hours, equating to approximately 1.8E11 NPs supplied, with on average, 0 NPs binding per substrate, see figure 4.4 (b). This is not surprising as an antibody will combine specifically with the corresponding antigen. Even a small change, for example, the substitution of one amino acid for another, moving a chemical group from one carbon to another, or using the mirror image of a chemical group may change the antibody-antigen fit from very good to weak or non-interacting.[4] It is expected that a small number of NPs could bind as proteins always adsorb to some extent onto a solid surface. This adsorption is energetically favoured because of the decrease in interfacial tension and resultant decrease in the Gibbs energy of the system.

(a) 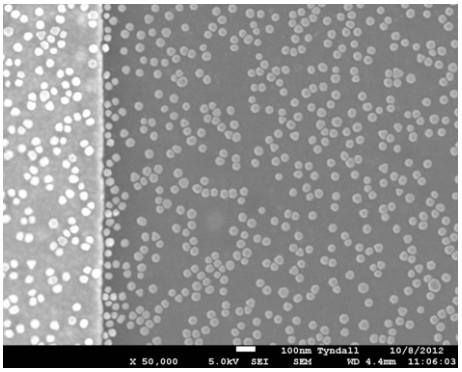

(b) 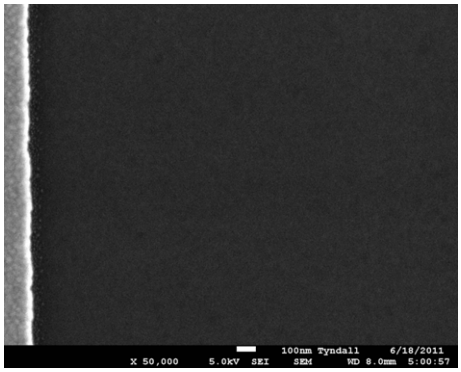

Figure 4.4 Scanning electron microscopy (SEM) images depicting the surface NP density of (a) the antiCRP NPs @ OD2 for 1 hour on the substrate surface marking the presence of the CRP antigen (20 µg/mL 2 hours), (b) 40 nm BSA passivated NP solution @ OD2 for 3 hours (≈ 1.8E11 NPs supplied ≈ 0 NPs binding per chip).

5 µg/mL CRP antigen for 2 hours resulted in sparse and inhomogeneous coverage with on average 675 antigens available per APTES binding site resulting in binding to ≈ 1 in 20 available APTES sites, see figure 4.5.

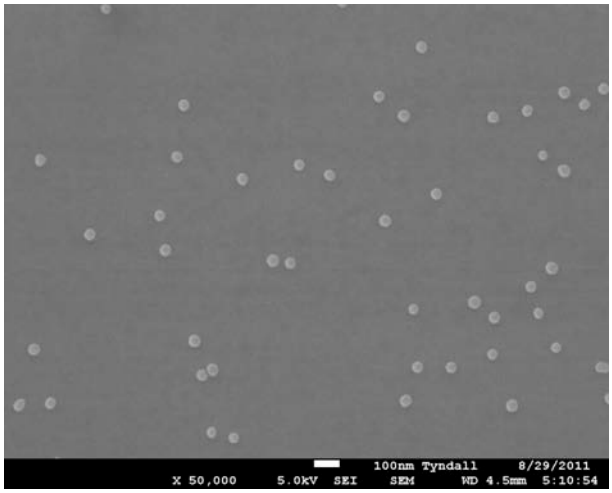

Figure 4.5: Scanning electron microscopy (SEM) image depicting the surface NP density of antiCRP NPs marking the presence of the CRP antigen (5 µg/mL 2 hours).

4.3.4 Image J analysis

ImageJ analysis enabled precise quantification of numbers of nanoparticles bound to the substrate surface. This enabled accurate relation of tracer signal – in this case nanoparticles, to concentration of CRP antigen present in the sample. Substrates (APTES functionalised; 100 μg/mL CRP antibody 4°C 16 hours) were exposed to 20 μg/mL CRP antigen RT for various times (a) 10 min (b) 60 min and (c) 120 min followed by immersion in antiCRP NP solution for 60 minutes. The number of individual NPs as well as the number of nanostructures (NS) of various sizes up to 10 NP were counted using Image J for each of 5 SEM images analysed per time point, see figure 4.6. The total of each sized NS entity across the 5 images was then established, followed by the average number of each. The ratio of individual NP to NS was then calculated for each of the 4 time points. This lead to estimation of the degree of NP binding to chemisorbed CRP antigen as opposed to binding of antiCRP NPs to physiosorbed antigen.

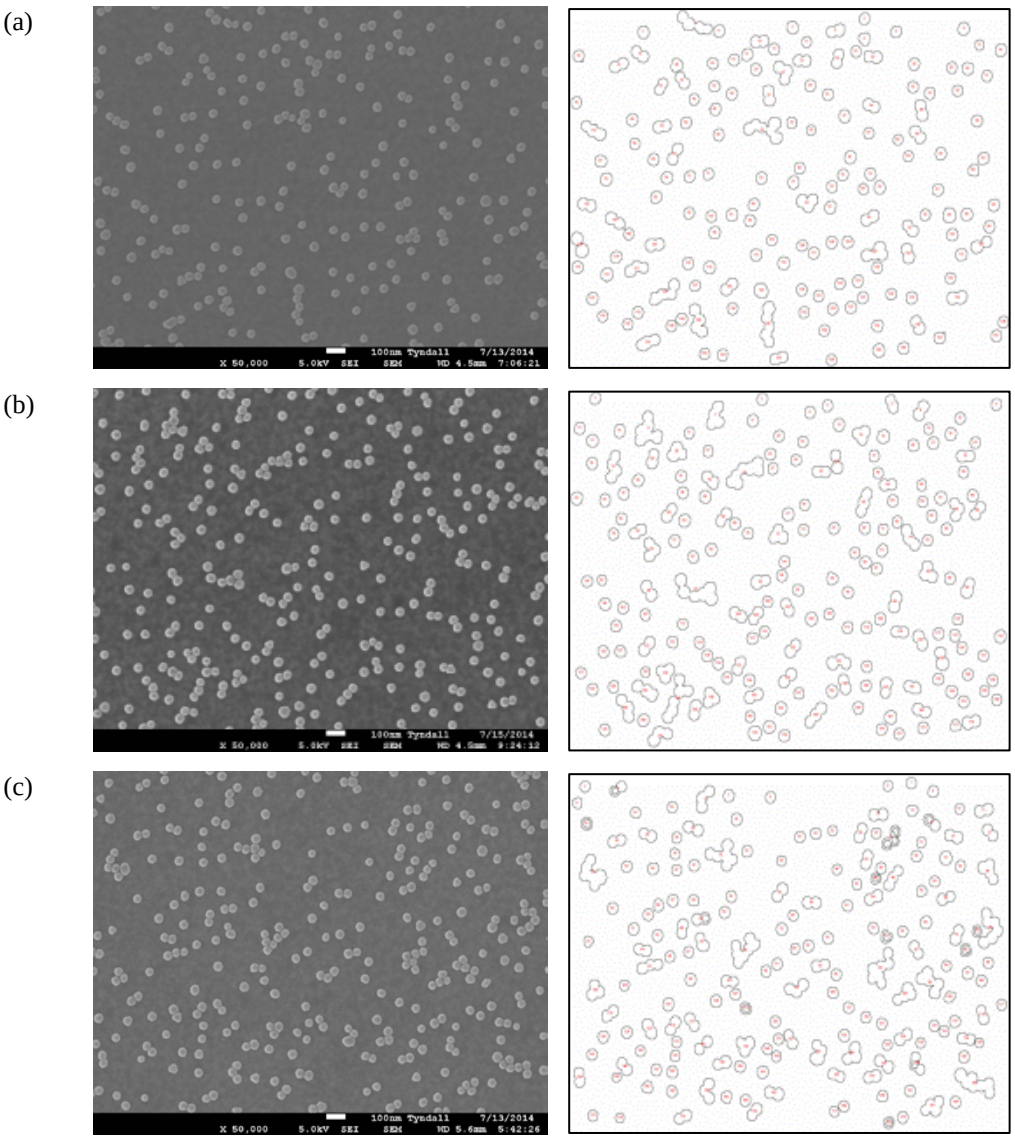

Figure 4.6: Scanning electron microscopy images depicting surface NP density and corresponding ImageJ output programme images outlining the various nanoparticles (NP)/nanostructures (NS) present at each time interval for 20 µg/mL CRP antigen RT for various lengths of time (a) 10 min (b) 60 min and (c) 120 min and immersion in antiCRP nanoparticle solution for 60 min.

Table 4.1 shows the total numbers of individual nanoparticles (NP) and nanostructures (NS) recorded for the 5 images for each time interval that the substrates were immersed in antiCRP nanoparticle solution for 60 minutes. The ratio of NP to NS is also shown in table 4.1. As the ratio of NS to individual NP decreases over time, it is suggestive that some length of time is required to facilitate formation of larger nanostructures. From this table of values the histogram in Figure 4.7 was plotted.

	Antigen (min)	NP (min)	Total Monomers	Ratio monomers :Nanostructures (NS)
(a)	10	60	86	1 : 0.94
(b)	60	60	97	1 : 0.76
(c)	120	60	110	1 : 0.58
(d)	120	10	82	1 : 0.29

Table 4.1: (a – c) Average numbers of nanoparticles (NP) and nanostructures (NS) recorded for the 5 scanning electron microscopy (SEM) images for each time point for which substrates (APTES functionalised; 100 µg/mL CRP antibody 4°C 16 hours) were exposed to (a – c) 20 µg/mL CRP antigen RT, followed by immersion in antiCRP nanoparticle solution for 60 min, including the ratio of individual NP to NS, (d) 20 µg/mL CRP antigen RT 2 hours followed by immersion in antiCRP nanoparticle solution for 10 min, including the ratio of individual NP to NS.

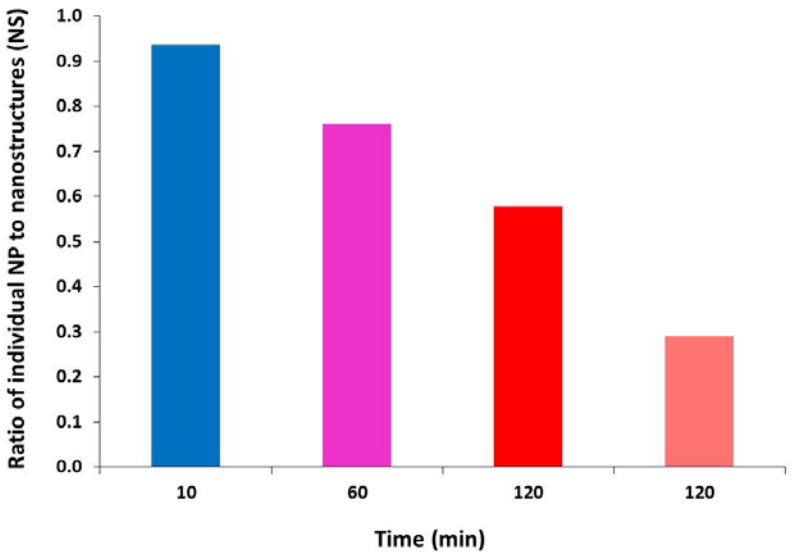

Figure 4.7: Histogram displaying the ratio of individual nanoparticles (NP) to nanostructures (NS) recorded for the 5 scanning electron microscopy (SEM) images for each time point for which substrates were exposed to 20 µg/mL CRP antigen RT, followed by immersion in antiCRP NP solution for 60 min. Also, the ratio of individual nanoparticles (NP) to nanostructures (NS) for substrates exposed to 20 µg/mL CRP antigen RT 2 hours followed by immersion in antiCRP nanoparticle solution for 10 minutes.

Further analysis of the data in the form of histogram plots of the % nanostructures containing numbers of nanoparticles from 1 to 10 when substrates were exposed to 20 μg/mL CRP antigen, followed by immersion in antiCRP nanoparticle solution for 60 minutes highlights the conversion of smaller nanostructures into larger assemblies over time, see figure 4.8. Unlike solution phase formation of nanostructures, however, where gentle mixing can facilitate more rapid formation of nanostructures this surface-based nanostructure formation relies on diffusion alone. Histogram plots of the % nanostructures containing numbers of nanoparticles from 1 to 3 (no nanostructures > those containing 3 NP were formed) when substrates were exposed to 5 μg/mL CRP antigen, followed by immersion in antiCRP nanoparticle solution for 60 minutes demonstrates the potential of visual detection of CRP antigen, differentiating between a CRP antigen concentration of 5 μg/mL (baseline level cut-off point) and elevated levels of 20 μg/mL, see figure 4.9.

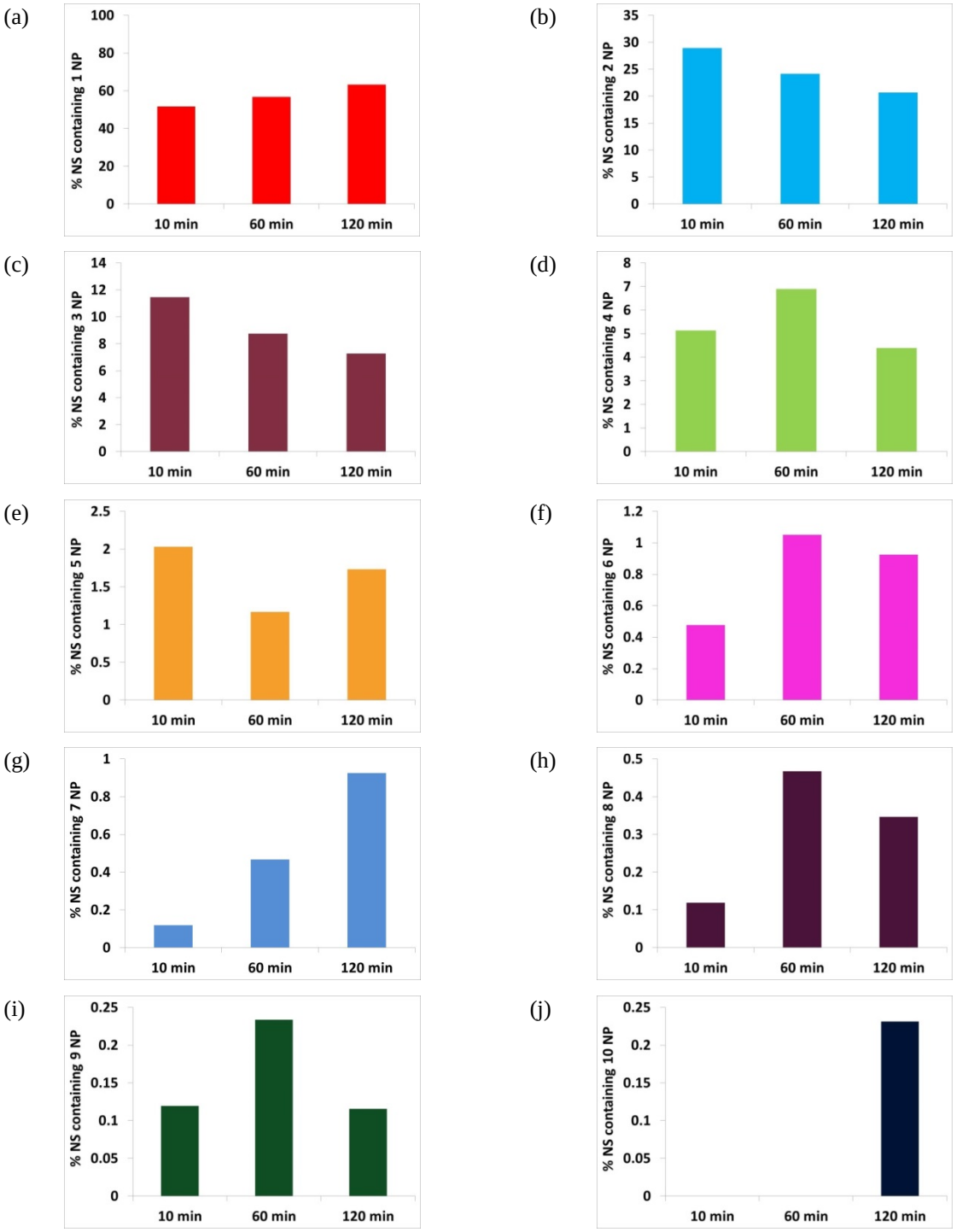

Figure 4.8: Histograms showing the distribution of nanostructures (NS) containing (a) one (b) two (c) three (d) four (e) five (f) six (g) seven (h) eight (i) nine (j) ten nanoparticles (NP) on substrate surfaces following immersion in 20 µg/mL CRP antigen solution for 10 minutes to 2 hours, followed by immersion in antiCRP NP solution for 60 minutes.

(a)

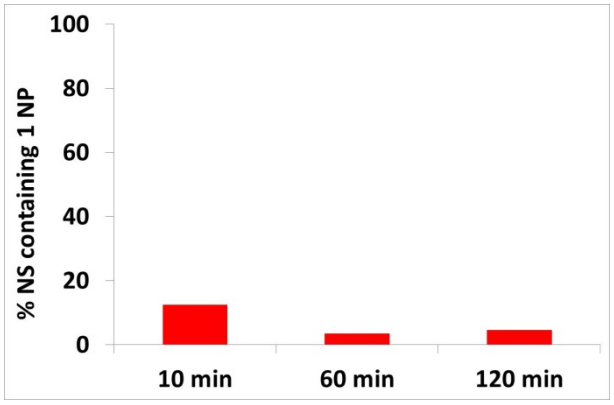

(b)

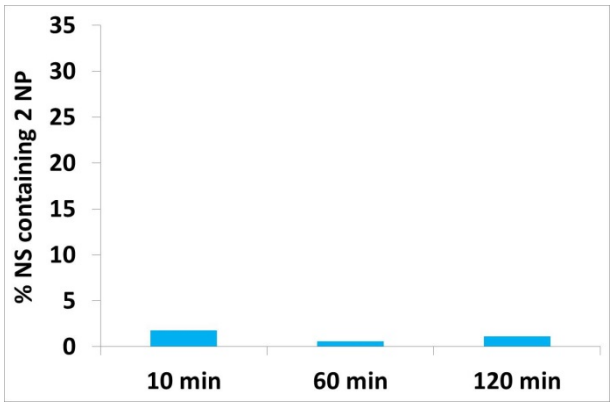

(c)

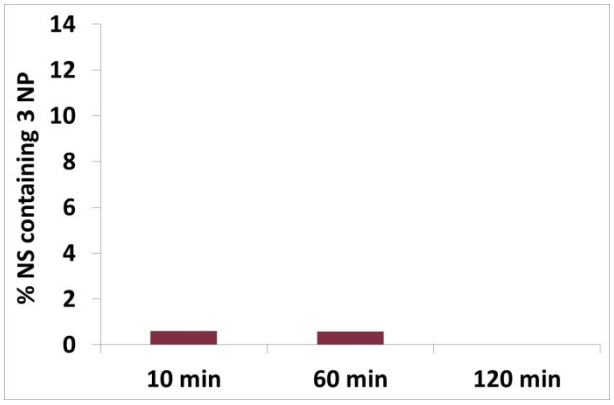

Figure 4.9: Histograms showing the distribution of nanostructures (NS) containing (a) one (b) two and (c) three nanoparticles (NP) on substrate surfaces following immersion in 5 µg/mL CRP antigen solution for 10 minutes to 2 hours, followed by immersion in antiCRP NP solution for 60 minutes.

The use of antiCRP NPs as tracers to mark the presence of bound antigen to generate an optical signal provided a simple, sensitive, visual detection means free of elaborate equipment to detect for the presence of CRP antigen in a clinically relevant range. Immersion of substrates in 5 µg/mL CRP antigen for 2 hours followed by immersion in antiCRP nanoparticle solution for 60 minutes resulted in no visually detectable colour change of the substrate surface while immersion of substrates in 20 µg/mL CRP antigen for 2 hours followed by immersion in antiCRP nanoparticle solution for 60 minutes resulted in a distinct substrate surface colour change to pink, see figure 4.10. Additionally, the data in figures 4.8 and 4.9 is suggestive that CRP antigen immersion times of 10 minutes and immersion in antiCRP nanoparticle solution could also facilitate this visual detection of CRP, demonstrating potential of such nanoparticle amplification to facilitate rapid surface-based POC detection of CRP. It is envisaged that future work can facilitate this.

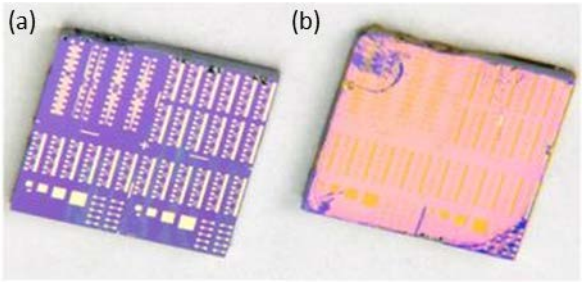

Figure 4.10: Silicon-silicon oxide substrates (APTES functionalised; 100 µg/mL CRP antibody 4°C 16 hours) which were exposed to (a) 5 µg/mL CRP antigen RT 2 hours followed by immersion in antiCRP nanoparticle solution for 60 min and (b) 20 µg/mL CRP antigen RT 2 hours followed by immersion in antiCRP nanoparticle solution for 60 minutes.

4.4 Conclusions

The binding of C-reactive Protein (CRP) antibody to silanised silicon oxide surfaces was implemented using the organosilane (3-Aminopropyl)triethoxysilane (APTES) and the subsequent binding of CRP antigen to this immobilised CRP antibody was marked by the presence of antiCRP gold NPs. Scanning electron microscopy (SEM) imaging was used throughout as a means to establish the build-up of layers during the antibody immobilisation and antigen binding processes. ImageJ software was employed to numerically analyse the number of surface bound nanoparticles.

Surface antiCRP NP coverage marking the presence of CRP antigen enabled estimation of the amount of bound antigen in the presence of limitations associated with surface-based attachment mechanisms, such as poor receptor binding, random orientation of the receptor molecule, alteration of conformation of the receptor molecule on interaction with the surface, steric factor and altered kinetics. This facilitated estimation of sensitivity and speed of response, where it was demonstrated that nanoparticle amplification could facilitate rapid visual surface-based detection of CRP.

In addition to solution-phase nanoparticle recognition-induced self-assembly, employing nanoparticle amplification in surface-based assays represents a detection means void of complex chemical processes and elaborate equipment which could compete with laboratory-based assays in terms of specificity, stability and sensitivity but also facilitate rapid surface-based point-of-care detection of CRP. The excellent binding specificity of gold nanoparticles offers a suitable platform for the selective binding and detection of biological targets. The advantages of integrating biomolecules with gold nanoparticles can generate materials that combine the properties of the nanoparticles with the molecular recognition properties of biomolecules. This provides for the analysis of cardiac markers such as CRP or diseases that can evolve rapidly in varying circumstances to be performed periodically at the point-of-care.

4.5 References

1. Alivisatos P. The use of nanocrystals in biological detection. *Nat Biotechnol*. **2004**;22(1):47-52.

2. Peng H-I, Miller BL. Recent advancements in optical DNA biosensors: Exploiting the plasmonic effects of metal nanoparticles. *Analyst*. **2011**;136(3):436-447.

3. Dykman L, Khlebtsov N. Gold nanoparticles in biomedical applications: recent advances and perspectives. *Chem Soc Rev*. **2012**;41(6):2256-2282.

4. Chen Y, Munechika K, Ginger DS. Bioenabled nanophotonics. *MRS Bull*. **2008**;33(5):536-542.

Chapter 5

Thesis summary

5.1 Conclusions

Nanoparticle self-assembly was demonstrated as an attractive technique to facilitate point-of-care detection of C-reactive protein (CRP). A CRP antigen concentration of 0.06 μg/mL was detected, evidenced as a distinct solution colour change from red to blue within 5 minutes. The strong light scattering of the gold nanoparticles facilitated this visual detection void of complex chemical processes and elaborate equipment, facilitating rapid inexpensive point-of-care detection while concurrently maintaining specificity, stability and sensitivity.

Employing just gold nanoparticles functionalized with CRP antibodies and CRP antigen as linker molecules, control of the rate of nanoparticle recognition-induced self-assembly was achieved between that of rapid formation of large nanostructures with associated solution colour change from red to blue within 5 minutes, and slow formation of small nanostructures over hours with no discernable solution color change. The key factor causative of that controlled self-assembly being the linker molecule-nanoparticle ratio and can be controlled to enable detection across a wide range of CRP concentrations.

Such control of the rate of nanoparticle self-assembly was corroborated employing nanoparticles of different functionality demonstrating applicability to detection of other molecules of interest. The self-assembly of d = 60 nm citrate-stabilized gold nanoparticle solution and $Re_2(DMAA)_4(NCS)_2$ linker molecules also resulted in a distinct solution colour change from red to blue within 5 minutes while elevated $Re_2(DMAA)_4(NCS)_2$ linker molecule concentrations resulted in slow/restricted nanostructure formation.

Such a sensitive, specific, stable, rapid detection mechanism could provide for point-of-care sensing at, for example, a GP surgery or hospital setting, using a hand-held spectrometer, facilitating provision of immediate and accurate test results. It also provides for detection at a range of near-patient settings, most particularly in resource-constrained settings, providing a simple, inexpensive visual detection means.

Surface-based assays also show much promise in application to point-of-care detection. The binding of CRP antibody to silanised silicon-silicon oxide substrates with gold micron-scale electrodes was implemented using the organosilane (3-Aminopropyl)triethoxysilane (APTES) and the subsequent binding of CRP antigen to this immobilised CRP antibody was explored. The formation of the antibody-antigen complex resulted in a corresponding decrease of the sensor capacitance employing a CRP antigen concentration of 20 μg/mL (2 hours).

It is concluded the molecular functionalization is successful for these devices and the net decrease in capacitance is a signature of successful binding of CRP antigen to CRP antibody immobilised on the substrate surface. Measurement protocols were reported and CRP was detected in a clinically relevant range mimicking point-of-care conditions. The binding of antigen to antibody however resulted in small charge related changes which were difficult to measure with great sensitivity.

The means to overcome limitations presented in using silicon-silicon oxide substrates in electrical detection of CRP was identified employing simulations performed in ANSYS. There lies potential in utilising this detection mechanism to establish a differential immunosensor where difference in response between a single antibody layer and an antibody layer to which antigen has bound can be detected. It presents a platform from which to work on to develop the electrical detection process further, using optimised electrode design, quartz substrates and potentially real time measurements in buffer ideally in a flow through cell involving the addition of the sample containing CRP antigen yielding the result.

While electrical characterisation facilitated characterisation of the reaction occurring at the biosensor surface in the presence of such limitations it was deemed advantageous to employ nanoparticle amplification to facilitate rapid point-of-care surface-based detection of CRP, void of elaborate equipment.

The binding of CRP antibody to silanised silicon oxide substrates was implemented using the organosilane (3-Aminopropyl)triethoxysilane (APTES) and the subsequent binding of CRP antigen to this immobilised CRP antibody was marked by the presence of antiCRP gold NPs. Scanning electron microscopy (SEM) imaging was used throughout as a means to establish the build-up of layers during the antibody immobilisation and antigen binding processes. ImageJ software was employed to numerically analyse the number of surface bound nanoparticles.

Surface antiCRP NP coverage marking the presence of CRP antigen enabled estimation of the amount of bound antigen in the presence of limitations associated with surface-based attachment detection mechanisms, such as poor receptor binding, random orientation of the receptor molecule, alteration of conformation of the receptor molecule on interaction with the surface, steric factor and altered kinetics. This facilitated estimation of sensitivity and speed of response, where it was demonstrated that nanoparticle amplification could facilitate rapid visual surface-based detection of between 5 μg/mL and 20 μg/mL CRP.

In addition to solution-phase nanoparticle recognition-induced self-assembly, employing nanoparticle amplification in surface-based assays represents a detection means void of complex chemical processes and elaborate equipment which could compete with laboratory-based assays in terms of specificity, stability and sensitivity but also facilitate rapid surface-based point-of-care detection of CRP. The excellent binding specificity of gold nanoparticles offers a suitable platform for the selective binding and detection of biological targets. The advantages of integrating biomolecules with gold nanoparticles can generate materials that combine the properties of the nanoparticles with the molecular recognition properties of biomolecules. This provides for the rapid, inexpensive analysis of cardiac markers such as CRP to be performed periodically at the POC.

Chapter 6

Appendices

A.1 Abbreviations and Acronyms

AC	Alternating current
APR	Acute phase response
APTES	(3-Aminopropyl)triethoxysilane
BSA	Bovine serum albumin
CHD	Coronary heart disease
CPG	Capacitance-conductance in parallel
CRP	C-reactive protein
CVD	Cardiovascular disease
DEP	Dielectrophoresis
DLVO	Derjaguin Landau Verwey Overbeek
DNA	Deoxyribonucleic acid
ELISA	Enzyme-linked immunosorbent assay
FDA	Food and drug administration
FWHM	Full width half maximum
GAM	Goat anti-mouse
GMM	Generalised Multiple Mie
LAT	Latex agglutination test
LCR	Inductance capacitance resistance
LOD	Limit of detection
NP	Nanoparticle
NP	Nanostructure
OD	Optical density
PBS	Phosphate buffered saline
POC	Point-of-care
RNA	Ribonucleic acid
RT	Room temperature

SAM	Self assembled monolayer
SEM	Scanning electron microscopy
SPR	Surface plasmon resonance
UV	Ultra violet

A.2 Publications

Schopf, C,; **Noonan, E**,; Quinn, A.J, Iacopino, Self-assembly of gold nanocrystals into discrete coupled plasmonic structures. *Crystals* **2016**, 6, 117 – 126.

A.3 Presentations

D. Lordan[1], A. Miranda, K. Linehan, **E. Noonan**, R. Puicervert, M. Russell, A. Pescaglini, M. Manning, M. Burke, A. Quinn, Molecular Functionalization of Exfoliated Graphene and Transferred CVD Graphene, MRS Spring Meeting 2014, San Francisco, California, April 2014.

E. Noonan, N. Sassiat, M. Manning, H. Braven, A. Quinn, Recognition-Induced Nanoparticle-Protein Binding for Optical and Electrical Sensing, Tyndall Internal Conference 2013, Cork, March 2013.

E. Noonan, M. Manning, H. Braven, N. Sassiat, A. Quinn, Recognition-Induced Nanoparticle-Protein Binding for Optical and Electrical Sensing, BCFN Nanomaterials Workshop 2013, University of Bristol, Bristol, February 2013.

E. Noonan, N. Sassiat, M, Manning, H. Braven, A. Quinn, Recognition-Induced Nanoparticle-Protein Binding for Optical and Electrical Sensing of C-Reactive Protein, UCC Research Day 2012, Cork, August 2012.

E. Noonan, N. Sassiat, M. Manning, H. Braven, A. Quinn, Recognition-Induced Nanoparticle-Protein Binding for Optical and Electrical Sensing, Tyndall Poster Competition 2012, Cork, July 2012.

E. Noonan, N. Sassiat, M. Manning, H. Braven, A. Quinn, Recognition-Induced Nanoparticle-Biomolecule Aggregates as Sensing Elements in Biomedical Diagnostic Devices, Postgraduate Symposium on Nanotechnology 2011, University of Birmingham, Birmingham, December 2011.

C. Schopf, **E. Noonan**, G. Leveque, A. Quinn, D. Iacopino, Correlated Optical/Electron Microscopy Imaging and Spectroscopy of Metal Nanostructures, Postgraduate

Symposium on Nanotechnology 2011, University of Birmingham, Birmingham, December 2011.

E. Noonan, M. Manning, H. Braven, A. Quinn, Formation and Characterisation of Nanocrystal-Biomolecule Nanostructures, Tyndall Poster Competition 2011, Cork, July 2011.

E. Noonan, M. Manning, H. Braven, A. Quinn, Recognition-Induced NC-Biomolecule *N*mer Nanostructures as Sensing Elements in Novel Low-Cost Biomedical Diagnostic Devices, Nanobio Europe 2011, Cork, June 2011.

E. Noonan, A. Quinn, Formation and Optical Properties of Nanocrystal-Molecule Nanostructures, INSPIRE-ICGEE "Fabrication to Application" School 2010, Cork, October 2010.

E. Noonan, D. Iacopino, A. Quinn, Formation of Plasmonic Nanoparticle-Molecule Nanostructures, Tyndall Poster Competition 2010, Cork, July 2010.